INVESTIGATION OF THE ATMOSPHERIC OZONE FORMATION POTENTIALS OF SELECTED $C_{\geq 12}$ NORMAL AND CYCLIC ALKANES

Report to the
Aluminum Association

by

William P. L. Carter, Dongmin Luo, and Irina L. Malkina

October 31, 2000

College of Engineering
Center for Environmental Research and Technology
University of California
Riverside, California 92521

00-AP-RT30-002-FR

ABSTRACT

As the second phase of our study of the atmospheric ozone formation potentials of constituents of aluminum rolling mill emissions, a series of environmental chamber experiments and computer model simulations were carried out to assess the atmospheric ozone formation potentials of the selected cycloalkanes hexyl cyclohexane and octyl cyclohexane. The experiments consisted of determining the effects on NO oxidation, ozone formation and OH radical levels when adding the compounds to varying simulated model photochemical smog systems. The chamber experiments employed both blacklight and xenon arc light sources. These data supplemented similar experiments carried out previously on C_{12} - C_{16} normal alkanes. Like the $C_{\geq 12}$ normal alkanes, these cycloalkanes were found to be strong inhibitors of radical levels, inhibited rates of NO oxidation and O_3 formation in experiments that are sensitive to radical effects, but had only relatively small effects on O_3 in experiments more representative of atmospheric conditions.

Model simulations using the recently developed SAPRC-99 atmospheric chemical mechanism was gave good simulations of the results of the $C_{\geq 12}$ normal and cyclic alkane data obtained in both phases of this project. This mechanism was then used to calculate that impacts of these compounds on ozone formation in a one day box model scenarios representing various urban areas around the United States. These were compared with ozone impacts calculated for ethane, the compound that has been used by the EPA to determine "negligible" ozone reactivity for regulatory exemption purposes. The ozone impacts for the $C_{\geq 12}$ alkanes were found to be highly dependent on scenario conditions and how the ozone impact was quantified. In most cases the $C_{\geq 12}$ alkane ozone impacts on a mass basis were less than 25% those of the mixture representing VOCs from all sources, but the impacts relative to ethane varied greatly. In general, the impacts of the $C_{\geq 12}$ alkanes on maximum 8-hour average ozone levels were found to less than those of ethane under most conditions, while their impacts on peak ozone yields tend to be greater than ethane, except for the lowest NO_x scenarios. However, the results are highly variable and dependent on other scenario conditions besides NO_x.

ACKNOWLEDGEMENTS

The authors acknowledge Mr. Dennis Fitz for assistance in administering this program, Mr. Kurt Bumiller for assistance in carrying out the environmental chamber experiments, and Dr. Roger Atkinson for helpful discussions. We also thank Dr Roger Atkinson for kindly providing the methyl nitrite used in the kinetic experiments carried out for this project.

This work was funded by the Aluminum Association through contract number AA 1345. However, the opinions and conclusions expressed in this report are entirely those of the primary author, Dr. William P. L. Carter. Mention of trade names or commercial products does not constitute endorsement or recommendation for use.

TABLE OF CONTENTS

LIST OF TABLES

LIST OF FIGURES

INTRODUCTION

Ozone in photochemical smog is formed from the gas-phase reactions of volatile organic compounds (VOCs) and oxides of nitrogen (NO_x) in sunlight. Although Houston and Los Angeles currently have the worst ozone problems in the United States, other areas of the country also have episodes where ozone exceeds the federal air quality standard. Ozone control strategies in the past have focused primarily on VOC controls, though the importance of NO_x control has become recognized in recent years. VOC and NO_x controls have differing effects on ozone formation. NO_x is required for ozone formation, and if the levels of NO_x are low compared to the levels of reactive VOCs, then changing VOC emissions will have relatively little effect on ozone. Since NO_x is removed from the atmosphere more rapidly than VOCs, ozone in areas far downwind from the primary sources tend to be more NO_x limited, and thus less responsive to VOC controls. VOC controls tend to reduce the rate that O_3 is formed when NO_x is present, so VOC controls are the most beneficial in reducing O_3 in the urban source areas, where NO_x is relatively plentiful, and where O_3 yields are determined primarily by how rapidly it is being formed. Because of this, any comprehensive ozone control strategy should involve reduction of emissions of both NO_x and VOCs.

Many different types of VOCs are emitted into the atmosphere, each reacting at different rates and having different mechanisms for their reactions. Because of this, they can differ significantly in their effects on ozone formation, or their "reactivity". Some compounds, such as CFCs, do not react in the lower atmosphere at all, and thus make no contribution to ground-level ozone formation. Others, such as methane, react and contribute to ozone formation, but react so slowly that their practical effect on ozone formation in urban atmospheres is negligible. Obviously, it does not make sense to regulate such compounds as ozone precursors. In recognition of this, the EPA has exempted certain compounds from such regulations on the basis of having "negligible" effects on ozone formation. Although the EPA has no formal policy on what constitutes "negligible" reactivity, in practice it has used the ozone formation potential of ethane as the standard in this regard is because ethane is the most reactive of the compounds that were initially exempted by the EPA. Therefore, the ozone formation potential of a compound relative to ethane is of particular interest when assessing whether it might be a likely candidate for exemption from regulation as an ozone precursor.

Many VOCs that would not be judged to have "negligible" reactivity under the current criterion might still have much lower ozone formation potential than average, and substituting emissions of highly reactive VOCs with such moderate-to-low reactivity VOCs would be expected to result in air quality improvements. Although the current EPA policies do not encourage such substitutions, it has been proposed to implement reactivity-based policies on a voluntary basis in consumer product regulations in California (CARB, 1999), and the EPA is currently re-evaluating its reactivity-based VOC policies (Dimitriades, 1999, RRWG, 1999). Mc.Bride et al (1977) showed that adopting reactivity-based VOC control policies could result in significant cost savings in ozone reduction strategies, though a number of

difficult policy and enforcement issues need to be resolved (RRWG, 1999). Although regulatory approaches that appropriately deal with differences in VOC reactivity are still evolving, it is clear that industries whose processes result in VOC emissions will need to know how those VOCs might be classified under any such system, so they can appropriately adapt to reactivity-based policies once they are implemented. This requires an ability to reliably estimated the ozone impacts of the VOCs of interest.

Aluminum rolling mills use high molecular weight alkane mixtures as lubricants, and normal rolling mill processes may result in sufficient emissions of these compounds to be of regulatory concern. However, high molecular weight alkanes, and high molecular weight normal alkanes in particular, have been estimated to have sufficiently low ozone impacts (e.g., Carter, 1994a, Carter and Venkataraman, 1995) that exempting them from regulation as VOC ozone precursors may not be inappropriate. Because of this, the Aluminum Association contracted with the College of Engineering Center for Environmental Research and Technology to provide the data and conduct the analysis needed to quantitatively assess the ozone impacts of representative components of aluminum rolling mill lubricants.

The process involved in of quantitatively assessing ozone impacts of compounds for which ozone impact data are not available involves at a minimum the following steps. (1) Environmental chamber experiments are carried out to determine the effects of the subject compounds on O_3 formation and other measures of air quality under various conditions. (2) Gas-phase atmospheric chemical mechanisms for the relevant atmospheric reactions of the compounds are developed based on available laboratory data and theoretical estimates and their ability to predict of ozone impacts and other relevant measures of reactivity are evaluated by comparing model predictions with the results of the environmental chamber experiments. If necessary, uncertain portions of the mechanism are modified to yield predictions that are consistent with the chamber data. (3) The experimentally evaluated mechanisms are then incorporated into models for ozone formation in the atmosphere, and these models are then used to determine the effects of adding these compounds to existing emissions in scenarios representing various urban conditions where ozone formation is a problem. The results are then compared with the ozone formation potentials of other representative compounds, including ethane. A comparison of the ozone impacts of the subject compounds to those of ethane can be used in judging whether it is appropriate to exempt the compound from regulation as a VOC ozone precursor under the current standard used by the EPA. A comparison of their ozone impacts compared to the mixture of reactive VOCs emitted from all anthropogenic sources can be used to assess the relative ozone benefits of regulating emissions of the subject compounds compared to regulating all VOC emissions equally.

The first phase of this project consisted of conducting such experiments and analysis on the ozone impacts of the C_{12} to C_{16} normal alkanes. This phase was completed and the results are documented by Carter et al (1996). It was found that as predicted these normal alkanes had relatively low ozone impacts that are comparable to those of ethane, though the impacts varied significantly from scenario to scenario. In the second phase of the program, experiments were carried out to assess the ability of current mechanisms to predict the ozone impacts of the representative high molecular weight cycloalkanes hexyl cyclohexane and octyl cyclohexane. During the intervening period the general atmospheric chemical

mechanism used in the 1996 Phase 1 report underwent a significant update (Carter, 2000), and thus the environmental chamber mechanism evaluation and atmospheric reactivity predictions for the $C_{\geq 12}$ normal alkanes as given by Carter et al (1996) are out of date. This Phase 2 report therefore updates the mechanism evaluations and reactivity calculations for the C_{12} - C_{16} normal alkanes, as well as documenting the Phase 2 experiments, mechanism evaluations, and reactivity calculations for the representative cycloalkanes.

EXPERIMENTAL AND DATA ANALYSIS METHODS

Environmental Chamber Experiments

Overall Experimental Approach

Most of the environmental chamber experiments for this program consisted of measurements of "incremental reactivities" of the subject VOCs under various conditions. These involve two types of irradiations of model photochemical smog mixtures. The first is a "base case" experiment where a mixture of reactive organic gases (ROGs) representing those present in polluted atmospheres (the "ROG surrogate") is irradiated in the presence of oxides of nitrogen (NO_x) in air. The second is the "test" experiment that consists of repeating the base case irradiation except that the VOC whose reactivity is being assessed is added. The differences between the results of these experiments provide a measure of the atmospheric impact of the test compound, and the difference relative to the amount added is a measure of its reactivity. To provide data concerning the reactivities of the test compound under varying atmospheric conditions, three types of base case experiments were carried out:

Mini-Surrogate Experiments. This base case employed a simplified ROG surrogate and relatively low ROG/NO_x ratios. Low ROG/NO_x ratios represent "maximum incremental reactivity" (MIR) conditions, which are most sensitive to VOC effects. This is useful because it provides a sensitive test for the model, and also because it is most important that the model correctly predict a VOC's reactivity under conditions where the atmosphere is most sensitive to the VOCs. The ROG mini-surrogate mixture employed consisted of ethene, n-hexane, and m-xylene. This surrogate was employed in our previous studies (Carter et al, 1993; 1995a-c, 1997a, 2000a), and was found to provide a more sensitive test of the mechanism than the more complex surrogates that more closely represent atmospheric conditions (Carter et al, 1995b). This high sensitivity to mechanistic differences makes the mini-surrogate experiments most useful for mechanism evaluation. The average initial reactant concentrations of these experiments were (in ppm): NO: 0.22, NO_2: 0.09, n-hexane: 0.5, ethene: 0.8, and m-xylene: 0.14

High NO_x Full Surrogate Experiments. This base case employed a more complex ROG surrogate under somewhat higher, though still relatively low, ROG/NO_x conditions. While less sensitive to the mechanism employed, experiments with a more representative ROG surrogate are needed to evaluate the mechanism under conditions that more closely resembling the atmosphere. The ROG surrogate employed was the same as the 8-component "lumped molecule" surrogate as employed in our previous study (Carter et al. 1995b), and consists of n-butane, n-octane, ethene, propene, trans-2-butene, toluene, m-xylene, and formaldehyde. Calculations have indicated that use of this 8-component mixture will give essentially the same results in incremental reactivity experiments as actual ambient mixtures (Carter et al. 1995b). The average initial reactant concentrations of these experiments were (in ppm): NO: 0.25, NO_2: 0.10, n-butane: 0.4, n-octane: 0.12, ethene: 0.08, propene: 0.07, trans-2-butene: 0.07, toluene: 0.11 and m-xylene: 0.10.

Full Surrogate, low NO_x Experiments. This base case employing the same 8-component "lumped molecule" surrogate as the full surrogate experiments described above, except that lower NO_x levels (higher ROG/NO_x ratios) were employed to represent NO_x-limited conditions. Such experiments are necessary to assess the ability of the model to properly simulate reactivities under conditions where NO_x is low. The initial ROG and NO_x reactant concentrations were comparable to those employed in our previous studies (Carter et al. 1995b, 1997a, 2000a). The average initial NO and NO_2 were 0.11 and 0.06 ppm, respectively, and the initial concentrations of the 8 ROG surrogate components were the same as in the high NO_x full surrogate experiments.

An appropriate set of control and characterization experiments necessary for assuring data quality and characterizing the conditions of the runs for mechanism evaluation were also carried out. These are discussed where relevant in the results or modeling methods sections (see also Carter et al, 1995c, 2000a).

Environmental Chambers

Two environmental chambers were employed in this program, which differed primarily in the type of light source employed. Most experiments were carried out using the CE-CERT "Dividable Teflon Chamber" (DTC) with a blacklight light source. This consists of two ~6000-liter 2-mil heat-sealed FEP Teflon reaction bags located adjacent to each other and fitted inside an 8' x 8' x 8' framework, and which uses two diametrically opposed banks of 32 Sylvania 40-W BL black lights as the light source. The lighting system in the DTC was found to provide so much intensity that only half the lights were used for irradiation. The air conditioner for the chamber room was turned on before and during the experiments. Four air blowers that are located in the bottom of the chamber were used to help cool the chamber as well as mix the contents of the chamber. The CE-CERT DTC is very similar to the SAPRC DTC which is described in detail elsewhere (Carter et al, 1995b,c).

The blacklight light source has the advantage of being relatively inexpensive to operate and provides a reasonably good simulation of natural sunlight in the region of the spectrum that is important in affecting most photolysis reactions of importance for non-aromatic VOCs (Carter et al, 1995c,d). This is therefore probably appropriate for studies of reactivities of compounds, such as alkanes, which are not photoreactive or believed to form significant yields of photoreactive products whose action spectra are not well characterized. However, to verify that this is the case, it is useful to carry out at least some experiments using a light source such as xenon arcs, which give a better simulation of sunlight throughout the full spectral range. Therefore, the CE-CERT xenon arc Teflon Chamber (CTC) was used for some of the experiments carried out for this project.

The CE-CERT CTC consists of two ~3500 –liter 4' x 4' x 8' FEP Teflon reaction bags located adjacent to each other at one end of an 8' x 12' room with reflective aluminum paneling on all surfaces. Four 6.5 KW xenon arc lights were mounted on the wall opposite the reaction bags, all in a room with walls and ceiling covered with reflective aluminum paneling to maximize light intensity and homogeneity. As discussed elsewhere (Carter et al. 1995d), this light source gives the closest approximation available of the ground-level solar spectrum for an indoor chamber. The room with the

chamber has a sufficiently powerful air conditioning system to remove the heat input caused by the lights to maintain an approximately constant ambient temperature of ~25^{o}C. A movable panel is used to block the lights when they are first turned on and warming up, which is raised to begin the irradiation. The chamber was very similar to the Statewide Air Pollution Research Center's Xenon arc Teflon Chamber (SAPRC XTC) which is described in detail elsewhere (Carter et al. 1995c,d).

Both the DTC and CTC are designed to allow simultaneous irradiations of experiments with and without added test reactants under the same reaction conditions. Since the chambers are actually two adjacent FEP Teflon reaction bags, two mixtures can be simultaneously irradiated using the same light source and with the same temperature control system. These two reaction bags are referred to as the two "sides" of the chambers (Side A and Side B) in the subsequent discussion. The sides are interconnected with two ports, each with a box fan, which rapidly exchange their contents to assure that base case reactants have equal concentrations in both sides. In addition, a fan is located in each of the reaction bags to rapidly mix the reactants within each chamber. The ports connecting the two reactors can then be closed to allow separate injections on each side, and separate monitoring of each side.

Experimental Procedures

The reaction bags were flushed with dry air produced by an AADCO air purification system for 14 hours (6pm-8am) on the nights before experiments. The continuous monitors were connected prior to reactant injection and the data system began logging data from the continuous monitoring systems. The reactants were injected as described below (see also Carter et al, 1993, 1995c). The common reactants were injected in both sides simultaneously using a three-way (one inlet and two outlets connected to side A and B respectively) bulb of 2 liters in the injection line and were well mixed before the chamber was divided. The contents of each side were blown into the other using two box fans located between them. Mixing fans were used to mix the reactants in the chamber during the injection period, but these were turned off prior to the irradiation. The sides were then separated by closing the ports that connected them, after turning all the fans off to allow their pressures to equalize. After that, reactants for specific sides (the test compound in the case of reactivity experiments) were injected and mixed. In case of CTC chamber the lights are turned on after lowering a metal baffle between the lights and the reactors, and the lights are allowed to warm up for at least 30 minutes. Irradiation in the chamber is begun by raising the baffle between the lights and the reactors, and the irradiation proceeds for 6 hours. After the run, the contents of the chamber were emptied by allowing the bags to collapse, and then the chamber was flushed with purified air. The contents of the reactors were vented into a fume hood.

The procedures for injecting the various types of reactants were as follows. The NO and NO_2 were prepared for injection using a high vacuum rack. Known pressures of NO, measured with MKS Baratron capacitance manometers, were expanded into Pyrex bulbs with known volumes, which were then filled with nitrogen (for NO) or oxygen (for NO_2). The contents of the bulbs were then flushed into the chamber with nitrogen. The gaseous reactants were prepared for injection either using a high vacuum rack or a gas-tight syringes whose amounts were calculated to achieve the desired concentrations in the

chamber. Sufficiently volatile liquid reactants (which included all the liquid surrogate components used in this study) were injected using a micro syringe into a 1-liter Pyrex bulb equipped with stopcocks on each end and a port for the injection of the liquid. Then one end of the bulb was attached to the injection port of the chamber and the other to a nitrogen source. The stopcocks were then opened, and the contents of the bulb were flushed into the chamber with a combination of nitrogen and heat gun for approximately 5 minutes. The high molecular weight cycloalkanes were injected by introducing the desired amount of liquid measured with a microsyringe into a tube wrapped with heat tape, then flushing the contents of the tube into the chamber with Aadco air at about 2 liters/minute for 10-20 minutes, with the tube was heated to ~250K.

Formaldehyde was prepared in a vacuum rack system by heating paraformaldehyde in an evacuated bulb until the pressure corresponded to the desired amount of formaldehyde. The bulb was then closed and detached from the vacuum system and its contents were flushed into the chamber with dry air through the injection port.

Kinetic Experiments

In addition to the environmental chamber experiments for mechanism evaluation, a limited number of experiments were carried out to determine the rate constant for the reactions of OH radicals with hexyl cyclohexane and octyl cyclohexane, using a relative rate technique. Experiments were carried out using either a ~3200-liter blacklight-irradiated chamber constructed of 2 mil FEP Teflon film that was used in our previously reported kinetic experiments (Carter et al, 2000a), or Side A of the DTC chamber described above. The light intensity in the ~3200 liter chamber was approximately twice that of the lights used in the DTC. Pure dry air from an AADCO air purification system was used for all experiments, and the experiments were carried out at ambient temperature (approximately 295-298^{o}K).

OH Radicals were generated by the photolysis of methyl nitrite in the presence of NO. The methyl nitrate was synthesized at Roger Atkinson's laboratory at the Air Pollution Research Center as described previously (Atkinson et al, 1981), and was transferred to our laboratory in the gas phase using ~0.6 liter Pyrex bulb covered with the black tape. The methyl nitrite was prepared for injection using a high vacuum rack as described above. The contents of the bulb were then flushed into the chamber with the Aadco air after all the reactants were already injected. Approximately 2 ppm of methyl nitrite, 3 ppm of NO and 0.25 ppb each of m-xylene, n-C_{12}, n-C_{14}, hexyl cyclohexane, and octyl cyclohexane were injected into the reactor in the dark. After the reactants were injected and mixed, the concentrations of the VOC reactants were monitored by gas chromatography until reproducible concentrations were measured. The analysis methods employed were the same as employed in the reactivity experiments for the hexyl and octyl cyclohexanes, as described below, and all the VOCs were analyzed simultaneously using the same instrument. Then the lights were turned on for brief periods (5-10 minutes, with the time increasing as the experiment progressed) and then turned off. The reactant concentrations were measured between each irradiation.

The experiments employed m-xylene as the reference compound, hexyl cyclohexane and octyl cyclohexane as the compounds whose OH rate constants were to be determined and n-dodecane and n-tetradecane for verification purposes.

Analytical Methods

Ozone and nitrogen oxides (NO_x) were continuously monitored using commercially available continuous analyzers with Teflon sample lines inserted directly into the chambers. The sampling lines from each side of the chamber were connected to solenoids that switched from side to side every 10 minutes, so the instruments alternately collected data from each side. Ozone was monitored using a Dasibi 1003-AH UV photometric ozone analyzer and NO and total oxides of nitrogen (including organic nitrates and perhaps HNO_3) were monitored using a Teco Model 42 chemiluminescent NO/NO_x monitor. The output of these instruments, along with that from the temperature sensors and the formaldehyde instrument, were attached to a computer data acquisition system, which recorded the data at 10 minutes intervals for ozone, NOx and temperature (and at 15 minutes for formaldehyde), using 30 second averaging times. This yielded a sampling interval of 20 minutes for taking data from each side.

The Teco instrument and Dasibi CO analyzer were calibrated prior to each experiment using a certified NO and CO source and CSI 1700 gas-phase titration calibrator. The Dasibi ozone analyzer was calibrated against transfer standard ozone analyzer using transfer standard method in an interval of three months and was check with CSI ozone generator for each experiment to assure that the instrument worked properly. The details were discussed elsewhere (Carter et al, 1995c)

Organic reactants other than formaldehyde were measured by gas chromatography with FID detection as described elsewhere (Carter et al. 1993; 1995c). GC samples were taken for analysis at intervals from 20 minutes to 30 minutes either using 100 ml gas-tight glass syringes or by collecting the 100 ml sample from the chamber onto Tenax-GC solid adsorbent cartridge. These samples were taken from ports directly connected to the chamber after injection and before irradiation and at regular intervals after irradiation was started. The sampling method employed for injecting the sample onto the GC column depended on the volatility or “stickiness” of the compound. For analysis of the more volatile species, which includes all the base ROG surrogate compounds monitored in this study, the contents of the syringe were flushed through a 10 ml and 5 ml stainless steel or 1/8' Teflon tube loop and subsequently injected onto the column by turning a gas sample valve. For analysis of the hexyl and octyl cyclohexanes, and also m-xylene, n-C_{12} and n-C_{14} during the kinetic experiments, the samples were collected using a Tenax-GC cartridge. The cartridge was then placed in series with the GC column, where it was heated to 300^{o}C to desorb the sample, which was then cryofocused on the column.

The calibrations for the GC analyses for most compounds were carried out by sampling from chambers or vessels of known volume into which known amounts of the reactants were injected, as described previously (Carter et al, 1995c).

Formaldehyde was monitored using an adaptation of the diffusion scrubber method developed by Dasgupta et al (1988, 1990), as described by Carter et al (1995c). It was calibrated using a formaldehyde diffusion tube whose weight loss was monitored over time. The system cycled between zero, calibrate, and sample modes to correct for zero and span drifts.

Characterization Methods

Temperature

Three temperature thermocouples were used to monitor the chamber temperature, two of which were located in the sampling line of continuous analyzers to monitor the temperature in each side. The third one was located in the outlet of the air conditioning system used to control the chamber temperature. The temperature range in these experiments was typically 25-30 C.

Xenon Arc Light Source

The spectrum of the xenon arc light source was measured several (usually five) times during each CTC experiment using a LiCor LI-1800 spectroradiometer. The absolute light intensity in this chamber was measured by "photostationary state" NO_2 actinometry experiments and by Cl_2 actinometry, which were primarily carried out prior to the period of the experiments discussed in this report (Carter et al, 1997a). The photostationary state experiments consisted of simultaneous measurements of photostationary state concentrations of NO, NO_2, and O_3 in otherwise pure air, with the NO_2 photolysis rate being calculated from the $[NO][O_3]/[NO_2]$ ratio (Carter et al. 1997a). The Cl_2 actinometry experiments consisted of photolyzing ~0.1 ppm of Cl_2 in ~1 ppm of n-butane, calculating the Cl_2 photolysis rate from the rate of consumption of n-butane, and then calculating the corresponding NO_2 photolysis rate from the absorption cross sections and quantum yields for NO_2 and Cl_2 (assuming unit quantum yields for Cl_2) and the spectral distribution of the light source (Carter et al, 1997a).

Relative trends in light intensity with time are obtained using the quartz tube method of Zafonte et al. (1977), modified as discussed by Carter et al. (1995c; 1997a). The results of these experiments were analyzed to determine the NO_2 photolysis rates for modeling as discussed by Carter et al (2000a). The NO_2 photolysis rate used for modeling these experiments was 0.178 min^{-1} for the first CTC run in the series (CTC167), and declined to 0.141 min^{-1} for the last such run in the series (CTC240).

Blacklight Light Source

The light intensity in the DTC chamber was monitored by periodic NO_2 actinometry experiments utilizing the quartz tube method of Zafonte et al (1977), with the data analysis method modified as discussed by Carter et al. (1995c). The results of these experiments were tracked over time, and there was a gradual decrease in light intensity over time during most of the operational lifetime of this chamber. The actinometry results around the time of these experiments were fit reasonably well by a straight line, which

was used to determine the NO_2 photolysis rates used for modeling. These were 0.211 min^{-1} for the first DTC run for this project (DTC315) and 0.209 min^{-1} for the last such run (DTC325).

The spectrum of the blacklight light source is periodically measured using a LiCor LI-1200 spectroradiometer, and found to be essentially the same as the general blacklight spectrum recommended by Carter et al (1995c) for use in modeling blacklight chamber experiments

Dilution

The dilution of the chambers due to sampling is expected to be small because the flexible reaction bags can collapse as samples are withdrawn for analysis. Also, the chambers were designed to operate under slightly positive pressure, so any small leaks would result in reducing the bag volume rather than diluting the contents of the chamber. Information concerning dilution in an experiment can be obtained from relative rates of decay of added VOCs that react with OH radicals with differing rate constants (Carter et al. 1993; 1995c). Most experiments had a more reactive compound such as m-xylene and n-octane present either as a reactant or added in trace amounts to monitor OH radical levels. Trace amounts (~0.1 ppm) of n-butane were also added to experiments if needed to provide a less reactive compound for monitoring dilution. In addition, specific dilution check experiments such as CO irradiations were carried out. Based on these results, the dilution rate was found to be negligible in this chamber in most experiments, generally being less than 0.3% per hour.

Reactivity Data Analysis Methods

As indicated above, most of the experiments for this program consisted of simultaneous irradiation of a "base case" reactive organic gas (ROG) surrogate - NO_x mixture in one of the dual reaction chambers, together with an irradiation, in the other reactor, of the same mixture with added. The results are analyzed to yield two measures of VOC reactivity: the effect of the added VOC on the amount of NO reacted plus the amount of ozone formed, and integrated OH radical levels. These are discussed in more detail below.

The first measure of reactivity is the effect of the VOC on the change in the quantity $[O_3]$-[NO], or $\Delta([O_3]$-[NO]). As discussed elsewhere (e.g., Johnson, 1983; Carter and Atkinson, 1987; Carter and Lurmann, 1990, 1991, Carter et al, 1993, 1995a), this gives a direct measure of the amount of conversion of NO to NO_2 by peroxy radicals formed in the photooxidation reactions, which is the process that is directly responsible for ozone formation in the atmosphere. (Johnson calls it "smog produced" or "SP".) The incremental reactivity of the VOC relative to this quantity, which is calculated for each hour of the experiment, is given by

$$IR[\Delta([O_3]-[NO])_t^{VOC}] = \frac{\Delta([O_3]-[NO])_t^{Test} - \Delta([O_3]-[NO])_t^{Base}}{[VOC]_0} \qquad (I)$$

where $\Delta([O3]\text{-}[NO])_t^{Test}$ is the $\Delta([O_3]\text{-}[NO])$ measured at time t from the experiment where the test VOC was added, $\Delta([O3]\text{-}[NO])_t^{Base}$ is the corresponding value from the corresponding base case run, and $[VOC]_0$ is the amount of test VOC added. An estimated uncertainty for IR[$\Delta([O_3]\text{-}[NO])$] is derived based on assuming an ~3% uncertainty or imprecision in the measured $\Delta([O_3]\text{-}[NO])$ values. This is consistent with the results of the side equivalency test, where equivalent base case mixtures are irradiated on each side of the chamber.

Note that reactivity relative to $\Delta([O3]\text{-}[NO])$ is essentially the same as reactivity relative to O_3 in experiments where O_3 levels are high, because under such conditions $[NO]_t^{base}$. $[NO]_t^{test}$. 0, so a change in $\Delta([O3]\text{-}[NO])$ caused by the test compound is due to the change in O_3 alone. However, $\Delta([O3]\text{-}[NO])$ reactivity has the advantage that it provides a useful measure of the effect of the VOC on processes responsible for O_3 formation even in experiments where O_3 formation is suppressed by relatively high NO levels.

The second measure of reactivity is the effect of the VOC on integrated hydroxyl (OH) radical concentrations in the experiment, which is abbreviated as "IntOH" in the subsequent discussion. This is an important factor affecting reactivity because radical levels affect how rapidly all VOCs present, including the base ROG components, react to form ozone. If a compound is present in the experiment that reacts primarily with OH radicals, then the IntOH at time t can be estimated from

$$\text{IntOH}_t = \frac{\ln([\text{tracer}]_0 / [\text{tracer}]_t) - Dt}{\text{kOH}^{\text{tracer}}} \qquad \text{(II)}$$

where $[tracer]_0$ and $[tracer]_t$ are the initial and time=t concentrations of the tracer compound, kOH^{tracer} its OH rate constant, and D is the dilution rate in the experiments. The latter was found to be small and was neglected in our analysis. The concentration of tracer at each hourly interval was determined by linear interpolation of the experimentally measured values. M-xylene was used as the OH tracer in these experiments because it is a surrogate component present in all experiments, its OH rate constant is known (the value used was 2.36×10^{-11} cm^3 $molec^{-1}$ s^{-1} [Atkinson, 1989]), and it reacts relatively rapidly.

The effect of the VOC on OH radicals can thus be measured by its IntOH incremental reactivity, which is defined as

$$\text{IR[IntOH]}_t = \frac{\text{IntOH}_t^{\text{Test}} - \text{IntOH}_t^{\text{Base}}}{[\text{VOC}]_0} \qquad \text{(III)}$$

where $IntOH^{Test}$ and $IntOH^{Base}$ are the IntOH values measured at time t in the added VOC and the base case experiment, respectively. The results are reported in units of 10^6 min. The uncertainties in IntOH and IR[IntOH] are estimated based on assuming an ~2% imprecision in the measurements of the m-xylene concentrations. This is consistent with the observed precision of results of replicate analyses of this compound.

CHEMICAL MECHANISMS

General Atmospheric Photooxidation Mechanism

The chemical mechanism used in the environmental chamber and atmospheric model simulations in this study is the "SAPRC-99" mechanism that is documented in detail by Carter (2000). This mechanism represents a complete update of the SAPRC-90 mechanism of Carter (1990) and the SAPRC-97 mechanism of Carter et al (1997a), and incorporates recent reactivity data from a wide variety of VOCs, including those discussed in this report. This includes assignments for ~400 types of VOCs, and can be used to estimate reactivities for ~550 VOC categories. A condensed version, developed for use in regional models, is used to represent base case emissions in the atmospheric reactivity simulations discussed in this report. A unique feature of this mechanism is the use of a computerized system to estimate and generate complete reaction schemes for most non-aromatic hydrocarbons and oxygenates in the presence of NO_x, from which condensed mechanisms for the model can be derived. This includes the mechanisms for the higher alkanes discussed in this report and the mechanisms used for their major reactive oxygenated products. The SAPRC-99 mechanism was evaluated against the results of almost 1700 environmental chamber experiments carried out at the University of California at Riverside, including experiments to test ozone reactivity predictions for over 80 types of VOCs. This includes experiments and VOCs discussed in this report.

A listing of the mechanism as used in the model simulations in this report is given in Appendix A. This consists of the "base mechanism" representing the reactions of the inorganics and common organic products, the reactions of the specific VOCs used in the environmental chamber experiments (including the three test compounds whose mechanisms are discussed in the following sections), and the reactions of the lumped model species used when representing base case VOCs in the ambient reactivity simulations. The mechanisms used for the higher molecular alkanes are discussed in more detail below. The report of Carter (2000) can be consulted for a more detailed discussion of the other portions of the mechanism.

Atmospheric Reactions of $C_{\geq 12}$ Alkanes

Available laboratory information concerning the gas-phase atmospheric reactions of the alkanes has been reviewed by Atkinson (1997), and the most recent relevant information is discussed by Carter (2000). The only significant gas-phase atmospheric reaction of alkanes is the reaction with OH radicals. Alkanes do not absorb light in the wavelength region provided by ground-level sunlight ($\lambda \geq 300$ nm) (Calvert and Pitts, 1966), and rate constants for their reactions with other reactive atmospheric species (e.g., O_3, NO_3 radicals, $O(^3P)$ atoms) are too low for them to be of significance (Atkinson 1997, and references therein). Therefore, we will consider only reactions of alkanes with OH radicals.

Data are available for the OH radical rate constants for all the n-alkanes through n-$C_{16,}$ for various branched alkane isomers up to ~C_{10}, and for various cyclic alkane up to C_{12}. The OH radical rate constants and temperature dependence expressions that are used in the SAPRC-99 mechanism (Carter, 2000) for the higher molecular weight ($C_{\geq 7}$) alkanes for which data are available are summarized on Table 1. Most of the rate constant expressions on Table 1 are those recommended in the review by Atkinson (1997), but a few more recently measured rate constants are also given. Based on the available kinetic data, Atkinson (1987) developed a structure-estimation method that can be used to estimate OH radical rate constants for alkanes and other types of compounds. The performance of this method, as updated by Kwok and Atkinson (1995), in predicting is shown on Table 1, where it can be seen that the rate constants for most compounds are predicted to within ±25%. Thus, the method of Kwok and Atkinson (1995) serves as a good basis for estimating OH radical rate constants for $C_{\geq 12}$ alkanes whose rate constants have not been measured. The one exception is 3,4-diethyl hexane, where steric effects may be slowing down the rate of reaction at the two tertiary hydrogens in the molecule.

The reaction of OH with alkanes occurs by the abstraction of an H atom from one of the various positions on the molecule, forming H_2O and the corresponding alkyl radical. The alkyl radical can then add O_2 to form the corresponding peroxy radical that, in the presence of NO_x, will primarily react with NO to form NO_2 and the corresponding alkoxy radical or the corresponding alkyl nitrate. These are shown below in the case of the radical formed from reaction of OH at the 3-position of n-octane.

$$CH_3CH_2CH_2CH_2CH_2CH_2CH_2CH_3 + OH \rightarrow H_2O + CH_3CH_2CH_2CH_2CH_2CH(\cdot)CH_2CH_3 \quad (1)$$

$$CH_3CH_2CH_2CH_2CH_2CH(\cdot)CH_2CH_3 + O_2 \rightarrow CH_3CH_2CH_2CH_2CH_2CH(OO\cdot)CH_2CH_3 \quad (2)$$

$$CH_3CH_2CH_2CH_2CH_2CH(OO\cdot)CH_2CH_3 + NO \rightarrow CH_3CH_2CH(ONO_2)CH_2CH_2CH_2CH_2CH_3 \quad (3)$$

$$CH_3CH_2CH_2CH_2CH_2CH(OO\cdot)CH_2CH_3 + NO \rightarrow NO_2 + CH_3CH_2CH_2CH_2CH_2CH(O\cdot)CH_2CH_3 \quad (4)$$

The higher molecular weight alkoxy radical can react either with O_2, by decomposition, or by 1,4-H shift isomerization via a 6-member ring transition state, e.g.,

$$CH_3CH_2CH_2CH_2CH_2CH(O\cdot)CH_2CH_3 + O_2 \rightarrow CH_3CH_2CH_2CH_2CH_2C(O)CH_2CH_3 + HO_2 \quad (5)$$

$$CH_3CH_2CH_2CH_2CH_2CH(O\cdot)CH_2CH_3 \rightarrow CH_3CH_2CH_2CH_2CH_2CHO + CH_3CH_2\cdot \quad (6)$$

$$CH_3CH_2CH_2CH_2CH_2CH(O\cdot)CH_2CH_3 \rightarrow CH_3CH_2CH(OH)CH_2CH_2CH(\cdot)CH_2CH_3 \quad (7)$$

Based on available information concerning the reactions of alkoxy radicals formed in alkane photooxidation systems, the 1,4-H shift isomerization reaction (e.g., Reaction 7) is expected to be the major process for those long chain alkoxy radicals where it can occur (Atkinson, 1997; Carter, 2000). The subsequent reactions of the bifunctional radical formed in Reaction (7) are expected to be:

$$CH_3CH_2CH(OH)CH_2CH_2CH(\cdot)CH_2CH_3 + O_2 \rightarrow CH_3CH_2CH(OH)CH_2CH_2CH(OO\cdot)CH_2CH_3 \quad (8)$$

$$CH_3CH_2CH(OH)CH_2CH_2CH(OO\cdot)CH_2CH_3 + NO \rightarrow CH_3CH_2CH(OH)CH_2CH_2CH(ONO_2)CH_2CH_3 \quad (9)$$

$$CH_3CH_2CH(OH)CH_2CH_2CH(OO\cdot)CH_2CH_3 + NO \rightarrow NO_2 + CH_3CH_2CH(OH)CH_2CH_2CH(O\cdot)CH_2CH_3 \quad (10)$$

Table 1. Experimental and estimated rate constants for the reactions of OH radicals with $C_{\geq 7}$ alkanes, as used in the SAPRC-99 mechanism (Carter, 2000). Experimental data are from the evaluation of Atkinson (1997) unless indicated otherwise.

Compound	Model Name	k(300) (cm^3 $molec^{-1}$ s^{-1})	A [a]	B	Ea kcal/mole	Refs [b]	Est'd k(300) k	(diff)
n-Heptane	N-C7	7.04e-12	1.43e-12	2.0	-0.950		6.91e-12	-2%
n-Octane	N-C8	8.76e-12	2.48e-12	2.0	-0.751		8.33e-12	-5%
n-Nonane	N-C9	1.00e-11	2.26e-12	2.0	-0.888		9.75e-12	-3%
n-Decane	N-C10	1.13e-11	2.82e-12	2.0	-0.827		1.12e-11	-1%
n-Undecane	N-C11	1.29e-11					1.26e-11	-2%
n-Dodecane	N-C12	1.39e-11					1.40e-11	1%
n-Tridecane	N-C13	1.60e-11					1.54e-11	-4%
n-Tetradecane	N-C14	1.80e-11					1.69e-11	-6%
n-Pentadecane	N-C15	2.10e-11					1.83e-11	-13%
n-Hexadecane	N-C16	2.30e-11					1.97e-11	-14%
2,2,3-Trimethyl Butane	223TM-C4	4.25e-12	7.61e-13	2.0	-1.025		3.24e-12	-24%
2,2-Dimethyl Pentane	22-DM-C5	3.40e-12					3.26e-12	-4%
2,4-Dimethyl Pentane	24-DM-C5	5.00e-12					6.87e-12	37%
2,2,3,3-Tetrame. Butane	2233M-C4	1.06e-12	1.72e-12	2.0	0.286		1.02e-12	-4%
2,2,4-Trimethyl Pentane	224TM-C5	3.60e-12	1.87e-12	2.0	-0.389		4.66e-12	30%
2,2-Dimethyl Hexane	22-DM-C6	4.80e-12					4.68e-12	-2%
2,3,4-Trimethyl Pentane	234TM-C5	7.10e-12					8.55e-12	20%
2,3,5-Trimethyl Hexane	235TM-C6	7.90e-12					9.97e-12	26%
2-Methyl Octane	2-ME-C8	1.01e-11					9.73e-12	-4%
3,3-Diethyl Pentane	33-DE-C5	4.90e-12					5.31e-12	8%
4-Methyl Octane	4-ME-C8	9.70e-12					1.00e-11	3%
2,6-Dimethyl Octane	26DM-C8	1.29e-11				1	1.14e-11	-12%
2-Methyl Nonane	2-ME-C9	1.28e-11				1	1.12e-11	-12%
3,4-Diethyl Hexane	34-DE-C6	7.40e-12				2	1.25e-11	69%
Cycloheptane	CYCC7	1.30e-11					9.94e-12	-24%
Methyl cyclohexane	ME-CYCC6	1.00e-11					1.02e-11	2%
Cyclooctane	CYCC8	1.40e-11					1.14e-11	-19%
1,1,3-Trimethyl Cyclohexane	113MCYC6	8.70e-12					9.12e-12	5%
Hexyl Cyclohexane	C6-CYCC6	1.78e-11				3	1.77e-11	-1%

[a] Temperature dependence given by $k(T) = A\ (T/300)^B\ e^{-Ea/RT}$, where T is the temperature in ^oK, and R is the gas constant. If no data are given for A, B and Ea, then temperature dependence data are not available.

[b] If no footnote number is given, then the rate constant is recommended by Atkinson (1997). Following are references for rate constants measured subsequently.

1. Carter et al (2000b)
2. Atkinson et al. (2000)
3. This work.

$$CH_3CH_2CH(OH)CH_2CH_2CH(O\cdot)CH_2CH_3 \rightarrow CH_3CH_2CH(OH)CH_2CH_2C(\cdot)(OH)CH_2CH_3 \quad (11)$$

$$CH_3CH_2CH(OH)CH_2CH_2C(\cdot)(OH)CH_2CH_3 + O_2 \rightarrow CH_3CH_2CH(OH)CH_2CH_2C(O)CH_2CH_3 + HO_2\cdot \quad (12)$$

Thus the major products formed after the reaction of OH at the 3-position of n-octane are expected to be 6-hydroxy-3-octanone and HO_2 with two NO to NO_2 conversions, 3-octyl nitrate with the consumption of 1 NO, and 6-hydroxy-2-octyl nitrate with one NO to NO_2 conversion and consumption of an additional NO. Analogous mechanisms and products are expected from the other higher n-alkanes. The predicted formation of these δ-hydroxy carbonyl products from higher molecular weight has been confirmed by recent experimental product data (Eberhard et al, 1995; Kwok et al, 1996; Arey et al, 2000).

Analogous reactions can occur in the case of the higher molecular weight branched and cyclic alkanes if they have sufficiently long chains that the 1,4-H shift can occur. Decompositions to form lower molecular weight oxygenated products and radicals that cause additional NO to NO_2 conversions become relatively more important in the case of the branched alkanes because (1) decompositions forming tertiary radicals or ketones are more favorable than those forming primary radicals or aldehydes (Carter, 2000), and (2) branched alkanes tend to have shorter chains, and the possibility of forming radicals that cannot under go 1,4-H shifts increases. It is also likely that 1,4-H shift isomerizations become relatively less important in the case of the cycloalkanes because the bicyclic transition states required may have greater strain. For example, in the case of cyclohexane, the initially formed alkoxy radical is estimated to react with O_2 about 70% of the time to form cyclohexanone (Reaction 17), with the remaining 30% reacting by decomposition with ring opening (Reaction 18), to ultimately give rise to polyfunctional products with additional NO to NO_2 conversion and nitrate formation, e.g.,

$$-CH_2CH_2CH_2CH_2CH_2CH_2- + OH \rightarrow -CH_2CH_2CH_2CH_2CH_2CH(\cdot)- \quad (13)$$

$$-CH_2CH_2CH_2CH_2CH_2CH(\cdot)- + O_2 \rightarrow -CH_2CH_2CH_2CH_2CH_2CH(OO\cdot)- \quad (14)$$

$$-CH_2CH_2CH_2CH_2CH_2CH(OO\cdot)- + NO \rightarrow -CH_2CH_2CH_2CH_2CH_2CH(ONO_2)- \quad (15)$$

$$-CH_2CH_2CH_2CH_2CH_2CH(OO\cdot)- + NO \rightarrow NO_2 + -CH_2CH_2CH_2CH_2CH_2CH(O\cdot)- \quad (16)$$

$$-CH_2CH_2CH_2CH_2CH_2CH(O\cdot)- + O_2 \dashrightarrow -CH_2CH_2CH_2CH_2CH_2C(O)- + HO_2 \quad (17)$$

$$-CH_2CH_2CH_2CH_2CH_2CH(O\cdot)- \rightarrow HCOCH_2CH_2CH_2CH_2CH_2\cdot \quad (18)$$

$$HCOCH_2CH_2CH_2CH_2CH_2\cdot + O_2 \rightarrow HCOCH_2CH_2CH_2CH_2CH_2OO\cdot \quad (19)$$

$$HCOCH_2CH_2CH_2CH_2CH_2OO\cdot + NO \rightarrow HCOCH_2CH_2CH_2CH_2CH_2ONO_2 \quad (20)$$

$$HCOCH_2CH_2CH_2CH_2CH_2OO\cdot + NO \rightarrow NO_2 + HCOCH_2CH_2CH_2CH_2CH_2O\cdot \quad (21)$$

$$HCOCH_2CH_2CH_2CH_2CH_2O\cdot \rightarrow HCOCH_2CH(\cdot)CH_2CH_2CH_2OH \quad (22)$$

$$HCOCH_2CH(\cdot)CH_2CH_2CH_2OH + O_2 \rightarrow HCOCH_2CH(OO\cdot)CH_2CH_2CH_2OH \quad (23)$$

$$HCOCH_2CH(OO\cdot)CH_2CH_2CH_2OH + NO \rightarrow HCOCH_2CH(ONO_2)CH_2CH_2CH_2OH \quad (24)$$

$$HCOCH_2CH(OO\cdot)CH_2CH_2CH_2OH + NO \rightarrow NO_2 + HCOCH_2CH(O\cdot)CH_2CH_2CH_2OH \quad (25)$$

$$HCOCH_2CH(O\cdot)CH_2CH_2CH_2OH \rightarrow HCOCH_2CH(OH)CH_2CH_2CH(\cdot)OH \quad (26)$$

$$HCOCH_2CH(OH)CH_2CH_2CH(\cdot)OH + O_2 \rightarrow HCOCH_2CH(OH)CH_2CH_2CHO + HO_2\cdot \quad (27)$$

As discussed by Atkinson (1997) and Carter (2000), except for nitrate yields in the reaction of NO with the initially formed peroxy radicals (discussed below) and qualitative information on bifunctional product formation, there is almost no experimental information on the branching ratios or product yields involved in these reactions. Therefore, the rate constant ratios involved have to be estimated in order to derive overall reaction mechanisms for these alkanes. Estimation methods exist for all the reactions involved (e.g., Carter and Atkinson, 1985; Atkinson, 1987; Carter, 2000) and serve as a basis for generating comprehensive detailed mechanisms for the atmospheric reactions of alkanes in the presence of NO_x (Carter, 1990, 2000). The most recent version is incorporated into the SAPRC-99 mechanism generation system that is documented by Carter (2000) and that was used to derive the higher alkane photooxidation mechanisms used in this study.

The major aspects of the mechanisms that affect the overall ozone impacts of these higher alkanes are the overall nitrate yields from the reactions of NO with the higher molecular weight peroxy radicals, and the numbers of NO to NO_2 conversions involved in product formation. The latter are determined by branching ratios involved in the alkoxy radical reactions that determine whether additional radicals are formed that result in multi-step mechanisms. The number of NO to NO_2 conversions is probably not a major uncertainty in the case of the normal alkanes because isomerizations are expected to dominate in almost all cases, but this may be a greater uncertainty in mechanisms for branched and cyclic alkanes where competing decompositions or reactions with O_2 may become relatively more important. Uncertainties in the predictions of product formation are probably not as important a factor affecting reactivity predictions of the alkanes. This is because the most likely mechanisms generally predict similar types of higher molecular weight bi- or polyfunctional oxygenates, and model calculations (at least for single day scenarios) tend to be relatively insensitive to assumptions about these product's mechanisms.

Probably the most important factor affecting predicted reactivities of the higher molecular concerns nitrate formation from the reactions of NO with the higher molecular weight peroxy radicals (e.g., Reactions 3, 19, 15, 20 and 24, above). This reaction, which becomes increasingly important as the size of the molecule increases (Carter and Atkinson, 1989a; Atkinson, 1997), represents both a radical and NO_x sink. If sufficiently important these reactions can cause significant reductions in overall ozone formation potentials of the reacting VOCs, and even ozone inhibition. This is the major reason why high molecular weight alkanes tend to have very low ozone formation potentials, despite their relatively high OH radical rate constants and relatively large number of estimated NO to NO_2 conversions (Carter and Atkinson, 1989b; Carter, 1994a, 2000). Information concerning the relative rates of this reaction compared to the competing formation of the alkoxy radical and NO_2 comes from primarily from measurements of yields of the various secondary alkyl nitrates formed from the radicals formed initial the initial reactions of the n-alkanes and cyclohexane, and from a very limited number of measurements of primary or tertiary alkyl nitrate yields from branched alkanes (Carter and Atkinson, 1989b; Atkinson, 1997). Yields of substituted nitrates formed from the hydroxy-substituted radicals formed after 1,5-H shift isomerizations (e.g., the rate constant ratio for Reactions 9 vs. 10, 20 vs. 21 and 24 vs. 25, above) are unknown and have to be estimated.

Updates to the Alkane Photooxidation Mechanisms

The nitrate yields used when deriving mechanisms for the higher alkanes in the SAPRC-90 (Carter, 2000) through SAPRC-97 (Carter et. al, 1997a) mechanisms are based on the data and recommendations given by Carter and Atkinson (1989a). These are shown on Figure 1 for the secondary peroxy radicals formed from the normal alkanes. Based on these data, nitrate yields of over 30% were calculated for the radicals initially formed in the oxidation of n-octane. increasing to yields of 40-45% for the initially formed radicals from the $C_{\geq 12}$ n-alkanes. However, the extrapolation above C_8 was uncertain and was determined primarily by the nature of the curve fit parameterization used.

Mechanisms using the nitrate yield data and estimates of Carter and Atkinson (1997a) gave a good fit to the environmental chamber reactivity data for n-octane (Carter et al, 1993, 1995b, 1997a; Carter, 1995), and reasonably good fits to the data for the C_{12} - C_{16} n-alkanes obtained in our Phase 1 study for this project (Carter et al, 1996). However, to obtain these fits it had to be assumed that nitrate formation from the reaction of NO from the hydroxy substituted peroxy radicals formed after the 1,4-H shift isomerization was negligible (e.g., in Reaction 8, above). Otherwise, the predicted total nitrate yields in the overall reaction are increased by a factor of 1.5 or more, and the model predicts much greater inhibitions of radical levels and NO oxidation rates than were consistent with the environmental chamber data. This was a concern because it is not chemically reasonable for the addition of one OH on peroxy

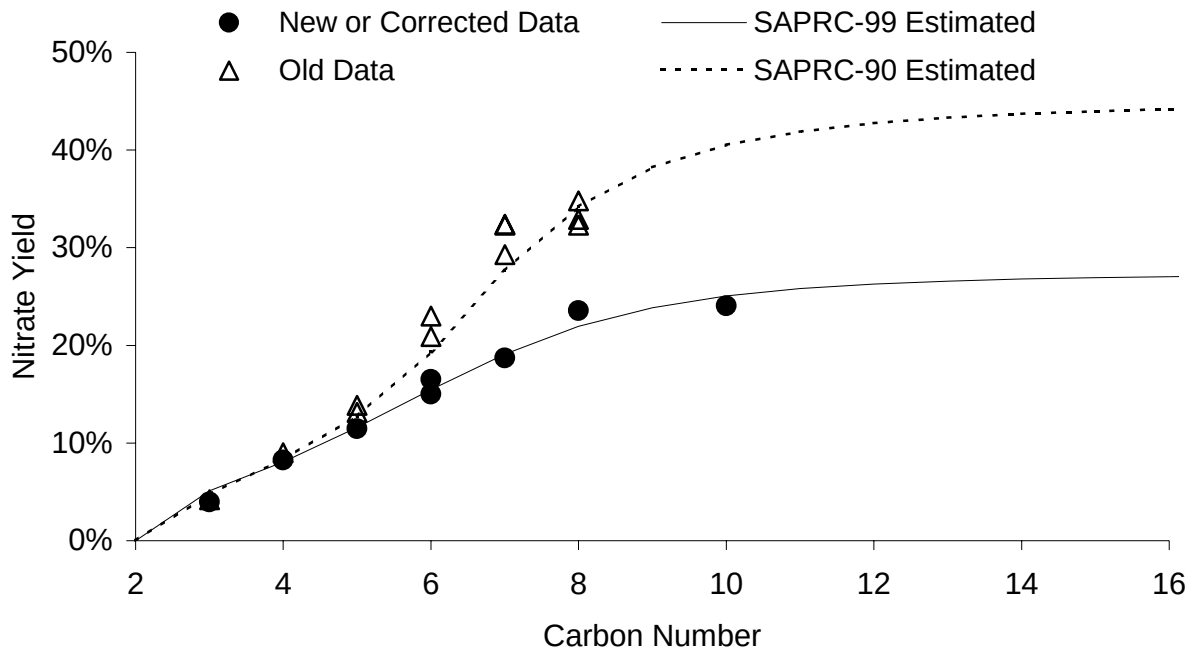

Figure 1. Plots of experimental nitrate yields for reactions of NO with the initially formed secondary peroxy radicals formed from the normal alkanes, and the estimates incorporated in the SAPRC-90 and SAPRC-99 mechanisms derived from these data.

radicals four carbons away from the peroxy center with 8 or more carbons to reduce the nitrate yields from 30% or more to negligible levels. However, there did no appear to be any other way to reconcile the existing nitrate yield and environmental chamber data into a consistent mechanism for n-alkanes. This assumption was therefore incorporated in the n-alkane mechanism used in our report on the atmospheric ozone impacts of the $C_{\geq 12}$ n-alkanes that was prepared previously (Carter et al, 1996).

The apparent inconsistency between environmental chamber and nitrate yield data was not the only problem associated with the previous mechanisms for the atmospheric reactions of the higher alkanes. Because the limited data indicated lower alkyl nitrate yields from the reactions of NO with primary and tertiary peroxy radicals, the SAPRC-97 and earlier mechanisms predicted that $C_{\geq 8}$ branched and cyclic alkanes tended to have considerably higher ozone reactivities than the normal alkanes with the same carbon numbers. There was limited data available to test this until environmental chamber experiments were carried out using various mineral spirits mixtures, which consist primarily of complex mixtures of $C_{\geq 10}$ alkanes, of which over 75% were branched or cyclic (Carter et al, 1997b). The ozone impacts of these mixtures in the environmental chamber reactivity experiments were very similar to those of n-alkanes in the same carbon number range, and were significantly less than predicted by mechanisms based on their branched and cyclic alkane contents (Carter et al, 1997b). This suggested that the nitrate yields in the reactions of OH radicals with these higher branched and cyclic alkanes may be closer to those for n-alkanes than was being assumed in the mechanism.

Most of the data concerning the effects of nitrate yields on carbon number come from the measurements of Atkinson et al (1982, 1984), and the temperature and pressure effects data come from Atkinson et al (1983b). More recently, using improved chromatographic methods, Arey et al (2000) remeasured the nitrate yields from the C_3-C_8 n-alkanes. They obtained significantly lower nitrate yields for the $C_{\geq 5}$ radicals. In addition, Atkinson and co-workers (unpublished results, 1999) also obtained lower nitrate yields from n-decane than estimated using the parameterization of Carter and Atkinson (1989a). These new data [and old data of Atkinson et al (1982, 1984) corrected the revised calibration factors as indicated by the results of Arey et al (2000)] are shown on Figure 1, where they can be compared with the previous data and estimates. The revised estimates of these secondary nitrate yields as a function of carbon number, derived by Carter (2000) based on reoptimizing the parameters of Carter and Atkinson (1989a) to fit the new data, are also shown on the figure. It can be seen that the predicted nitrate yields for the $C_{\geq 12}$ peroxy radicals are about 40% lower than predicted by the parameterization derived from the older data. In addition, the new data on the nitrate yield for n-decane tended to support the predictions that the rate of increase of the nitrate yields with the size of the molecule will fall off with carbon numbers above 8.

As a result of these reduced nitrate yields from the initially formed peroxy radicals, it is now possible for mechanisms to successfully simulate the environmental chamber data without having to make chemically unreasonable assumptions about no nitrate formation from the reactions of NO with OH-substituted peroxy radicals. Only a slight reduction caused by OH substitution is assumed, based on assumed overall nitrate yields that give best fits to the chamber data for a variety of OH-substituted

organic compounds (Carter, 2000). Thus it is now possible for model predictions to simulate reactivity data for n-alkanes using a mechanism that is chemically reasonable and consistent with nitrate yield estimates used for other compounds. Thus, the SAPRC-99 mechanism estimation methods incorporate nitrate yield estimates based on these new data (Carter, 2000).

This revision in the nitrate yield estimates for secondary peroxy radicals did not totally resolve the problems indicated by the model simulations of the experiments with the mineral spirits mixtures with the branched and cyclic $C_{\geq 10}$ alkanes. As indicated above, the results of these experiments indicated that the $C_{\geq 10}$ branched and cyclic alkanes are much closer in reactivity to the normal alkanes than previously estimated. Two approaches were used to when deriving the revised nitrate yield estimation methods for the SAPRC-99 mechanism to reduce the differences between the model predictions of reactivities of branched and cyclic alkanes vs. normal alkanes. These are as follows:

Revised Nitrate Yield Corrections for Primary and Tertiary Radicals. The limited product data indicated that nitrate yields from primary and tertiary peroxy radicals are lower than those from the secondary peroxy radicals. In the previous mechanism, estimates for nitrate yields for these radicals were made by applying a correction factor of 0.4 for primary radicals and 0.3 for tertiary radicals, regardless of the size of the radical. Instead of using this approach, in the SAPRC-99 mechanism, the estimates for these radicals are made by reducing the effective carbon number by 1.5 when calculating the nitrate yields using the parameterization derived to fit the data for the secondary radicals (Carter, 2000). This gives about the same predicted nitrate yields for the lower molecular weight primary and tertiary radicals for which there are data (Carter and Atkinson, 1989a), but predicts that the differences between the secondary and primary or tertiary radicals decrease with size of the molecule. This is because of the leveling off of the rate of increase in the nitrate yield as the size of the molecule increases, as shown on Figure 1.

Revised Representation of Unspeciated Branched and Cyclic Alkanes in Complex Hydrocarbon Mixtures. Most of the branched and cyclic alkane constituents of mineral spirits and similar higher molecular weight petroleum-derived substances consist of highly complex mixtures of many isomers whose exact structures are unknown. In order to model the reactivities of such substances, a few representative compounds are chosen to be representative of all the branched or all the cyclic alkanes of with the same molecular weights. In the previous mechanism the compounds chosen as representative were relatively highly branched and only a single compound was used. However, GC-MS analyses of mineral spirits samples indicated that less branched compounds, whose mechanisms would be closer to those of normal alkanes, tend to be relatively more important (O'Donnell, Safety-Kleen Corp., private communication, 1997). For the updated mechanism, the unspeciated branched and cyclic alkanes on complex mixtures are represented using three compounds for each carbon number rather than a single one, and the compounds used are generally less highly branched (Carter, 2000). For example, the branched C_{12} alkanes, which previously were represented by 3,6-diethyl octane, are now represented by 50% 3,6-dimethyl decane, 25% 5-methyl undecane and 25% 3-methyl undecane. The cyclic C_{12} alkanes, which were previously represented by 1,3,5-diethylcyclohexane are now represented by 35% hexyl cyclohexane and 33% each 1,3,5 diethyl cyclohexane and 1-methyl 4-pentyl cyclohexane. This should

tend to reduce differences in reactivities between normal alkanes and branched and cyclic alkanes with the same carbon number.

Representation of C_{12} - C_{16} Normal and Cyclic Alkanes in the SAPRC-99 Mechanism

The detailed mechanisms for the atmospheric reactions of the higher alkanes in the presence of NO_x were derived using the SAPRC-99 mechanism generation and estimation system based on the considerations discussed in the previous sections. These then were used to derive the condensed representation of these products in terms of SAPRC-99 model species, as shown in Table A-2 in Appendix A for the specific branched and cyclic compounds that were represented in the model simulations in this report. The OH radical rate constants used for the normal alkanes were the experimental values as shown on Table 1, above. For hexyl cyclohexane the rate constant used was that derived in this study as shown on Table 1. For octyl cyclohexane it was judged that experimental measurement was sufficiently uncertain that the estimate derived using the structure-reactivity methods of Kwok and Atkinson is more likely to be reliable, so the estimated rate constant was used. These data for the alkyl cyclohexanes are discussed n the Results section, below.

Table 2 gives a summary of the yields of the SAPRC-99 product or radical operator model species that were derived for the $C_{\geq 12}$ normal and branched alkanes that were studied in this project. Here, RO2-R. represents the formation of peroxy radicals that ultimately react to convert NO to NO_2 and form HO_2, RO2-N. represents the formation of peroxy radicals that ultimately react with NO to form alkyl nitrates, R2O2. represents extra NO to NO_2 conversions formed by peroxy radicals formed in multi-step mechanisms, RCHO represents higher aldehyde products, and PROD2 represents reactive ketones and non-aldehyde bifunctional products that are predicted to be formed.

Table 2. Summary of radical operator and product yields used when representing the $C_{\geq 12}$ normal and branched alkanes in the SAPRC-99 mechanism

Compound	Radical Operator or Product Yields				
	RO2-R.	RO2-N.	R2O2.	RCHO	PROD2 [b]
n-Dodecane	0.54	0.46	0.77	0.01	0.53
n-Tetradecane	0.53	0.47	0.76	0.01	0.52
n-Pentadecane	0.53	0.47	0.76	0.01	0.52
n-Hexadecane	0.52	0.48	0.76	0.01	0.52
Hexyl Cyclohexane	0.53	0.47	0.85	0.09	0.46
Octyl Cyclohexane	0.51	0.49	0.85	0.06	0.46

[a] Represented by separate model species with parameters derived based on the set of products they represent, as discussed in the text.

Note that C_{12} - C_{16} normal alkanes have very similar representations in the SAPRC-99 mechanism, with the only difference being that the overall nitrate yields slowly increase with the size of the molecule. The alkyl cyclohexanes are predicted have very similar overall nitrate yields to the normal alkanes in the same molecular weight, but somewhat more NO to NO_2 conversions caused by peroxy radicals formed in multi-step mechanisms. The slightly higher overall nitrate yields from the alkyl cyclohexanes may seem surprising in that their reactions are predicted to involve formation of tertiary peroxy radicals that are estimated to have lower nitrate yields. However, this is countered by the fact that their overall reactions involve tend to involve more steps, and therefore more peroxy radical formation, than the reactions of the corresponding n-alkanes (compare Reactions 1 - 12, above, with Reactions 12 - 27). This is the reason that the cycloalkanes have more NO to NO_2 conversions in the overall mechanisms, as indicated by the higher R2O2. yields.

As indicated on Table 2, these normal alkanes and alkyl cyclohexanes are predicted to form significant yields of bifunctional ketone products that are normally represented by the PROD2 model species. However, for more accurate representation of the contributions of these products for use when calculating the reactivities of the individual compounds, they can also be represented using compound-product model species whose rate constants and parameters are adjusted based on the specific mixture of products they represent. As discussed by Carter (2000), the SAPRC-99 mechanism generation system is used to derive estimated mechanisms for these product species, and these are then used to derive he parameters in the lumped product-specific species used to represent them. This approach was employed when representing these normal and cyclic $C_{\geq 12}$ alkanes in the model simulations of the chamber experiments and atmospheric reactivity calculations used in this work.

Table 3 shows the mixture of the higher ketone products that are predicted to be formed in the photooxidations of n-dodecane and hexyl cyclohexane. These serve as the basis for deriving the mechanisms shown for the lumped "PRD" model species for these compounds shown, which are shown on Table A-2 in Appendix A. Note that for n-dodecane the products are all just the various δ-hydroxy ketones resulting from reaction at the different positions in the molecule, while a somewhat more varied mixture is predicted to be formed from hexyl cyclohexane. The product mixtures for the higher molecular weight normal and cycloalkanes discussed in this work are similar.

Table 3. Mixtures of higher ketone products predicted to be formed in the reactions of n-dodecane and hexyl cyclohexane with OH radicals in the presence of NO_x.

Relative Yields	Products
	Products from n-Dodecane (Total yield = 53%)
19%	$CH_3CH_2CH_2CH_2CH_2CH_2CH(OH)CH_2CH_2C(O)CH_2CH_3$
19%	$CH_3CH_2CH_2CH_2CH_2CH(OH)CH_2CH_2C(O)CH_2CH_2CH_3$
15%	$CH_3CH_2CH_2CH_2CH_2CH_2CH_2CH(OH)CH_2CH_2C(O)CH_3$
11%	$CH_3CH_2CH_2CH_2CH(OH)CH_2CH_2C(O)CH_2CH_2CH_2CH_3$
10%	$CH_3CH_2CH_2CH(OH)CH_2CH_2C(O)CH_2CH_2CH_2CH_2CH_3$
10%	$CH_3CH_2CH(OH)CH_2CH_2C(O)CH_2CH_2CH_2CH_2CH_2CH_3$
9%	$CH_3CH(OH)CH_2CH_2C(O)CH_2CH_2CH_2CH_2CH_2CH_2CH_3$
	Products from Hexyl Cyclohexane (Total yield = 46%)
14%	$–CH_2CH_2CH_2CH_2CH_2C[CH_2CH_2C(O)CH_2CH_2CH_2OH](OH)–$
13%	$–CH_2CH_2CH_2C(O)CH_2CH[CH_2CH_2CH_2CH_2CH_2CH_3]–$
13%	$– CH_2CH_2CH_2CH_2C(O)CH[CH_2CH(OH)CH_2CH_2CH_2CH_3]–$
13%	$–CH_2CH_2CH_2CH_2CH_2C[CH_2CH_2C(O)CH_2CH_2CH_3](OH)–$
9%	$–CH_2CH_2CH_2CH_2CH_2CH[CH(OH)CH_2CH_2C(O)CH_2CH_3]–$
9%	$–CH_2CH_2C(O)CH_2CH_2CH[CH_2CH_2CH_2CH_2CH_2CH_3]–$
7%	$–CH_2CH_2CH_2CH_2CH_2CH[COCH_2CH_2CH(OH)CH_2CH_3]–$
7%	$–CH(OH)CH_2CH_2CH_2CH_2CH[CH_2C(O)CH_2CH_2CH_2CH_3]–$
6%	$–CH_2CH_2CH_2CH_2CH_2CH[CH_2CH(OH)CH_2CH_2C(O)CH_3]–$

EXPERIMENTAL RESULTS

Relative Rate Constant Measurements

The rate constants for the reactions of OH radicals with hexyl cyclohexane and octyl cyclohexane and (for control purposes) n-dodecane and n-tetradecane were measured using a relative rate method, with m-xylene used as the reference compound. The relative rate method employed has been used extensively in other laboratories for many years [see references cited by Atkinson (1989), e.g., Atkinson et al, 1981)], and involves measurements of the consumption of the various compounds in the presence of OH radicals. In this work, the OH radicals were generated either by the photolysis of methyl nitrite

$$CH_3ONO + h\nu \rightarrow CH_3O\cdot + NO$$
$$CH_3O\cdot + O_2 \rightarrow HO_2 + HCHO$$
$$HO_2 + NO \rightarrow OH + NO_2$$

(overall: $CH_3ONO + h\nu + O_2 \rightarrow HCHO + NO_2 + OH$)

Excess NO is added to avoid the formation of O_3 and NO_3 radicals.

Assuming that the organics react only with OH radicals, the kinetic differential equations for the organics can be solved and rearranged to yield

$$\ln(\frac{[Organic]_{t0}}{[Organic]_t}) - D_t = \frac{k_{Organic}}{k_{Reference}} \ln\left[(\frac{[Reference]_{t0}}{[Reference]_t}) - D_t \right] \qquad (IV)$$

where $[Organic]_{t0}$ and $[Organic]_t$, $[Reference]_{t0}$, and $[Reference]_t$ are the initial and time=t concentrations of the test and reference compounds, respectively, $k_{Organic}$ and $k_{Reference}$ are the test and reference compound's OH rate constant, and D_t is a factor added to account for dilution due to reactant injections, leaks, etc, from the beginning of the experiment up to time t. Since no reactant injections were made during the experiments and the leaks in this chamber are believed to be negligible during the time period of the experiments, D_t is assumed to be negligible in our analysis. Therefore plots of $\ln([Organic]_{t0}/[Organic]_t)$ against $\ln([Reference]_{t0}/[Reference]_t)$ should yield a straight line with intercept of approximately zero and a slope that is the ratio of rate constants. Given the known value of $k_{Reference}$, then $k_{Organic}$ can then be derived. In principle all of the compounds could be present in the same experiment but because of GC interferences and other factors generally only 2-4 test compounds are present in any given experiment.

To verify the method as employed in this study, relative rate constants were also determined for n-dodecane and n-tetradecane. These were used because their rate constants have already been measured, their physical characteristics and volatilities are similar to the test compounds of interest, and the same analytical methods are employed. Thus if there are analytical or wall loss problems associated with

conducting the experiments with the test compounds, they should also show up and yield incorrect results for these control compounds as well.

Two kinetic experiments were carried out for this project, and their conditions and detailed measurement data are given on Table 4. Plots of Equation (IV) are shown on Figure 2 for each of the four test compounds. Note that the initial reactant concentrations used when deriving these plots were determined using a least squares optimization method to minimize least squares errors in fits of the data to Equation (IV), with the initial reactant concentrations as well as the ratios of rate constants being simultaneously optimized during this process. This procedure minimizes biases introduced by experimental uncertainties in the initial reactant measurements, and allows all of the measurements to be weighted equally when determining rate constant ratios according to Equation (IV). The results are summarized on Table 5.

Table 4. Measurement data for the kinetic experiments carried out for this program.

	m-Xylene	n-C12	n-C14	Hexyl Cyclohexane	Octyl Cyclohexane
			Run 1 (~3200 liter reactor)		
Init.	0.227	0.208		0.258	0.185 [a]
Init.	0.219	0.200	0.163 [a]	0.250	0.204 [a]
Init.	0.225	0.205	0.164 [a]	0.258	0.217 [a]
Init.	0.224	0.206	0.169 [a]	0.259	
	0.084	0.114		0.135	
	0.083	0.105	0.108	0.119	0.149
	0.084	0.105	0.102	0.116	0.141
	0.080	0.102	0.088	0.118	0.117
	0.060	0.084	0.069	0.091	0.094
	0.063	0.085	0.068	0.093	0.086
	0.064	0.080	0.063	0.090	0.081
	0.039	0.074	0.062	0.079	0.076
	0.055	0.077	0.058	0.081	0.072
			Run 2 (DTC Side A)		
Init.	0.121	0.136	0.140	0.180	0.196
Init.	0.130	0.122	0.125	0.172	0.190
Init.	0.132	0.138	0.130	0.189	0.206
	0.105	0.115	0.110	0.154	0.151
	0.105	0.114	0.108	0.151	0.143
	0.105	0.116	0.113	0.152	0.147
	0.077	0.095	0.094	0.121	0.110
	0.075	0.096	0.076	0.115	0.108
	0.076	0.094	0.082	0.114	0.105
	0.062	0.081	0.073	0.097	0.086
	0.061	0.081	0.068	0.096	0.085
	0.059	0.079	0.067	0.094	0.085

[a] More consistent results are obtained if these points are assumed to be anomalous and are not used in the data analysis. See text.

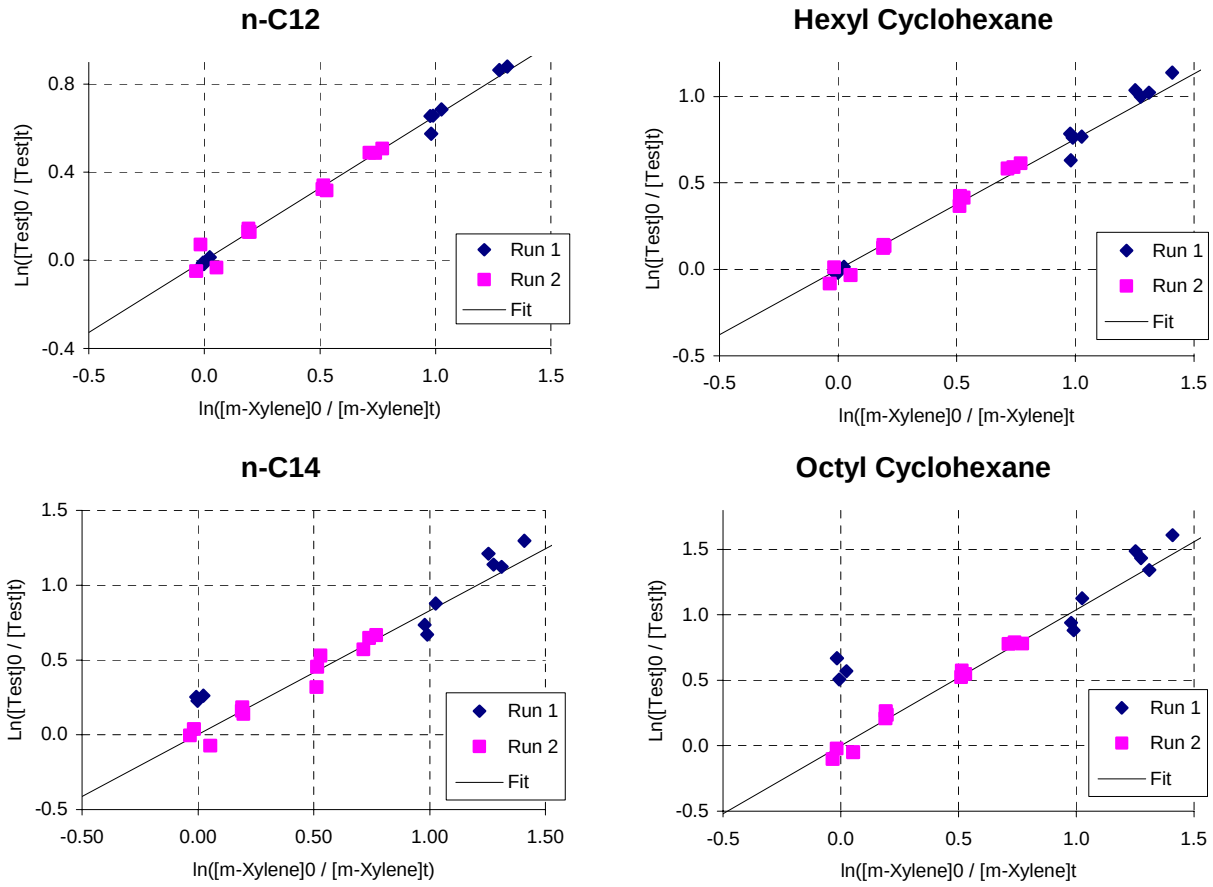

Figure 2. Plots of Equation (IV) for n-dodecane, n-tetradecane, hexyl cyclohexane, and octyl cyclohexane, with m-xylene as the test compound.

Figure 2 shows that good precision was obtained in the measurements of the relative rate constants for n-dodecane and hexyl cyclohexane, and fair precision in the measurements for the relative rate constants for the other two compounds if the initial data points in Run 1 are excluded. As indicated on Table 4 and shown on Figure 2, the initial measurements of n-dodecane and (especially) octyl cyclohexane in the first experiment appear to be anomalous, and were not used when computing the best fit to Equation (IV). The rates of decay of these compounds relative to m-xylene in the subsequent measurements in this experiment are consistent with the data in the second run, and the second experiment indicates no problems with the data or nonlinear plots of Equation (IV). Also, if all the data points are used the rate constant derived for octyl cyclohexane is lower than that derived for hexyl cyclohexane, which is not reasonable. However, all the data points were used when estimating the uncertainty of the rate constant ratios derived from these data, as shown on Table 4.

The rate constants determined in this work for n-dodecane and n-tetradecane are in good agreement with the literature values, suggesting that there are no systematic problems in our

Table 5. Summary of Results of OH Radical Rate Constant Measurements.

Compound	kOH / kOH (m-Xylene) [a]	kOH (cm^3 $molec^{-1}$ s^{-1})		
		This Work [b]	Literature	Reference
n-C12	0.66 ± 0.2	1.55×10^{-11}	1.39×10^{-11}	Atkinson (1997)
n-C14	0.83 ± 0.7	1.96×10^{-11}	1.80×10^{-11}	Atkinson (1997)
Hexyl Cyclohexane	0.77 ± 0.2	1.78×10^{-11}	1.77×10^{-11}	Kwok and Atkinson (1995) (Estimate)
Octyl Cyclohexane	1.04 ± 1.7	2.45×10^{-11}	2.05×10^{-11}	Kwok and Atkinson (1995) (Estimate)

[a] Rate constant ratio determined to minimize least squares errors between $\ln([VOC]_0/[VOC]_t)$ calculated using Equation (IV) and the experimentally measured values. The initial m-xylene and test VOC concentrations in each experiment were also optimized as part of this determination, to avoid biases introduced by uncertainties in initial reactant concentrations used in Equation (IV). Dilution is assumed to be negligible in all experiments. The stated error limits reflect precision on measurement only. Uncertainties for n-dodecane and hexyl cyclohexane based on standard deviations of least squares fits of lines to data. Uncertainties for n-tetradecane and octyl cyclohexane based on differences in rate constant ratios obtained if the initial points of the second experiment are used in the analysis.

[b] Placed on an absolute basis using kOH for m-xylene of 2.36×10^{-11} cm^3 $molec^{-1}$ s^{-1} at 298K (Atkinson, 1989).

measurements. The rate constant derived for hexyl cyclohexane is in good agreement with the rate constant estimated using the methods of Kwok and Atkinson (1995), consistent with the results observed for most of the higher alkanes and the substituted cyclohexanes, as shown on Table 1. The rate constant derived for octyl cyclohexane is about 20% higher than the estimated value, which is not outside the observed for other alkanes, but not as good as expected based on the data for hexyl cyclohexane and the other substituted cyclohexanes.

Based on these data, we conclude that the rate constant for the reaction of OH radicals with hexyl cyclohexane is 1.78×10^{-11} cm^3 $molec^{-1}$ s^{-1}, with an estimated uncertainty of around ±20%. Because of the problems with the initial measurements of the octyl cyclohexane in the first experiment, the rate constant measurement for the octyl cyclohexane is considered to be more uncertain than the estimate derived using the method of Kwok and Atkinson (1995). For this reason, the estimated rate constant is used in the model simulations for this compound in this work.

Phase 2 Environmental Chamber Experiments

Summary of Experiments and Characterization Results

Table 6 gives a chronological listing of all the experiments carried out for the second phase of this program. These consisted primarily of the experiments with the hexyl and octyl cyclohexanes, whose results are summarized in the following section. In addition, several characterization runs were carried out

Table 6. Chronological listing of the environmental chamber experiments carried out to evaluate the ozone formation potentials of hexyl cyclohexane and octyl cyclohexane.

Run ID	Date	Title	Comments
			DTC Experiments
DTC299	11/29/95	n-Butane - NO_x	Characterization run to measure the chamber radical source. Some indication of leakage on Side A, and Side A also had a slightly higher NO consumption rate. NO consumption rate on Side A was well fit by predictions of chamber model. NO consumption rate on Side B was slightly lower than predicted by chamber model, but results were within the experimental variability.
DTC300	1/19/96	NO_2 Actinometry	Measured NO_2 photolysis rate was 0.216 min^{-1}, in good agreement with the prediction of the curve fit to the full set of actinometry results, which was 0.215 min^{-1}.
DTC301	1/24/96	Propene - NO_x	Control run for comparison with other propene runs carried out in this and other chambers. The results are in the normal range. Good side equivalency was observed.
DTC302	1/25/96	Mini-surrogate - NO_x	Control run and side equivalency test. Good side equivalency observed. Ozone formation rate slightly slower than predicted by model, but results within the normal range.
DTC310	2/8/96	CO - NO_x	Characterization run to measure chamber radical source. Results rejected because CO may not have been purified, and the CO concentrations were above the reliable operating range of the CO monitor.
DTC315	2/21/96	Mini Surrogate + Hexyl Cyclohexane	Mini-surrogate reactivity experiment with 0.22 ppm of hexyl cyclohexane added to Side B. Results on Table 7 and Figure 4.
DTC316	2/22/96	CO - NO_x	Characterization run to measure chamber radical source. CO was purified. Results were in good agreement with predictions of chamber model.
DTC317	2/23/96	Full Surrogate + Hexyl Cyclohexane	High NO_x full surrogate reactivity experiment with 0.25 ppm of hexyl cyclohexane added to Side A. Results on Table 7 and Figure 7.
DTC318	2/27/96	Mini Surrogate + Hexyl Cyclohexane	Mini-surrogate reactivity experiment with 0.13 ppm of hexyl cyclohexane added to Side B. Results on Table 7 and Figure 4.
DTC319	2/28/96	Full Surrogate + Hexyl Cyclohexane	High NO_x full surrogate reactivity experiment with 0.34 ppm of hexyl cyclohexane added to Side B. Results on Table 7 and Figure 7.

Table 6 (continued)

Run ID	Date	Title	Comments
DTC322	3/4/96	CO - NO_x	Characterization run to measure the chamber radical source. NO consumption rate well fit by predictions of the chamber model. CO consumption rate indicates relatively low dilution, but with dilution in Side A being somewhat greater than in side B.
DTC324	3/6/96	Mini Surrogate + Octyl Cyclohexane	Mini-surrogate reactivity experiment with 0.12 ppm of octyl cyclohexane added to Side A. Results on Table 7 and Figure 4.
DTC325	3/7/95	Low NO_x Full Surrogate + Octyl Cyclohexane	Low NO_x full surrogate reactivity experiment with 0.34 ppm of octyl cyclohexane added to Side B. Results on Table 7 and Figure 8.
DTC326	3/11/96	NO_2 Actinometry	Measured NO_2 photolysis rate was 0.212 min^{-1}, in good agreement with the prediction of the curve fit to the full set of actinometry results, which was 0.208 min^{-1}.
DTC331	4/3/96	Propene - NO_x	Control run for comparison with other propene runs carried out in this and other chambers. The results were within the normal range. Good side equivalency was observed.
DTC333	4/11/96	Pure air irradiation	After 6 hours of irradiation, approximately 31 ppb O_3 formed on side A and 27 on side B. Results are within the normal range, but amounts of ozone formed were somewhat lower than the predictions of the chamber effects model.
DTC334	4/12/96	CO - NO_x	NO consumption rate well fit by predictions of the chamber model. CO consumption rate indicates relatively low dilution, but with dilution in Side A being somewhat greater than in side B.
DTC343	4/29/96	NO_2 Actinometry	Measured NO_2 photolysis rate was 0.209 min^{-1}, in good agreement with the prediction of the curve fit to the full set of actinometry results, which was 0.204 min^{-1}.
			<u>CTC Experiments</u>
CTC155	1/5/96	n-Butane - NO_x	Characterization run to measure the chamber radical source. The rate of NO oxidation is slightly less than the predictions of the chamber model, but the results are within the normal range. Good side equivalency observed.
CTC157	1/10/96	NO_2 Actinometry	NO_2 photolysis rate determined by tube method was 0.259 min^{-1}, which yields a corrected value of 0.191 min^{-1} (Carter et al, 2000a). This is reasonably close to the 0.18 min^{-1} predicted by the overall trends in the actinometry results for this chamber (Carter et al, 2000a).
CTC161	1/18/96	Pure Air Irradiation	Characterization run to test for background effects. Sides differ in ozone formation. Side A forms ~30 ppb O_3 in 6 hours, in good agreement with chamber model predictions. Side B forms ~40 ppb O_3, which is consistent with chamber model predictions if ~1 ppb of NO is assumed to be present initially.

Table 6 (continued)

Run ID	Date	Title	Comments
CTC162	2/6/96	CO - Air Leak Test	Run conducted to measure dilution due to leakage, which was found to be negligible.
CTC163	3/13/96	Propene - NO_x	Control run for comparison with other propene runs carried out in this and other chambers. The results were within the normal range. Good side equivalency was observed.
CTC164	3/14/96	Pure Air Irradiation	Characterization run to test for background effects. Approximately 35 ppb O_3 formed on each side in 6 hours, somewhat more than predicted by chamber model.
CTC165	3/15/96	Full Surrogate - NO_x	Standard full surrogate - NO_x mixture irradiated on both sides to test for side equivalency for this type of experiments. Good side equivalency was observed.
CTC166	3/18/96	NO_2 Actinometry	NO_2 photolysis rate determined by tube method was 0.263 min^{-1}, which yields a corrected value of 0.194 min^{-1} (Carter et al, 2000a). This is reasonably close to the 0.18 min^{-1} predicted by the overall trends in the actinometry results for this chamber (Carter et al, 2000a).
CTC167	3/19/96	Full Surrogate + Hexyl Cyclohexane	High NO_x full surrogate reactivity experiment with 0.55 ppm of hexyl cyclohexane added to Side A. Results on Table 7 and Figure 7.
CTC168	3/20/96	Full Surrogate + Octyl Cyclohexane(B)	High NO_x full surrogate reactivity experiment with 0.47 ppm of octyl cyclohexane added to Side B. Results on Table 7 and Figure 7.
	The chamber was inactive for a period and then was used for experiments for other projects		
CTC230	12/12/97	n-Butane - NO_x	Characterization run to measure the chamber radical source. The rate of NO oxidation is slightly less than the predictions of the chamber model, but the results are within the normal range. Good side equivalency observed.
CTC231	12/16/97	Mini Surrogate + Octyl Cyclohexane	Mini-surrogate reactivity experiment with 0.25 ppm of octyl cyclohexane added to Side A. Results on Table 7 and Figure 4.
CTC232	12/17/97	Full Surrogate + Octyl Cyclohexane	High NO_x full surrogate reactivity experiment with 0.31 ppm of octyl cyclohexane added to Side B. Results on Table 7 and Figure 7.
CTC233	12/18/97	Low NO_x Full Surrogate + Hexyl Cyclohexane (A)	Low NO_x full surrogate reactivity experiment with 0.33 ppm of hexyl cyclohexane added to Side A. Results on Table 7 and Figure 8.
CTC234	12/19/97	Propene - NO_x	Control run for comparison with other propene runs carried out in this and other chambers. The results were within the normal range. Good side equivalency was observed.
CTC236	12/23/97	n-Butane + Chlorine Actinometry	The chlorine photolysis rate measured in this experiment corresponded to an NO_2 photolysis rate of 0.148 min^{-1}. This is in good agreement with the NO_2 photolysis rate derived from the overall trends in all the actinometry experiments, which is 0.142 min^{-1} (Carter et al, 2000a).

Table 6 (continued)

Run ID	Date	Title	Comments
CTC237	1/6/98	Pure air irradiation	Characterization run to test for background effects. Sides differ in ozone formation. Both sides formed ~18 ppb in 6 hours, somewhat greater than predicted by the standard chamber model.
CTC239	1/8/98	Full Surrogate + Octyl Cyclohexane	High NO_x full surrogate reactivity experiment with 0.49 ppm of octyl cyclohexane added to Side B. Results on Table 7 and Figure 7.
CTC240	1/9/98	Low NO_x Full Surrogate + Octyl Cyclohexane	Low NO_x full surrogate reactivity experiment with 0.52 ppm of octyl cyclohexane added to Side A. Results on Table 7 and Figure 8.
CTC241	1/16/98	n-Butane - NO_x	Characterization run to measure the chamber radical source. The rate of NO oxidation agreed very well with the predictions of the standard chamber model. Good side equivalency observed.
CTC242	1/21/98	n-Butane + Chlorine Actinometry	The chlorine photolysis rate measured in this experiment corresponded to an NO_2 photolysis rate of 0.108 min^{-1}. This is less than the NO_2 photolysis rate derived from the overall trends in all the actinometry experiments, which is 0.142 min^{-1}, but is within the scatter of the data (Carter et al, 2000a).
CTC244	9/14/98	n-Butane - NO_x	Characterization run to measure the chamber radical source. The rate of NO oxidation agreed reasonably well with the predictions of the standard chamber model.
CTC245	9/15/98	Propene - NO_x	Control run for comparison with other propene runs carried out in this and other chambers. The results were within the normal range. Good side equivalency was observed.
CTC247	9/17/98	NO_2 Actinometry	NO_2 photolysis rate determined by tube method was 0.198 min^{-1}, which yields a corrected value of 0.146 min^{-1} (Carter et al, 2000a). This is reasonably close to the 0.14 min^{-1} predicted by the overall trends in the actinometry results for this chamber (Carter et al, 2000a).

to determine the chamber-dependent inputs needed for the model simulations of the experiments. Table 6 summarizes the purposes and relevant results from these runs. As indicated there, the results of most of these experiments were as expected based on our previous experience with these and similar chambers in our laboratories (Carter et al., 1995c and references therein; Carter et al, 2000a). Carter et al (2000a) gives a more detailed more discussion of the characterization results for these chambers during this time period, particularly with respect to light intensity and the chamber radical source. The results of these characterization experiments were taken into account when deriving the chamber dependent parameters used in the model simulations of these experiments, as discussed above and indicated on Table A-4 in Appendix A.

Hexyl and Octyl Cyclohexane Experiments

As indicated on Table 6, six incremental reactivity experiments were carried out with hexyl cyclohexane and seven incremental reactivity experiments were carried out with octyl cyclohexane. These consisted of at least two experiments for each compound using the mini-surrogate, at least three using the higher NO_x full surrogate and at least one for each compound using the low NO_x full surrogate. Experiments for each compound were carried out using the blacklight-irradiated DTC and using the CTC with the xenon arc light source. The results of these experiments are summarized on Table 7. For comparison purposes, the results of the Phase 1 experiments with the $C_{\geq 12}$ normal alkanes are also shown on Table 7. Concentration-time plots of selected data are given in the following section, in conjunction with the discussion of the results of the model simulations of these and the n-alkane experiments.

The results of these experiments indicate that the reactivity characteristics of these C_{12} and C_{14} alkyl cyclohexanes are very similar to those for the C_{12} and C_{14} normal alkanes studied previously (Carter et al, 1996). All compounds significantly inhibit OH radical levels in the experiments, and they also have significant negative effects on NO oxidation and O_3 formation rates in the mini-surrogate experiments. Their effects on NO oxidation and O_3 formation is much less in the full surrogate experiments, with their negative effect on O_3 declining essentially to zero by the end of the irradiations. The magnitudes of the $\Delta([O3]-[NO])$ and IntOH incremental reactivities are generally in the same range as observed in comparable experiments with the normal alkanes, suggesting that the amounts of inhibition caused by the reactions of these compounds are similar.

The large radical inhibiting effects in the reactions of these higher molecular weight alkanes can be attributed to the relatively high nitrate formation in the reactions of the peroxy radicals with NO, as discussed above. The NO oxidation and O_3 formation rates in the mini-surrogate experiments tend to be the most sensitive to radical inhibition or initiation effects (Carter et al, 1995a), and consequently the $\Delta([O_3]-[NO])$ reactivities are also highly negative in these experiments. On the other hand the full surrogate experiments are relatively more sensitive to the effects of the NO to NO_2 conversions involved in the alkane photooxidation mechanisms, which tend to work in the opposite direction. For alkanes such as n-octane, with lower overall nitrate yields, this is sufficient to counteract the inhibiting effect of the radical inhibition involved with nitrate formation and result in positive $\Delta([O_3]-[NO])$ reactivities in the full surrogate experiments (Carter et al, 1995a). In the case of the C_{12} or higher alkanes the positive effects of the NO to NO_2 conversions are not quite enough to counter the radical inhibiting effects in the full surrogate experiments, so the $\Delta([O_3]-[NO])$ reactivities are still generally negative in most experiments.

The mechanistic implications of these results will be discussed further in the following section, in conjunction with the discussion of the model simulations of these experiments.

Table 7 Summary of conditions and selected results of the environmental chamber experiments for both phases of this project. The data for the n-alkane experiments are from Carter et al. (1996).

Run	Test VOC (ppm)	NO_x (ppm)	Surg. (ppm C)	$\Delta([O_3]-[NO])$ (ppm) 2nd Hour Base	2nd Hour Test	2nd Hour IR [a]	6th Hour Base	6th Hour Test	6th Hour IR [a]	5th Hour IntOH (10^{-6} min) Base	5th Hour IntOH Test	5th Hour IntOH IR [a]
Phase II Experiments												
Mini-Surrogate + Hexyl Cyclohexane												
DTC318B	0.13	0.33	5.62	0.12	0.07	-0.40	0.43	0.28	-1.18	13.0	7.1	-47
DTC315B	0.22	0.33	5.36	0.15	0.08	-0.35	0.50	0.28	-0.99	16.3	5.7	-48
High NO_x Full Surrogate + Hexyl Cyclohexane												
DTC317A	0.25	0.17	3.88	0.30	0.27	-0.12	0.46	0.45	-0.08	28.6	16.2	-49
DTC319B	0.34	0.18	3.76	0.27	0.20	-0.19	0.44	0.42	-0.05	29.4	12.4	-50
CTC167A	0.55	0.41	5.90	0.36	0.28	-0.15	0.66	0.66	-0.01	23.6	12.5	-20
Low NO_x Full Surrogate + Hexyl Cyclohexane												
CTC233A	0.33	0.17	6.03	0.38	0.37	-0.03	0.43	0.45	0.05	19.4	12.1	-22
Mini-Surrogate + Octyl Cyclohexane												
DTC324A	0.12	0.32	6.09	0.16	0.09	-0.57	0.55	0.34	-1.71	16.5	9.2	-59
CTC231A	0.25	0.27	5.64	0.08	0.04	-0.16	0.38	0.18	-0.81	11.7	5.0	-27
High NO_x Full Surrogate + Octyl Cyclohexane												
CTC232B	0.31	0.46	5.80	0.20	0.14	-0.18	0.50	0.47	-0.09	14.4	8.4	-20
CTC168B	0.47	0.41	5.98	0.37	0.27	-0.20	0.67	0.62	-0.12	23.5	11.4	-26
CTC239B	0.49	0.44	5.92	0.28	0.18	-0.20	0.59	0.55	-0.08	17.1	8.1	-18
Low NO_x Full Surrogate + Octyl Cyclohexane												
DTC325B	0.34	0.18	4.72	0.31	0.25	-0.18	0.46	0.43	-0.09	30.3		
CTC240A	0.52	0.17	5.97	0.37	0.33	-0.07	0.43	0.42	-0.01	20.2	10.6	-18
Phase I Experiments [See Carter et al, (1996) for details]												
Mini-Surrogate + n-C_{12}												
DTC271B	0.18	0.30	5.49	0.12	0.07	-0.29	0.43	0.29	-0.74	17.1	11.0	-34
DTC273A	0.10	0.31	5.54	0.14	0.09	-0.41	0.49	0.38	-1.13	16.5	10.5	-58
DTC283B	0.23	0.32	5.63	0.12	0.06	-0.24	0.45	0.26	-0.82	14.5	5.0	-41
High NO_x Full Surrogate + n-C_{12}												
DTC272A	0.16	0.14	3.68	0.26	0.24	-0.13	0.40	0.38	-0.13	29.1	22.0	-44
DTC274B	0.11	0.16	3.66	0.30	0.28	-0.17	0.46	0.45	-0.07	31.1	24.2	-65
DTC284A	0.19	0.15	3.94	0.31	0.28	-0.14	0.48	0.45	-0.12	28.4	19.2	-48
CTC150B	0.27	0.42	5.45	0.36	0.30	-0.20	0.68	0.66	-0.05	21.6	15.2	-24
CTC154A	0.60	0.42	5.54	0.41	0.32	-0.14	0.70	0.70	-0.01	23.5	14.4	-15
Low NO_x Full Surrogate + n-C_{12}												
DTC293A	0.20	0.08	4.12	0.28	0.26	-0.11	0.32	0.31	-0.04	20.4	15.7	-24
Mini-Surrogate + n-C_{14}												
DTC275A	0.19	0.32	5.51	0.12	0.06	-0.32	0.46	0.27	-1.03	17.3	11.7	-30
DTC277B	0.11	0.31	5.68	0.13	0.07	-0.47	0.47	0.32	-1.42	16.4	9.7	-62
DTC289B	0.28	0.35	5.64	0.12	0.05	-0.25	0.43	0.19	-0.85	15.3	3.9	-41

Table 7 (continued)

Run	Test VOC (ppm)	NO_x (ppm)	Surg. (ppm C)	$\Delta([O_3]-[NO])$ (ppm)						5^{th} Hour IntOH (10^{-6} min)		
				2^{nd} Hour			6^{th} Hour					
				Base	Test	IR [a]	Base	Test	IR [a]	Base	Test	IR [a]
<u>High NO_x Full Surrogate + n-C_{14}</u>												
DTC276B	0.20	0.17	3.72	0.33	0.29	-0.22	0.50	0.48	-0.14	31.7	19.3	-63
DTC278A	0.07	0.16	4.17	0.32	0.29	-0.45	0.49	0.47	-0.32	28.5	23.2	-80
DTC290A	0.16	0.17	3.98	0.31	0.24	-0.40	0.47	0.42	-0.33	29.2	19.4	-63
CTC151A	0.26	0.50	5.49	0.37	0.34	-0.13	0.64	0.62	-0.09	19.9	13.6	-24
CTC158A	0.62	0.36	5.56	0.35	0.22	-0.21	0.69	0.60	-0.14	24.6	11.1	-22
<u>Mini-Surrogate + n-C_{15}</u>												
DTC279B	0.20	0.32	5.87	0.09	0.04	-0.23	0.43	0.23	-1.01	14.0	6.6	-37
<u>High NO_x Full Surrogate + n-C_{15}</u>												
DTC280A	0.08	0.16	4.01	0.32	0.26	-0.69	0.49	0.44	-0.58	30.3	21.4	-107
<u>Mini-Surrogate + n-C_{16}</u>												
DTC282A	0.09	0.33	5.64	0.15	0.08	-0.84	0.53	0.31	-2.50		9.5	
DTC291B	0.26	0.33	5.78	0.12	0.05	-0.26	0.44	0.21	-0.89	14.4	4.9	-36
<u>High NO_x Full Surrogate + n-C_{16}</u>												
DTC281B	0.16	0.16	3.85	0.30	0.26	-0.23	0.47	0.45	-0.09	30.7	19.8	-66
CTC152B	0.26	0.37	3.95	0.27	0.22	-0.17	0.48	0.48	0.00	18.0	11.9	-24
CTC156B	0.48	0.41	5.06	0.36	0.25	-0.24	0.67	0.59	-0.16	23.9	12.5	-24

[a] IR = Incremental Reactivity = ([Test] - [Base]) / [Test Compound Added]

MECHANISM EVALUATION

The ability of the SAPRC-99 chemical mechanism to appropriately simulate the atmospheric impacts of the higher molecular weight normal and cyclic alkanes studied was evaluated by conducting model simulations of the environmental chamber experiments carried out for both phases of this project. Although the Phase 1 study of the normal alkanes also included mechanism evaluation (Carter et al, 1996), this needed to be redone for this work because of the significant changes to the nitrate yield estimates for the higher alkanes, as discussed above. In addition, since the Phase I report of Carter et al, 1996) the overall mechanism was completely updated as discussed by Carter (2000), making the previous work out of date.

Methods

The environmental chamber modeling methods used in this work are based on those discussed in detail by Carter and Lurmann (1990, 1991), updated as discussed by Carter et al. (1995c; 1997a, 2000a). Model simulations of environmental chamber experiments requires including in the model appropriate representations of chamber-dependent effects such as wall reactions and characteristics of the light source. The photolysis rates were derived from results of NO_2 actinometry experiments and measurements of the relative spectra of the light source. In the case of the xenon arc lights used in the CTC, the spectra were derived from those measured during the individual experiments, assuming continuous linear changes in relative intensity at the various wavelengths, as discussed by Carter et al. (1997a). The thermal rate constants were calculated using the temperatures measured during the experiments, with the small variations in temperature with time during the experiment being taken into account. The computer programs and modeling methods employed are discussed in more detail elsewhere (Carter et al, 1995c). The specific values of the chamber-dependent parameters used in the model simulations of the experiments for this study are given in Table A-4 in Appendix A.

As indicated above, the chemical mechanism used in all the model simulations in this work was the SAPRC-99 mechanism documented by Carter (2000). The species, reactions, rate constants, and parameters used to calculate photolysis rates are listed in Tables A-1 through A-3 in Appendix A. Note that the mechanisms used for the higher alkanes are those derived using the SAPRC-99 mechanism generation system, as discussed in the previous sections. No adjustments were made to improve the fits of model calculations to the chamber data.

Results

The experiments modeled are the various alkane reactivity experiments carried out in the two phases of this project, whose conditions and selected results are summarized on Table 7, above. The results of the model simulations of these experiments are shown in Figure 3 through Figure 8, which give plots of the major experimental and calculated results of these incremental reactivity experiments. These

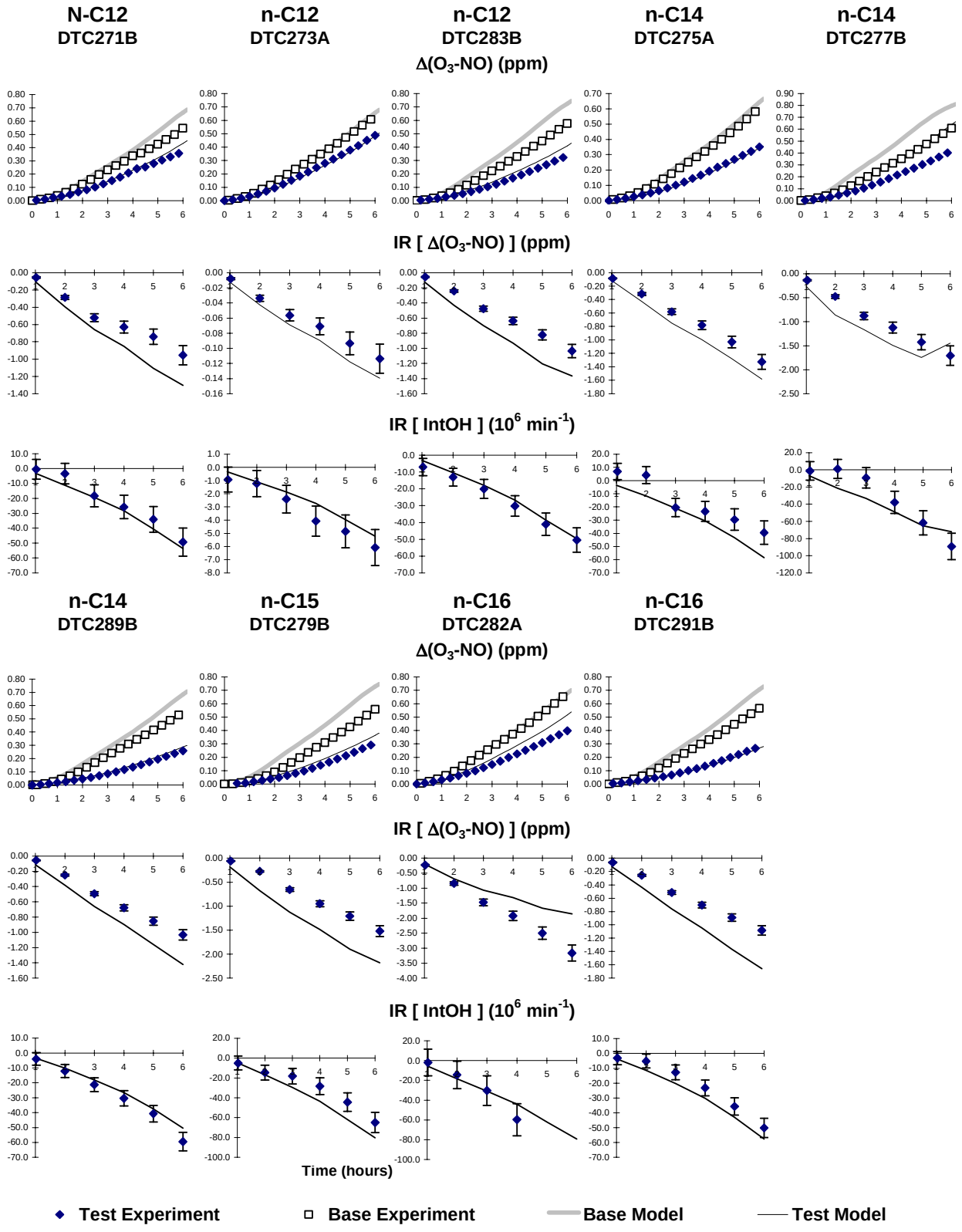

Figure 3. Selected experimental and calculated results of the mini surrogate incremental reactivity experiments with the C_{12} - C_{16} n-alkanes.

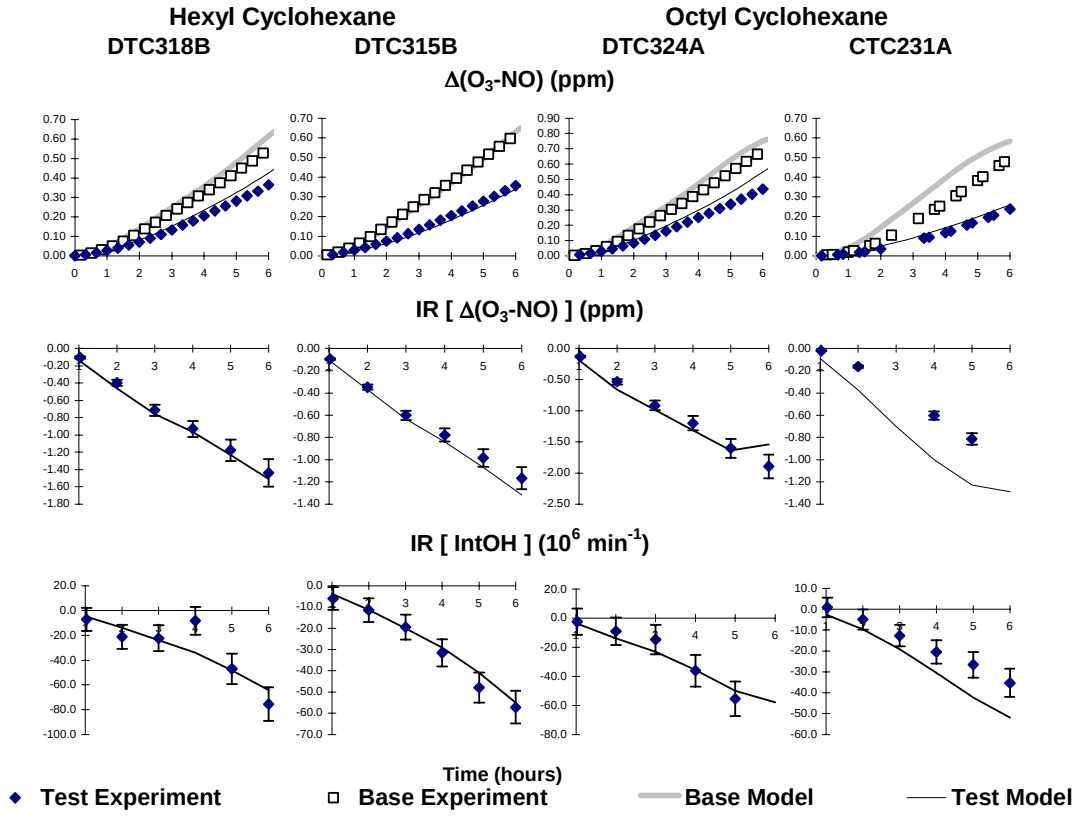

Figure 4. Selected experimental and calculated results of the mini-surrogate incremental reactivity experiments with hexyl cyclohexane and octyl cyclohexane.

include, for each experiment, the $\Delta([O_3]-[NO])$ data for both the base case and the added alkane experiment, the $\Delta([O_3]-[NO])$ incremental reactivities, calculated as the change in $\Delta([O_3]-[NO])$ caused by adding the alkane divided by the amount of alkane added, and the IntOH incremental reactivities, caused by the change in the IntOH measurements derived from the m-xylene consumption rates, divided by the amount of alkane added. The simulated incremental reactivities were calculated from the simulated using the same approach as the experimental incremental reactivities were calculated from the experimental data.

The results of the mini-surrogate experiments are shown on Figure 3 for the experiments with the n-alkanes, and on Figure 4 for the experiments with the hexyl cyclohexane and octyl cyclohexane. It can be seen that good fits of model simulations to the $\Delta([O_3]-[NO])$ and IntOH reactivity data are obtained in most experiments, particularly the DTC experiments with the alkyl cyclohexanes and the IntOH reactivity simulations in almost all runs. There may be a slight tendency for the model to underpredict $\Delta([O_3]-[NO])$ inhibition by the n-alkanes, but the discrepancy is relatively minor. Somewhat more variable fits are obtained for n-hexadecane and octyl cyclohexane than for the C_{12} compounds, as might be expected given

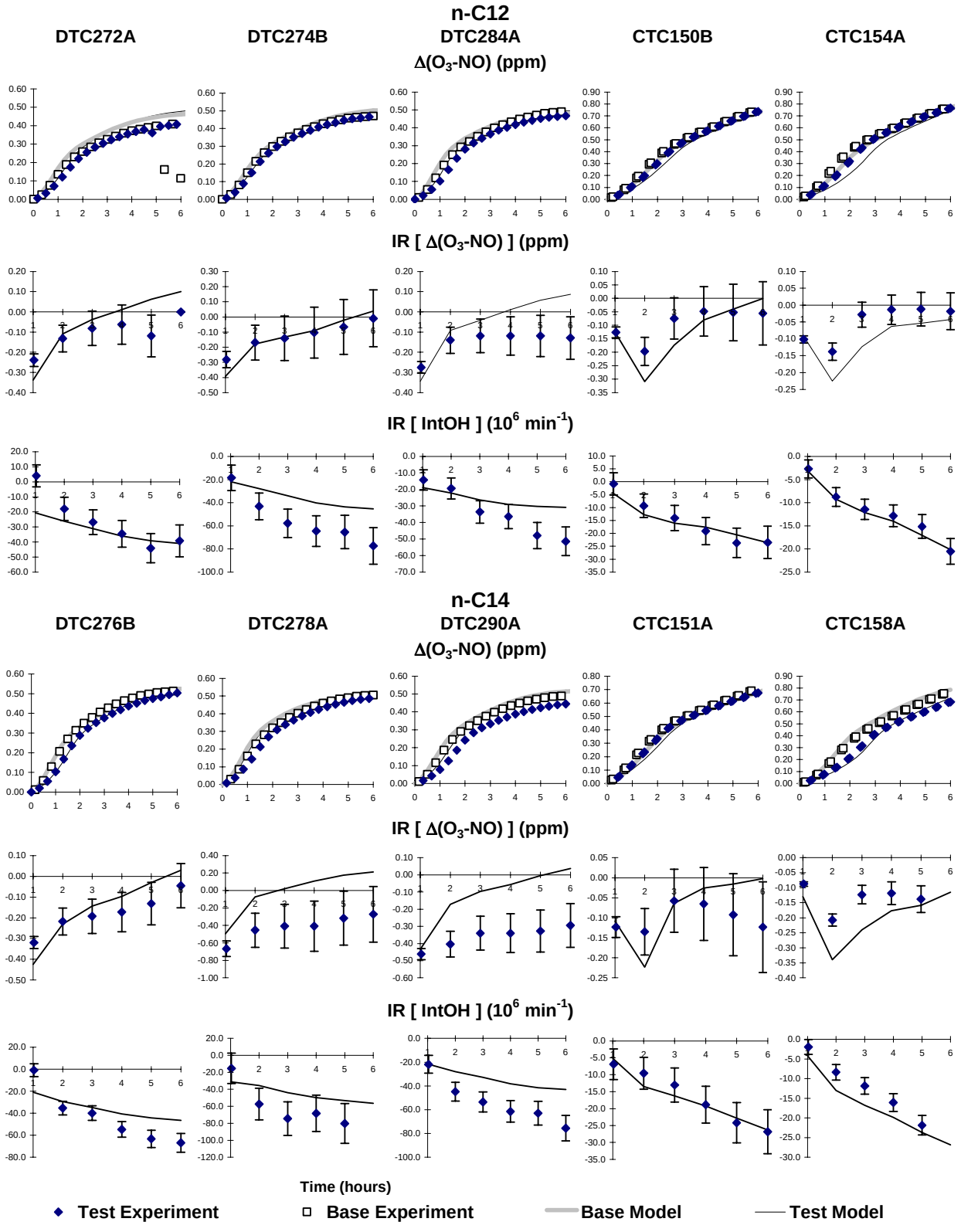

Figure 5. Selected experimental and calculated results of the high NO_x full surrogate incremental reactivity experiments with n-dodecane and n-tetradecane.

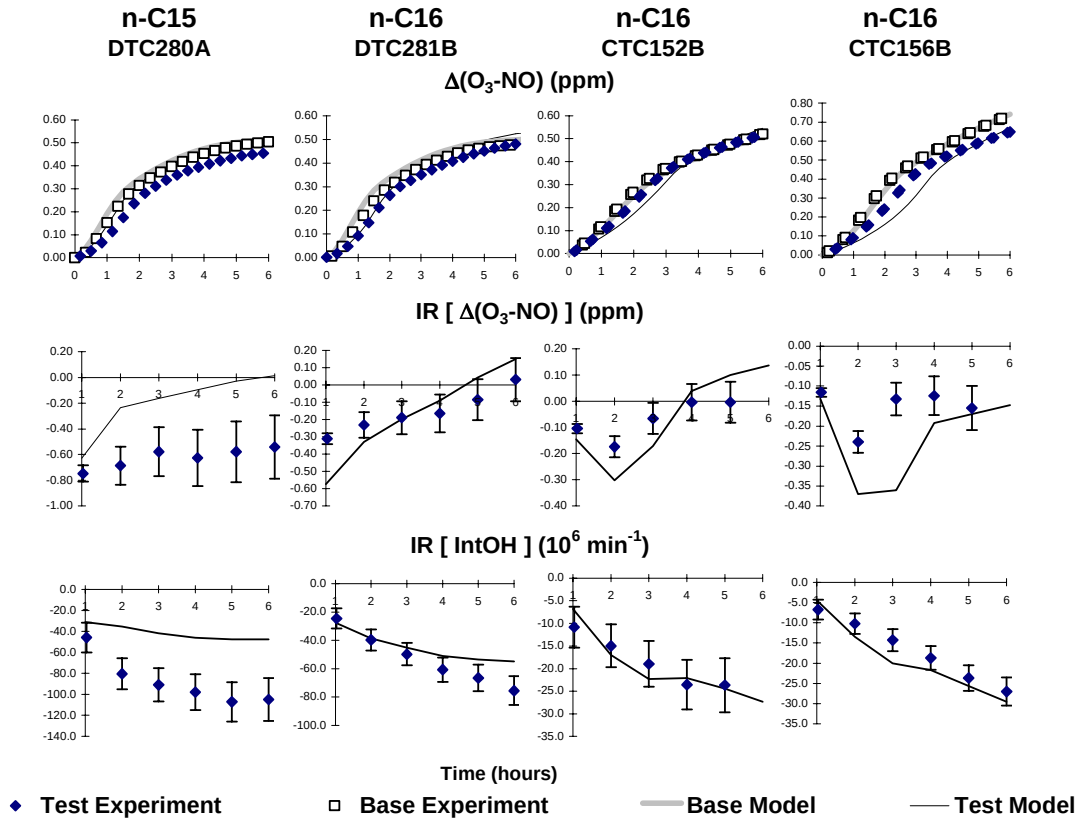

Figure 6. Selected experimental and calculated results of the high NO_x full surrogate incremental reactivity experiments with n-pentadecane and n-hexadecane.

the greater uncertainties involved with handling or analyzing the higher molecular weight compounds. The difference between the fits for the DTC and CTC experiments for octyl cyclohexane is more likely due to this than to any effects of the different light source employed, since the other experiments, discussed below, indicated no significant light source differences in the mechanism performance results.

The results of the high NO_x full surrogate experiments are shown on Figure 5 and Figure 6 for the n-alkanes and on Figure 7 for the cycloalkanes. Again reasonably good fits of model simulations to the data are obtained, with the model correctly predicting relatively small effects on $\Delta([O_3]-[NO])$ but large negative effects on IntOH. Almost as many CTC as DTC experiments were carried out for each compound, and no significant difference is observed between model simulations in the two chambers, indicating no significant light source effects. As with the mini-surrogate experiments, the ability of the model to simulate the alkyl cyclohexane experiments is comparable or even slightly better than its ability to simulate the experiments with the normal alkanes. In this case, the model performance in simulating the experiments with the C_{12} and the C_{16} alkanes is comparable.

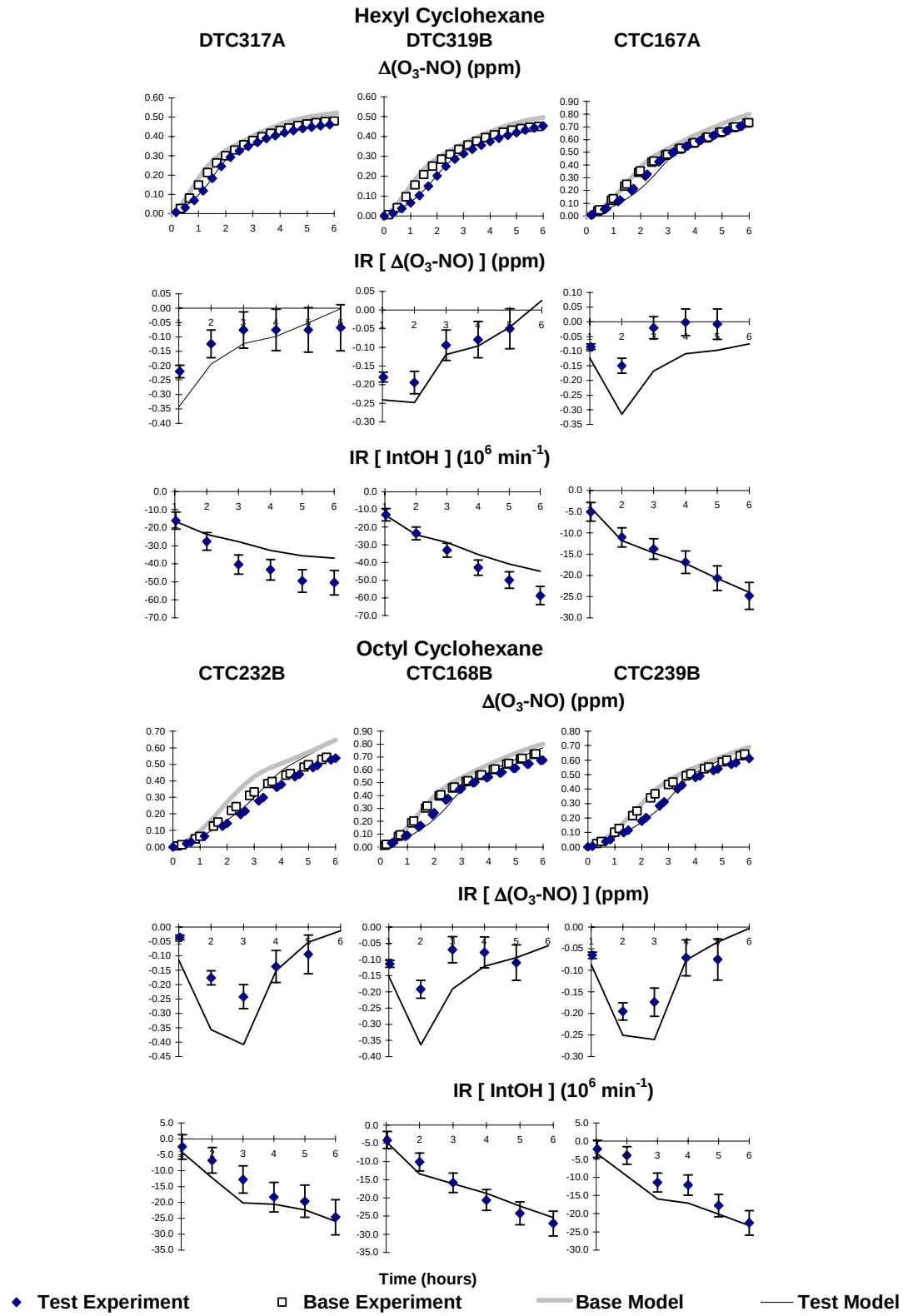

Figure 7. Selected experimental and calculated results of the high NO_x full surrogate incremental reactivity experiments with hexyl cyclohexane and octyl cyclohexane.

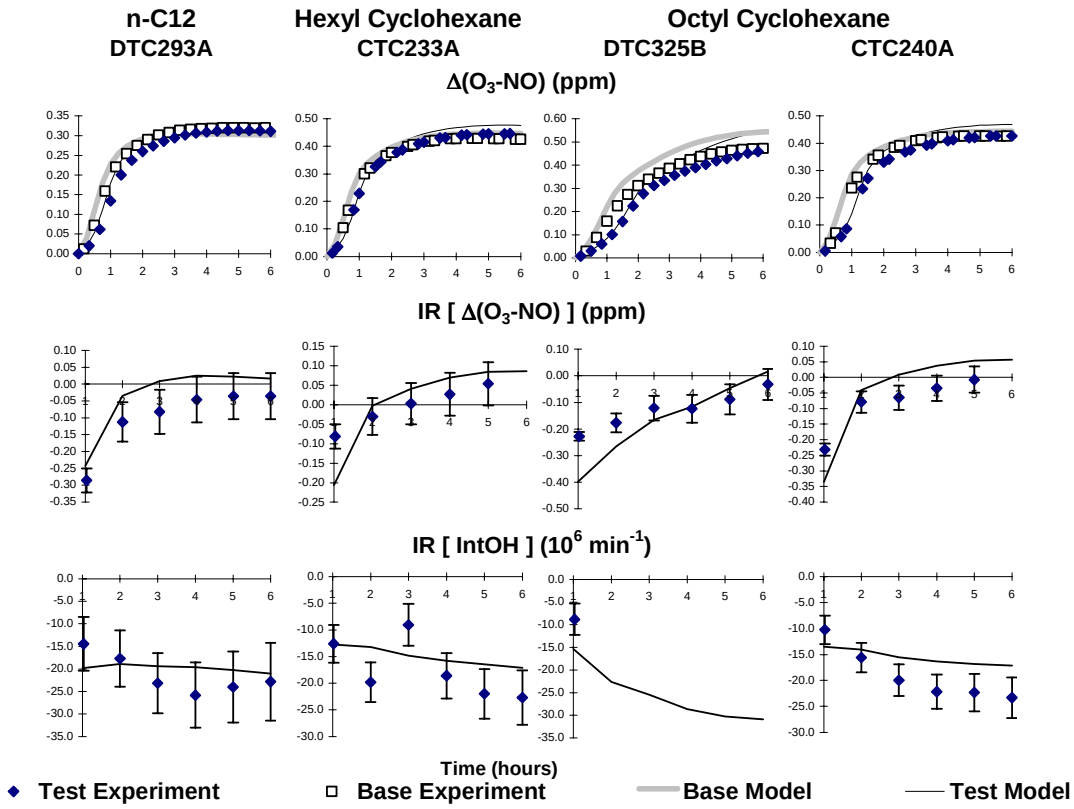

Figure 8. Selected experimental and calculated results of the low NO_x full surrogate incremental reactivity experiments with hexyl cyclohexane and octyl cyclohexane.

The results of the limited number of low NO_x full surrogate experiments carried out for this project are shown on Figure 8. Again the model performance in simulating these data is reasonably good, with the model correctly predicting the IntOH inhibition and the small effects on the $\Delta([O_3]-[NO])$ data and the peak ozone yields. The performance of the model in simulating the octyl cyclohexane experiments is not significantly affected by the light source employed.

Overall, it can be seen that the model can simulate the results of the reactivity experiments both for the $C_{\geq 12}$ normal alkanes and the $C_{\geq 12}$ alkyl cyclohexanes quite well considering the difficulties in handling and analyzing these low volatility compounds. Since these include experiments with different ROG surrogates that have differing sensitivities to various aspects of the mechanism (Carter et al, 1995a) and at different NO_x levels and employing different light sources, the mechanisms can be considered to be reasonably well tested. No large systematic biases were observed that indicated that adjustments to the estimated mechanism would be appropriate to improve the ability of the model to simulate these data.

ATMOSPHERIC REACTIVITY CALCULATIONS

Incremental reactivities of VOCs have been shown to be highly dependent on environmental conditions, so reactivities measured in environmental chamber experiments cannot necessarily be assumed to be the same as those under atmospheric conditions (Carter and Atkinson, 1989b; Carter et al, 1995b). Because of this, the only method available to obtain quantitative estimates of incremental reactivities of VOCs in ambient air pollution episodes is to conduct airshed model simulations of the episodes. Since these simulations cannot be any more reliable than the chemical mechanisms used, the major objective of this program was to assess the reliability of the mechanisms for the compounds of interest for use in such calculations. As discussed above, the results of this study suggest that the SAPRC-99 alkane mechanisms serve as an appropriate basis for estimating the effects of higher molecular weight normal and cyclic alkanes on ozone under atmospheric conditions. The atmospheric reactivity estimates based on these mechanisms are discussed in this section.

Scenarios Used for Reactivity Assessment

The set of airshed scenarios employed to assess the reactivities for this study is the same as those used for calculating the MIR and other reactivity scales in our previous work (Carter, 1994a), and also in the update using the SAPRC-99 mechanism (Carter, 2000). These scenarios, and the reasons for using them, are briefly described below. Note that the scenarios used in this work are exactly the same as used in the atmospheric reactivity estimates in our Phase 1 study (Carter et al, 1996).

The objective is to use a set of scenarios that represents, as much as possible, a comprehensive distribution of the environmental conditions where unacceptable levels of ozone are formed. Although a set of scenarios has not been developed for the specific purpose of VOC reactivity assessment, the EPA developed an extensive set of scenarios for conducting analyses of effects of ROG and NO_x controls on ozone formation using the EKMA modeling approach (Gipson et al. 1981; Gipson and Freas, 1983; EPA, 1984; Gery et al. 1987; Baugues, 1990). The EKMA approach involves the use of single-cell box models to simulate how the ozone formation in one day episodes is affected by changes in ROG and NO_x inputs. Although single-cell models cannot represent realistic pollution episodes in great detail, they can represent dynamic injection of pollutants, time-varying changes of inversion heights, entrainment of pollutants from aloft as the inversion height raises, and time-varying photolysis rates, temperatures, and humidities (Gipson and Freas, 1981; EPA, 1984; Gipson, 1984; Hogo and Gery, 1988). Thus, they can be used to simulate a wide range of the chemical conditions which affect ozone formation from ROG and NO_x, and which affect VOC reactivity. Therefore, at least to the extent they are suitable for their intended purpose, an appropriate set of EKMA scenarios should also be suitable for assessing reactivities over a wide range of conditions.

Base Case Scenarios

The set of EKMA scenarios used in this study were developed by the United States EPA for assessing how various ROG and NO_x control strategies would affect ozone nonattainment in various areas of the country (Baugues, 1990). The characteristics of these scenarios and the methods used to derive their input data are described in more detail elsewhere (Baugues, 1990; Carter, 1994b). Briefly, 39 urban areas in the United States were selected based on geographical representativeness of ozone nonattainment areas and data availability, and a representative high ozone episode was selected for each. The initial non-methane organic carbon (NMOC) and NO_x concentrations, the aloft O_3 concentrations, and the mixing height inputs were based on measurement data for the various areas, the hourly emissions in the scenarios were obtained from the National Acid Precipitation Assessment Program emissions inventory (Baugues, 1990), and biogenic emissions were also included. Table 8 gives a summary of the urban areas represented and other selected characteristics of the scenarios.

Several changes to the scenario inputs were made based on discussions with the California ARB staff and others (Carter, 1994a,b). Two percent of the initial NO_x and 0.1% of the emitted NO_x in all the scenarios was assumed to be in the form of HONO. The photolysis rates were calculated using solar light intensities and spectra calculated by Jeffries (1991) for 640 meters, the approximate mid-point of the mixed layer during daylight hours. The composition of the non-methane organic pollutants entrained from aloft was based on the analysis of Jeffries et al. (1989). The composition of the initial and emitted reactive organics was derived as discussed below. Complete listings of the input data for the scenarios are given elsewhere (Carter, 1994b).

This set of 39 EKMA scenarios are referred to as “base case” to distinguish them from the scenarios derived from them by adjusting NO_x inputs to yield standard conditions of NO_x availability as discussed below. No claim is made as to the accuracy of these scenarios in representing any real episode, but they are a result of an effort to represent, as accurately as possible given the available data and the limitations of the formulation of the EKMA model, the range of conditions occurring in urban areas throughout the United States. When developing general reactivity scales it is more important that the scenarios employed represent a realistic distribution of chemical conditions than accurately representing the details of any one particular episode.

The Base ROG mixture is the mixture of reactive organic gases used to represent the chemical composition of the initial and emitted anthropogenic reactive organic gases from all sources in the scenarios. Consistent with the approach used in the original EPA scenarios, the same mixture was used for all scenarios. The speciation for this mixture was derived by Croes (1991) based on an analysis of the EPA database (Jeffries et al. 1989) for the hydrocarbons and the 1987 Southern California Air Quality Study (SCAQS) database for the oxygenates (Croes et al. 1994; Lurmann and Main. 1992). This mixture consists of 52% (by carbon) alkanes, 15% alkenes, 27% aromatics, 1% formaldehyde, 2% higher aldehydes, 1% ketones, and 2% acetylene. The detailed composition of this mixture is given elsewhere (Carter, 1994b; Carter, 2000).

Table 8. Summary of the conditions of the scenarios used for atmospheric reactivity assessment.

	Scenario	Max O_3 (ppb)	Max 8-Hr Avg O_3 (ppb)	ROG / NO_x	NO_x / MOIR NO_x	Height (kM)	Init., Emit ROG (m. mol m^{-2})	O_3 aloft (ppb)	Integrated OH (ppt-min)
Avg.	MIR	187	119	3.1	1.5	1.8	15	70	128
Cond.	MOIR	239	165	4.5	1.0	1.8	15	70	209
	EBIR	227	172	6.4	0.7	1.8	15	70	210
Base	Atlanta, GA	179	132	7.3	0.7	2.1	12	63	200
Case	Austin, TX	175	144	9.3	0.5	2.1	11	85	179
	Baltimore, MD	334	215	5.2	1.1	1.2	17	84	186
	Baton Rouge, LA	241	173	6.8	0.9	1.0	11	62	186
	Birmingham, AL	244	202	6.9	0.5	1.8	13	81	208
	Boston, MA	197	167	6.5	0.6	2.6	14	105	262
	Charlotte, NC	143	126	7.8	0.3	3.0	7	92	212
	Chicago, IL	278	226	11.6	0.5	1.4	25	40	164
	Cincinnati, OH	205	153	6.4	0.7	2.8	17	70	220
	Cleveland, OH	252	179	6.6	0.9	1.7	16	89	187
	Dallas, TX	208	141	4.7	1.2	2.3	18	75	176
	Denver, CO	204	139	6.3	1.1	3.4	29	57	143
	Detroit, MI	246	177	6.8	0.7	1.8	17	68	235
	El Paso, TX	182	135	6.6	1.0	2.0	12	65	138
	Hartford, CT	172	144	8.4	0.5	2.3	11	78	220
	Houston, TX	312	217	6.1	0.9	1.7	25	65	225
	Indianapolis, IN	212	148	6.6	0.9	1.7	12	52	211
	Jacksonville, FL	155	115	7.6	0.6	1.5	8	40	206
	Kansas City, MO	159	126	7.1	0.6	2.2	9	65	233
	Lake Charles, LA	286	209	7.4	0.6	0.5	7	40	233
	Los Angeles, CA	568	406	7.6	1.0	0.5	23	100	134
	Louisville, KY	212	155	5.5	0.8	2.5	14	75	260
	Memphis, TN	229	180	6.8	0.6	1.8	15	58	249
	Miami, FL	132	111	9.6	0.4	2.7	9	57	181
	Nashville, TN	167	138	8.0	0.4	1.6	7	50	225
	New York, NY	365	294	8.1	0.7	1.5	39	103	159
	Philadelphia, PA	247	169	6.2	0.9	1.8	19	53	227
	Phoenix, AZ	277	193	7.6	1.0	3.3	40	60	153
	Portland, OR	166	126	6.5	0.7	1.6	6	66	233
	Richmond, VA	242	172	6.2	0.8	1.9	16	64	217
	Sacramento, CA	204	142	6.6	0.8	1.1	7	60	209
	St Louis, MO	324	209	6.1	1.1	1.6	26	82	176
	Salt Lake City, UT	186	150	8.5	0.6	2.2	11	85	182
	San Antonio, TX	133	98	3.9	1.0	2.3	6	60	192
	San Diego, CA	193	150	7.1	0.9	0.9	8	90	146
	San Francisco, CA	229	126	4.8	1.8	0.7	25	70	61
	Tampa, FL	230	153	4.4	1.0	1.0	8	68	211
	Tulsa, OK	231	160	5.3	0.9	1.8	15	70	264
	Washington, DC	283	209	5.3	0.8	1.4	13	99	239

Adjusted NO_x scenarios

Incremental reactivities in the base case scenarios would be expected to vary widely, since incremental reactivities depend on the ROG/NO_x ratio, and that ratio varies widely among the base case scenarios. To obtain reactivity scales for specified NO_x conditions, separate scenarios, designated MIR (for maximum incremental reactivity), MOIR (for maximum ozone incremental reactivity), and Equal Benefit Incremental Reactivity (EBIR) were developed (Carter, 1994a). In the MIR scenarios, the NO_x inputs were adjusted so the base ROG mixture (and most other VOCs) has its highest incremental reactivity. This is representative of the highest NO_x conditions of relevance to VOC reactivity assessment because at higher NO_x levels O_3 yields become significantly suppressed, but is also the condition where O_3 is most sensitive to VOC emissions. In the MOIR scenarios, the NO_x inputs were adjusted to yield the highest ozone concentration. In the EBIR scenarios, the NO_x inputs were adjusted so that the relative effects of NO_x reductions and total ROG reductions on peak ozone levels were equal. This represents the lowest NO_x condition of relevance for VOC reactivity assessment, because O_3 formation becomes more sensitive to NO_x emissions than VOC emissions at lower NO_x levels. As discussed by Carter (1994a) the MIR and EBIR ROG/NO_x ratios are respectively ~1.5 and ~0.7 times those for the MOIR scenarios in all cases.

NO_x Conditions in the Base Case Scenarios

The variability of ROG/NO_x ratios in the base case scenarios suggests a variability of reactivity characteristics in those scenarios. However, as discussed previously (Carter, 1994a), the ROG/NO_x ratio is also variable in the MIR or MOIR scenarios, despite the fact that the NO_x inputs in these scenarios are adjusted to yield a specified reactivity characteristic. Thus, the ROG/NO_x ratio, by itself, is not necessarily a good predictor of reactivity characteristics of a particular scenario. The NO_x/NO_x^{MOIR} ratio is a much better predictor of this, with values greater than 1 indicating relatively high NO_x conditions where ozone formation is more sensitive to VOCs, and values less than 1 indicating NO_x-limited conditions. NO_x/NO_x^{MOIR} ratios less than 0.7 represent conditions where NO_x control is a more effective ozone control strategy than ROG control (Carter, 1994a). Note that more than half of the base case scenarios represent NO_x-limited conditions, and ~25% of them represent conditions where NO_x control is more beneficial than VOC control. A relatively small number of scenarios represent MIR or near MIR conditions. However, as discussed elsewhere (Carter, 1994a), this set of scenarios is based on near-worst-case conditions for ozone formation in each of the airsheds. Had scenarios representing less-than-worst-case conditions been included, one might expect a larger number of MIR or near MIR scenarios. This is because NO_x is consumed more slowly on days with lower light intensity or temperature, and thus the scenario is less likely to become NO_x-limited.

Quantification of Atmospheric Reactivity

The reactivity of a VOC in an airshed scenario is measured by its incremental reactivity. For ambient scenarios, this is defined as the change in ozone caused by adding the VOC to the emissions,

divided by the amount of VOC added, calculated for sufficiently small amounts of added VOC that the incremental reactivity is independent of the amount added[1].

$$IR(VOC, Scenario) = \lim_{VOC \to 0} \left[\frac{O_3(\text{Scenario with VOC added}) - O_3(\text{Base Scenario})}{\text{Amount of VOC Added}} \right] \qquad (V)$$

The specific calculation procedure is discussed in detail elsewhere (Carter, 1994a,b).

Incremental reactivities derived as given above tend to vary from scenario to scenario because they differ in their overall sensitivity of O_3 formation to VOCs. These differences can be factored out to some extent by using "relative reactivities", which are defined as ratios of incremental reactivities to the incremental reactivity of the base ROG mixture, which is used to represent emissions of reactive VOCs from all sources.

$$RR(VOC, Scenario) = \frac{IR(VOC, Scenario)}{IR(\text{Base ROG}, Scenario)} \qquad (VI)$$

These relative reactivities can also be thought of as the relative effect on O_3 of controlling emissions of the particular VOC by itself, compared to controlling emissions from all VOC sources equally. Thus, they are more meaningful in terms of control strategy assessment than absolute reactivities, which can vary greatly depending on the episode and local meteorology.

In addition to depending on the VOC and the scenario, the incremental and relative reactivities depend on how the amounts of VOC added are quantified. In this work, this is quantified on a mass basis, since this is how VOCs are regulated, and generally approximates how VOC substitutions are made in practice. Note that relative reactivities will be different if they are quantified on a molar basis, with VOCs with higher molecular weight having higher reactivities on a mole basis than a gram basis.

Relative reactivities can also depend significantly on how ozone impacts are quantified (Carter, 1994a). Two different ozone quantification methods are used in this work, as follows:

"Ozone Yield" reactivities measure the effect of the VOC on the total amount of ozone formed in the scenario at the time of its maximum concentration. Incremental reactivities are quantified as grams O_3 formed per gram VOC added. Most previous recent studies of ozone reactivity (Dodge, 1984; Carter and Atkinson, 1987, 1989, Chang and Rudy, 1990; Jeffries and Crouse, 1991) have been based on this quantification method. The MIR, MOIR, and EBIR scales of Carter (1994a) also use this quantification.

"Maximum 8 Hour Average" reactivities measure the effect of the VOC on the average ozone concentration during the 8-hour period when the average ozone concentration was the greatest, which in

[1] Note that this differs from how the term "incremental reactivity" is used in the context of chamber experiments. In that case, the incremental reactivity refers to the relative change observed in the individual experiments, which in general depends on the amount added.

these one-day scenarios was the last 8 hours of the simulation. This provides a measure of ozone impact that is more closely related to the new Federal ozone standard that is given in terms of an 8-hour average. This quantification is used for relative reactivities in this work.

In previous reports, we have reported reactivities in terms of integrated O_3 over a standard concentration of 0.09 or 0.12 ppm. This provides a measure of the effect of the VOC on exposure to unacceptable levels of ozone. This is replaced by the maximum 8-hour average reactivities because it is more representative of the proposed new Federal ozone standard and because reactivities relative to integrated O_3 over a standard tend to be between those relative to ozone yield and those relative to 8-hour averages. Therefore, presenting both ozone yield and maximum 8-hour average relative reactivities should be sufficient to provide information on how relative reactivities vary with ozone quantification method. Incremental reactivities are quantified as ppm O_3 per milligram VOC emitted per square meter, but maximum 8-hour average reactivities are usually quantified as relative reactivities quantified on a mass basis.

Note that incremental reactivities are calculated for a total of 156 scenarios, consisting of the 39 base case scenarios and the three adjusted NO_x scenarios for each of the 39 base case scenarios. However, the incremental reactivities in the MIR, MOIR, or EBIR) scales are reported as averages of the incremental reactivities in the corresponding adjusted NO_x scenarios, because adjusting the NO_x conditions reduces the scenario variability, and this allows for a derivation single reactivity scales representing each type of NO_x condition. On the other hand, the individual scenario results will be shown for the base case scenarios, to give an indication of the scenario-to-scenario variability of the calculated reactivity results.

Results

Table 9 lists the ozone yield incremental reactivities calculated for selected represented C_{12} - C_{16} normal and cyclic alkanes, ethane, and the mixture of emitted reactive organic compounds (the base ROG). Table 10 gives the ozone yield and Table 11 gives maximum 8-hour average reactivities relative to the base ROG for these compounds and also for acetone. Ethane is chosen for comparison because it has been used by the EPA as the informal standard to determine “negligible” reactivity for VOC exemption purposes (Dimitriades, 1999). Acetone is also shown because it is a compound of similar reactivity as ethane that has been exempted from regulation as an ozone precursor. Distribution plots of the relative reactivities of ethane and selected $C_{\geq 12}$ normal and cyclic alkanes are shown on Figure 9 through Figure 12 for the base case, MIR, MOIR, and EBIR scenarios, respectively.

The results show that the incremental and relative reactivities of these $C_{\geq 12}$ normal and branched alkanes are highly variable and dependent on scenario conditions and on how ozone impacts are quantified. This variability cannot be attributed to variability in NO_x conditions alone since, as can be seen from Figure 10 through Figure 12, relatively wide distributions of the $C_{\geq 12}$ alkane relative reactivities are observed in the adjusted NO_x scenarios. By comparison, ethane (and most other VOCs) has much

Table 9. Atmospheric incremental calculated for the base ROG mixture, ethane, and selected $C_{\geq 12}$ normal and cyclic alkanes.

Scenario		Incremental Reactivities (gm O3 / gm VOC)						
		Base ROG	Ethane	n-C12	n-C14	n-C16	C6-CycC6	C8-CycC6
Adj'd NOx	Max React	3.68	0.30	0.65	0.57	0.51	0.74	0.59
	Max Ozone	1.46	0.20	0.42	0.37	0.33	0.46	0.38
	Equal Benefit	0.85	0.15	0.21	0.19	0.18	0.24	0.19
Base Case	Average	1.03	0.15	0.21	0.19	0.17	0.24	0.19
	St.Dev	0.42	0.04	0.17	0.16	0.15	0.19	0.17
	ATL GA	0.82	0.13	0.12	0.11	0.10	0.13	0.10
	AUS TX	0.63	0.12	0.01	0.01	0.00	0.00	0.00
	BAL MD	1.59	0.20	0.47	0.42	0.38	0.53	0.43
	BAT LA	0.85	0.11	0.12	0.08	0.07	0.11	0.09
	BIR AL	0.72	0.16	0.18	0.17	0.17	0.22	0.18
	BOS MA	0.72	0.14	0.28	0.25	0.25	0.31	0.26
	CHA NC	0.53	0.11	-0.01	-0.01	0.01	-0.01	-0.02
	CHI IL	0.26	0.07	-0.11	-0.13	-0.12	-0.13	-0.14
	CIN OH	1.12	0.20	0.44	0.41	0.38	0.49	0.43
	CLE OH	1.17	0.15	0.27	0.25	0.23	0.31	0.26
	DAL TX	2.14	0.23	0.39	0.32	0.29	0.43	0.33
	DEN CO	1.66	0.15	0.20	0.15	0.14	0.19	0.17
	DET MI	0.98	0.18	0.38	0.36	0.34	0.44	0.37
	ELP TX	1.45	0.14	0.10	0.08	0.06	0.12	0.06
	HAR CT	0.77	0.16	0.13	0.13	0.15	0.18	0.14
	HOU TX	1.10	0.17	0.37	0.31	0.29	0.38	0.32
	IND IN	1.24	0.18	0.25	0.25	0.21	0.28	0.24
	JAC FL	0.67	0.11	-0.02	-0.03	-0.02	-0.01	-0.03
	KAN MO	1.07	0.20	0.41	0.39	0.37	0.46	0.39
	LAK LA	0.42	0.09	0.01	0.01	-0.01	0.00	-0.02
	LOS CA	0.76	0.08	0.09	0.07	0.00	0.10	0.05
	LOU KY	1.24	0.22	0.43	0.38	0.33	0.46	0.38
	MEM TN	0.76	0.15	0.24	0.22	0.21	0.26	0.23
	MIA FL	0.49	0.10	-0.20	-0.19	-0.16	-0.21	-0.21
	NAS TN	0.67	0.15	0.01	0.01	0.00	0.01	-0.01
	NEW NY	0.39	0.07	0.11	0.09	0.07	0.12	0.10
	PHI PA	1.08	0.17	0.37	0.32	0.30	0.40	0.34
	PHO AZ	1.46	0.18	0.25	0.23	0.21	0.30	0.22
	POR OR	0.96	0.17	0.21	0.19	0.17	0.22	0.20
	RIC VA	1.06	0.18	0.41	0.39	0.36	0.46	0.39
	SAC CA	1.22	0.19	0.27	0.24	0.21	0.30	0.23
	SAI MO	1.38	0.16	0.32	0.27	0.25	0.35	0.28
	SAL UT	0.90	0.15	0.12	0.12	0.11	0.15	0.11
	SAN TX	1.62	0.21	0.39	0.36	0.34	0.44	0.37
	SDO CA	0.85	0.09	0.07	0.05	0.04	0.08	0.04
	SFO CA	1.87	0.09	0.06	0.05	0.03	0.08	0.06
	TAM FL	1.52	0.19	0.35	0.29	0.26	0.37	0.29
	TUL OK	1.17	0.20	0.48	0.45	0.39	0.53	0.46
	WAS DC	0.99	0.18	0.39	0.35	0.31	0.42	0.37

Table 10. Atmospheric relative ozone yield reactivities calculated for ethane, acetone, and selected $C_{\geq 12}$ normal and cyclic alkanes.

Scenario		Ozone Yield Reactivities relative to the base ROG (mass basis)						
		Ethane	Acetone	n-C12	n-C14	n-C16	C6-CycC6	C8-CycC6
Adj'd NOx	MIR	0.08	0.11	0.17	0.15	0.14	0.20	0.16
	MOIR	0.13	0.12	0.28	0.24	0.22	0.30	0.25
	EBIR	0.17	0.13	0.23	0.20	0.19	0.25	0.20
Base Case	Average	0.16	0.13	0.18	0.16	0.14	0.20	0.16
	St.Dev	0.04	0.02	0.19	0.18	0.17	0.21	0.20
	ATL GA	0.16	0.13	0.14	0.13	0.12	0.16	0.12
	AUS TX	0.19	0.13	0.02	0.01	0.00	0.00	0.00
	BAL MD	0.12	0.12	0.30	0.26	0.24	0.33	0.27
	BAT LA	0.13	0.12	0.14	0.10	0.08	0.13	0.10
	BIR AL	0.22	0.15	0.25	0.24	0.24	0.30	0.26
	BOS MA	0.20	0.13	0.38	0.35	0.34	0.42	0.36
	CHA NC	0.21	0.14	-0.02	-0.01	0.01	-0.01	-0.03
	CHI IL	0.28	0.19	-0.42	-0.48	-0.44	-0.50	-0.53
	CIN OH	0.18	0.12	0.39	0.37	0.34	0.44	0.38
	CLE OH	0.13	0.12	0.23	0.21	0.20	0.27	0.22
	DAL TX	0.11	0.11	0.18	0.15	0.13	0.20	0.15
	DEN CO	0.09	0.12	0.12	0.09	0.08	0.12	0.10
	DET MI	0.18	0.12	0.38	0.36	0.35	0.45	0.38
	ELP TX	0.10	0.12	0.07	0.06	0.04	0.08	0.04
	HAR CT	0.20	0.13	0.16	0.16	0.20	0.23	0.18
	HOU TX	0.16	0.12	0.34	0.28	0.26	0.35	0.30
	IND IN	0.14	0.12	0.20	0.20	0.17	0.23	0.19
	JAC FL	0.16	0.13	-0.03	-0.05	-0.03	-0.02	-0.05
	KAN MO	0.19	0.12	0.38	0.36	0.34	0.43	0.37
	LAK LA	0.22	0.14	0.03	0.01	-0.03	0.00	-0.04
	LOS CA	0.11	0.12	0.12	0.09	0.00	0.13	0.07
	LOU KY	0.17	0.12	0.35	0.30	0.27	0.37	0.31
	MEM TN	0.20	0.13	0.31	0.28	0.27	0.33	0.30
	MIA FL	0.20	0.15	-0.41	-0.38	-0.33	-0.43	-0.42
	NAS TN	0.23	0.16	0.02	0.02	0.00	0.02	-0.02
	NEW NY	0.17	0.12	0.27	0.22	0.19	0.30	0.25
	PHI PA	0.16	0.12	0.34	0.30	0.28	0.37	0.31
	PHO AZ	0.12	0.12	0.17	0.16	0.15	0.20	0.15
	POR OR	0.17	0.12	0.22	0.19	0.18	0.23	0.21
	RIC VA	0.17	0.12	0.38	0.36	0.34	0.43	0.37
	SAC CA	0.15	0.13	0.22	0.20	0.18	0.25	0.19
	SAI MO	0.11	0.12	0.23	0.20	0.18	0.25	0.20
	SAL UT	0.17	0.14	0.14	0.13	0.12	0.17	0.12
	SAN TX	0.13	0.11	0.24	0.22	0.21	0.27	0.23
	SDO CA	0.11	0.10	0.08	0.06	0.04	0.09	0.05
	SFO CA	0.05	0.14	0.03	0.03	0.02	0.04	0.03
	TAM FL	0.12	0.11	0.23	0.19	0.17	0.25	0.19
	TUL OK	0.17	0.12	0.41	0.38	0.34	0.45	0.39
	WAS DC	0.18	0.12	0.39	0.36	0.31	0.42	0.37

Table 11. Atmospheric relative maximum 8-hour average reactivities calculated for ethane, acetone, and selected $C_{\geq 12}$ normal and cyclic alkanes.

Scenario		Ozone Yield Reactivities relative to the base ROG (mass basis)						
		Ethane	Acetone	n-C12	n-C14	n-C16	C6-CycC6	C8-CycC6
Adj'd NOx	MIR	0.07	0.11	0.13	0.11	0.10	0.15	0.11
	MOIR	0.08	0.10	0.10	0.08	0.06	0.11	0.07
	EBIR	0.10	0.10	0.03	0.01	-0.01	0.02	-0.01
Base Case	Average	0.10	0.10	0.01	-0.02	-0.03	0.00	-0.03
	St.Dev	0.02	0.01	0.13	0.13	0.13	0.15	0.15
	ATL GA	0.09	0.10	-0.01	-0.02	-0.04	-0.02	-0.05
	AUS TX	0.11	0.09	-0.08	-0.10	-0.11	-0.11	-0.13
	BAL MD	0.08	0.11	0.11	0.08	0.07	0.12	0.08
	BAT LA	0.08	0.10	-0.01	-0.05	-0.06	-0.04	-0.07
	BIR AL	0.12	0.11	-0.01	-0.03	-0.04	-0.02	-0.05
	BOS MA	0.13	0.10	0.18	0.15	0.14	0.19	0.15
	CHA NC	0.14	0.10	-0.13	-0.14	-0.13	-0.15	-0.17
	CHI IL	0.13	0.11	-0.30	-0.36	-0.37	-0.39	-0.42
	CIN OH	0.10	0.09	0.14	0.12	0.10	0.15	0.11
	CLE OH	0.08	0.10	0.09	0.07	0.06	0.10	0.06
	DAL TX	0.08	0.09	0.09	0.06	0.05	0.09	0.05
	DEN CO	0.06	0.11	0.03	0.01	0.00	0.02	0.00
	DET MI	0.10	0.09	0.12	0.09	0.08	0.13	0.09
	ELP TX	0.07	0.10	-0.01	-0.03	-0.04	-0.02	-0.05
	HAR CT	0.12	0.10	-0.04	-0.06	-0.05	-0.04	-0.07
	HOU TX	0.09	0.10	0.10	0.06	0.04	0.09	0.06
	IND IN	0.09	0.09	0.01	-0.01	-0.04	-0.02	-0.04
	JAC FL	0.09	0.10	-0.16	-0.19	-0.20	-0.20	-0.23
	KAN MO	0.11	0.09	0.12	0.09	0.08	0.12	0.08
	LAK LA	0.11	0.10	-0.21	-0.25	-0.30	-0.29	-0.33
	LOS CA	0.07	0.10	-0.01	-0.03	-0.06	-0.02	-0.07
	LOU KY	0.11	0.10	0.12	0.08	0.06	0.11	0.07
	MEM TN	0.11	0.10	0.05	0.03	0.01	0.04	0.01
	MIA FL	0.11	0.10	-0.38	-0.38	-0.37	-0.44	-0.44
	NAS TN	0.15	0.12	-0.27	-0.29	-0.30	-0.33	-0.35
	NEW NY	0.08	0.09	0.09	0.06	0.03	0.08	0.05
	PHI PA	0.09	0.10	0.12	0.09	0.07	0.12	0.09
	PHO AZ	0.08	0.10	0.01	-0.01	-0.03	0.00	-0.03
	POR OR	0.11	0.10	0.02	0.00	-0.02	0.01	-0.01
	RIC VA	0.09	0.10	0.12	0.10	0.08	0.13	0.09
	SAC CA	0.09	0.11	-0.02	-0.04	-0.06	-0.04	-0.07
	SAI MO	0.07	0.11	0.08	0.05	0.04	0.08	0.05
	SAL UT	0.10	0.10	-0.05	-0.06	-0.08	-0.06	-0.09
	SAN TX	0.09	0.09	0.11	0.09	0.08	0.12	0.09
	SDO CA	0.08	0.08	-0.01	-0.03	-0.05	-0.02	-0.06
	SFO CA	0.04	0.13	-0.01	-0.02	-0.03	-0.01	-0.02
	TAM FL	0.08	0.10	0.08	0.05	0.03	0.08	0.04
	TUL OK	0.10	0.09	0.17	0.14	0.12	0.18	0.14
	WAS DC	0.10	0.10	0.12	0.10	0.06	0.13	0.09

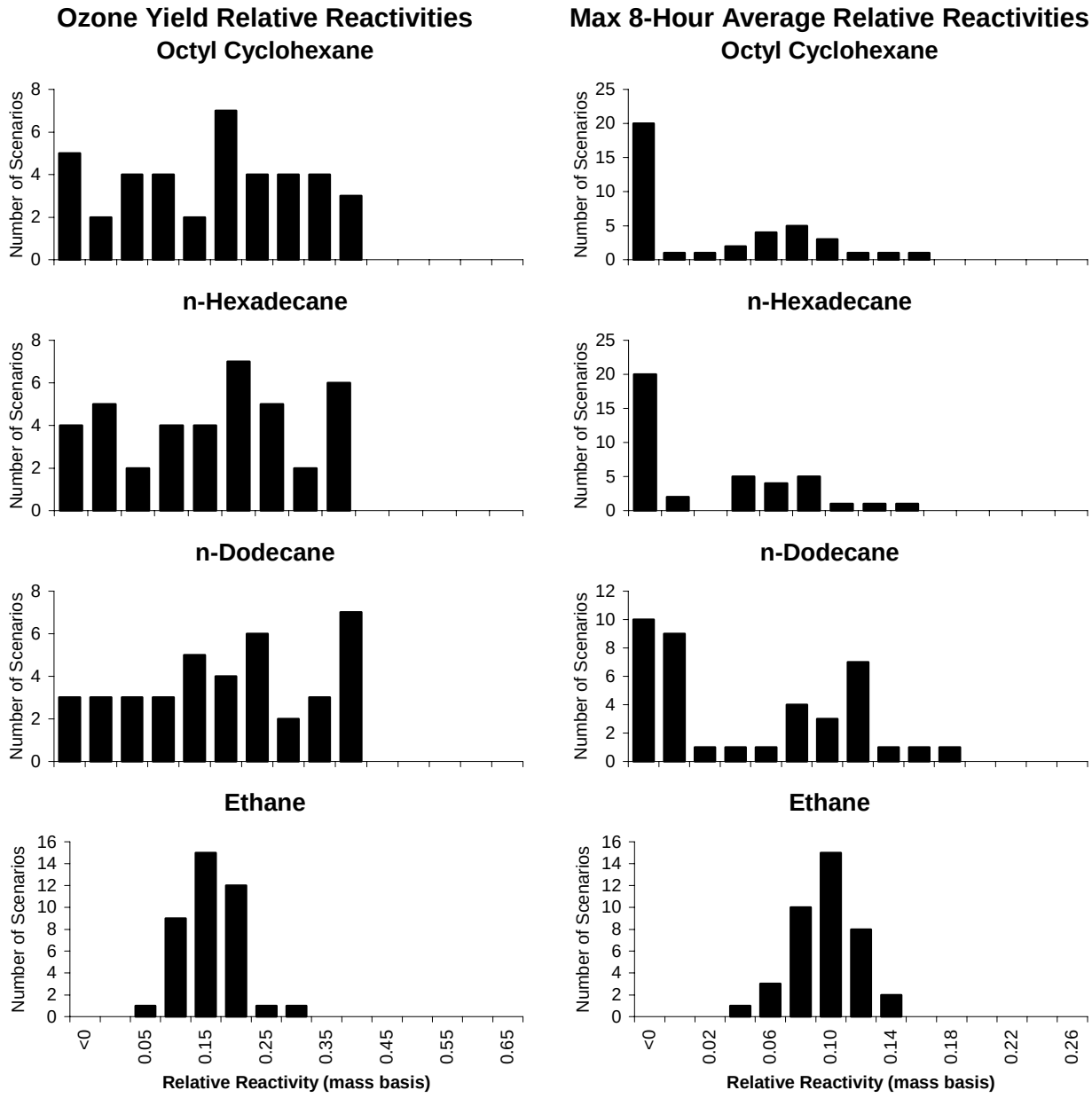

Figure 9. Distribution plots of relative reactivities of ethane, n-dodecane, n-hexadecane and octyl cyclohexane in the base case scenarios. Reactivities are relative to the base ROG mixture.

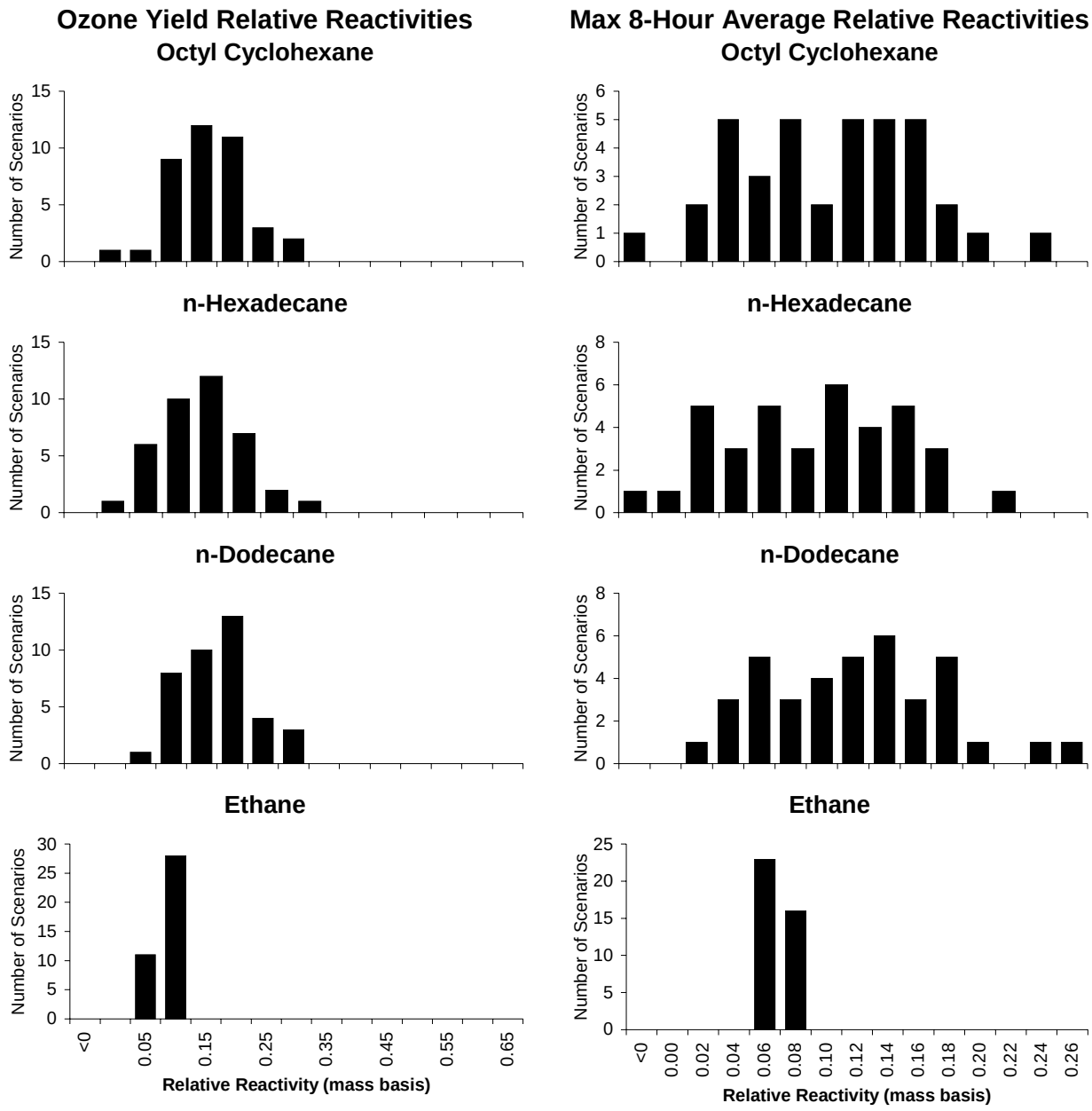

Figure 10. Distribution plots of relative reactivities of ethane, n-dodecane, n-hexadecane and octyl cyclohexane in the MIR scenarios. Reactivities are relative to the base ROG mixture.

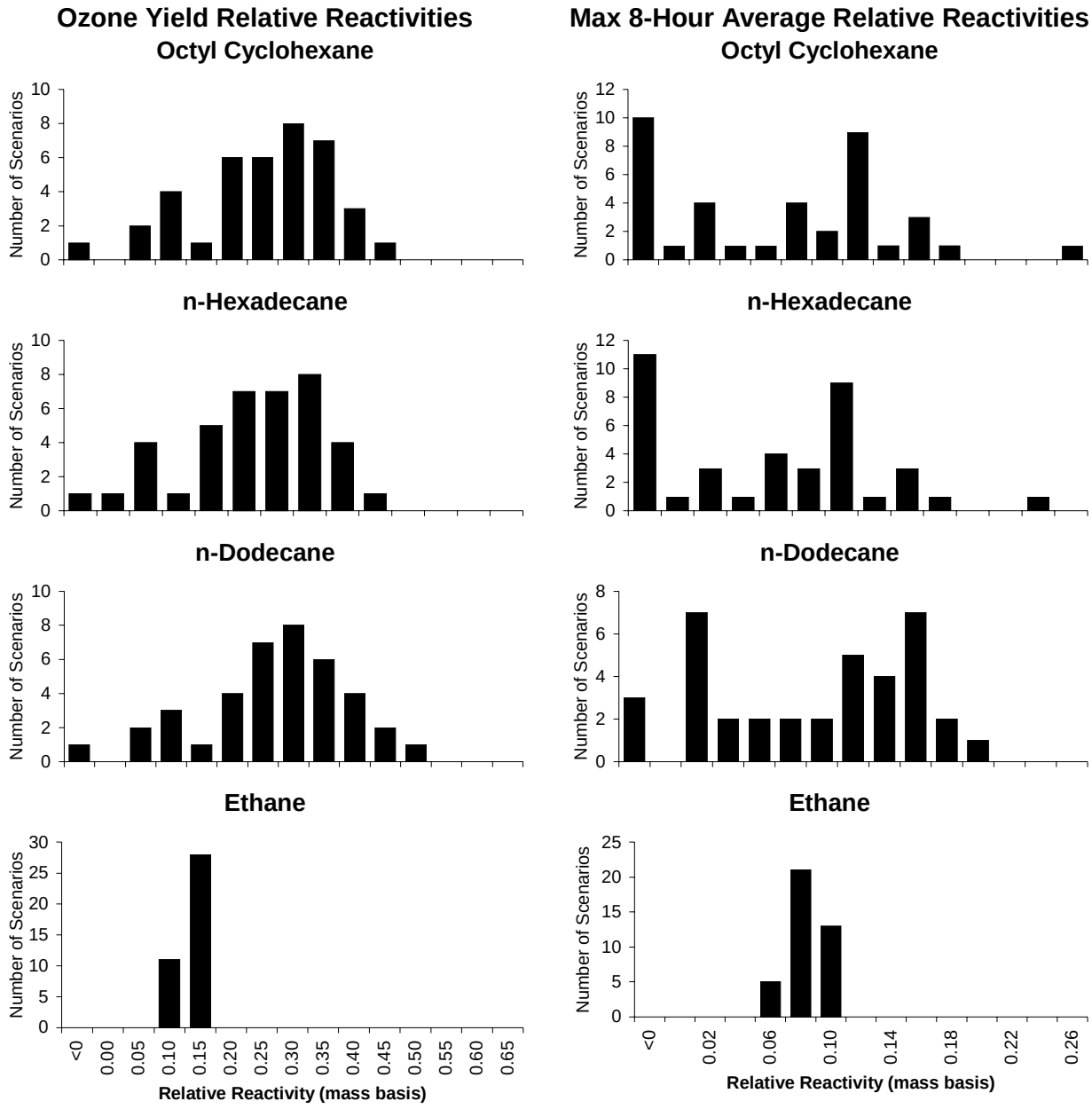

Figure 11. Distribution plots of relative reactivities of ethane, n-dodecane, n-hexadecane and octyl cyclohexane in the MOIR scenarios. Reactivities are relative to the base ROG mixture.

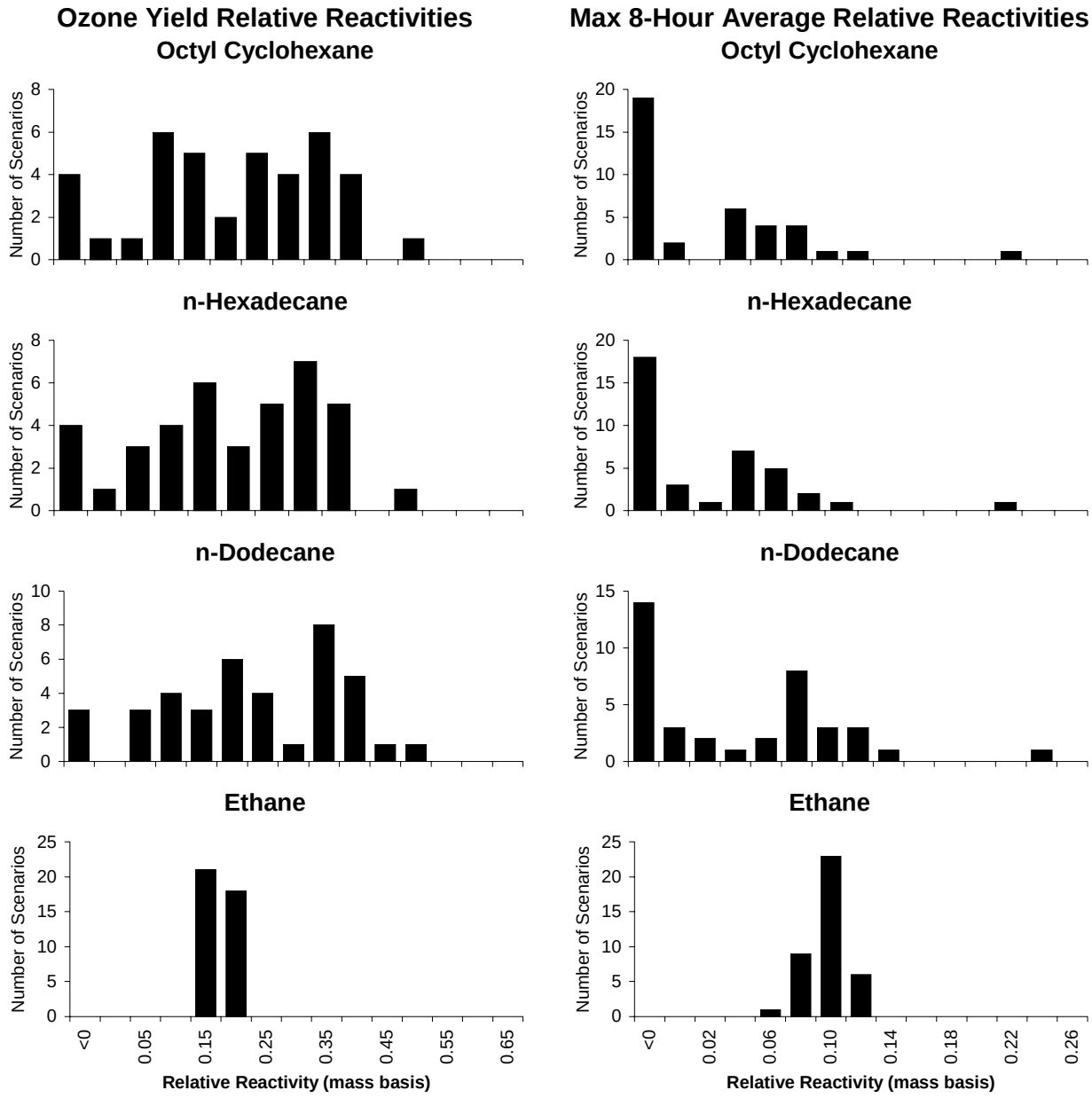

Figure 12. Distribution plots of relative reactivities of ethane, n-dodecane, n-hexadecane and octyl cyclohexane in the EBIR scenarios. Reactivities are relative to the base ROG mixture.

narrower distributions of relative reactivities once the NO_x conditions have been adjusted. However, the average relative reactivities of the $C_{\geq 12}$ alkanes tend to decrease with decreasing NO_x conditions, with the average relative reactivities being highest in the high NO_x MIR scenarios, and lowest in the base case scenarios, which include many scenarios with lower than EBIR NO_x levels.

The highly variable relative reactivities of the $C_{\geq 12}$ alkane can be explained by considering the different factors affecting their reactivities. The higher alkanes have a large positive effect on O_3 formation in that they react relatively rapidly and form a relatively large number of peroxy radicals that convert NO to NO_2. This positive impact is important under all NO_x conditions, though the efficiency of O_3 formation from NO to NO_2 conversions tends to decrease as NO_x levels decrease (Carter and Atkinson, 1989b). This positive effect is counteracted by the radical inhibition and NO_x removal processes caused by the nitrate formation reaction. Under high NO_x MIR conditions, it is the radical inhibition factor that is dominant, and the variability of overall reactivity from scenario to scenario is due to the variability of the relative importance of the radical inhibition vs. direct NO to NO_2 conversion effects. The NO_x removal effect of the nitrate formation reaction is unimportant. However, under low NO_x conditions, the NO_x removal factor becomes much more important than the radical inhibition factor, and thus the variability is due to the varying balance between this factor and the direct NO to NO_2 conversions.

It is interesting to note that the relative reactivities of the $C_{\geq 12}$ alkanes tend to be considerably less when ozone is quantified by the maximum 8-hour average than is the case when it is quantified by peak O_3 yields. The difference between the ozone yield and the 8-hour average relative reactivities increase with NO_x conditions. For example, the 8-hour average relative reactivities for the $C_{\geq 12}$ alkanes are about 40% higher in the MIR scenarios, about a factor of 2-4 higher in the MOIR scenarios, and in many cases negative in the EBIR scenarios. Apparently NO_x and radical inhibition effects tend to be more important in affecting average ozone levels than they are in affecting peak ozone yields.

In terms of comparing the individual n-alkane compounds, the calculations indicate that, as expected, the ozone impact decreases monotonically as the size of the compound increases. This is attributed to the fact that the nitrate yields decrease as the size of the molecule increase. In addition, the alkyl cyclohexanes tend to have somewhat higher reactivities, by about 5-25% on the average, than their normal alkane isomers. This is attributed to the somewhat larger number of NO to NO_2 conversions estimated to occur in the overall reactions of the alkyl cyclohexanes, as shown on Table 2, above. It cannot be due to differences in nitrate formation, since the overall nitrate yields for the alkyl cyclohexanes are slightly higher than from their normal alkane isomers (see Table 2).

The data are ambiguous in terms of the reactivities of these $C_{\geq 12}$ alkanes relative to ethane. No matter which ozone quantifications or NO_x levels are considered, there are scenarios where the $C_{\geq 12}$ alkane form more ozone than does an equal mass of ethane, and there are others where they either form less ozone or actually inhibit ozone levels. In terms of averages, the impacts of the $C_{\geq 12}$ alkanes on

maximum 8-hour average ozone levels are less than those of ethane under most conditions, while their impacts on peak ozone yields tend to be greater than ethane, except for the lower NO_x base case scenarios.

It is interesting to note that the average reactivities of the $C_{\geq 12}$ alkanes relative to ethane tend to be lower in the base case scenarios than in any of the adjusted NO_x scenarios. This is because many of the base case scenarios have lower relative NO_x levels than the lowest adjusted NO_x, EBIR scenarios. As indicated above, the relative NO_x levels of a scenario can be measured by the ratio of the NO_x inputs to the NO_x inputs yield the maximum ozone levels (the MOIR NO_x). It can be seen that a substantial number of base case scenarios have NO_x levels lower than EBIR, and it is these scenarios where the ozone yield reactivities tend to be lower than that for ethane or negative. Indeed, n-dodecane is calculated to have ozone yield reactivities less than that of ethane, and also to have negative maximum 8-hour average reactivities, for all scenarios where the NO_x levels are less than half that of MOIR levels. The NO_x dependence of the reactivities relative to NO_x is relatively small when NO_x is above EBIR levels, and other aspects of the scenarios appear to be relatively more important in determining reactivities relative to ethane. The specific factors that are the most important in this regard have not been identified.

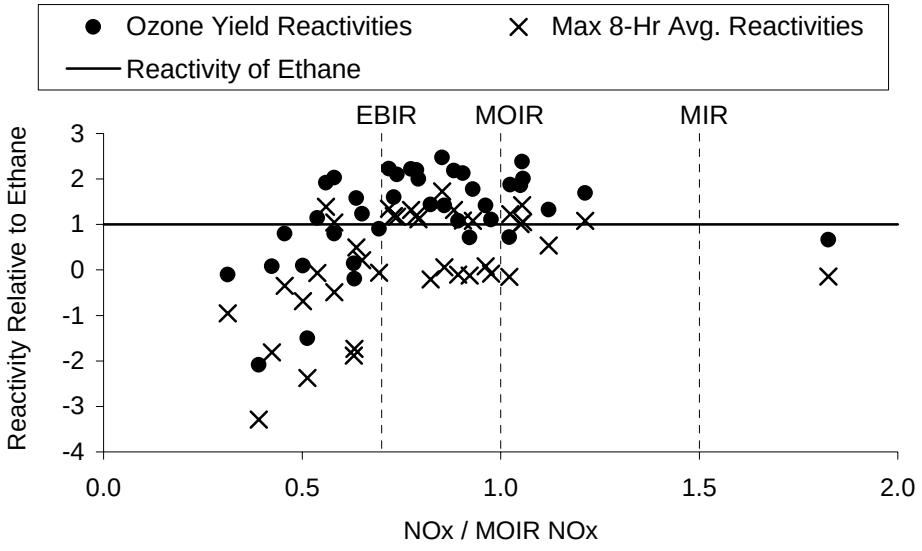

Figure 13. Plots of reactivities of n-dodecane relative to ethane in the base case scenarios against the ratio of NO_x inputs to the MOIR NO_x inputs.

CONCLUSIONS

The decision whether it is appropriate to regulate a group of compounds as ozone precursors requires a qualitative assessment of their ozone impacts under a variety of environmental conditions. This requires developing mechanisms for the relevant reactions of the subject compounds, verifying that the mechanisms can accurately predict the impacts of these compounds on ozone formation and other relevant measures or reactivity, and then using the mechanisms in airshed models to predict the impacts in representative atmospheric scenarios. Although estimated mechanisms for the higher alkanes have been available for some time (Carter, 1990), until the first phase of this project there have been no data to test the predictive capabilities of estimated mechanisms for the higher ($C_{\geq 12}$) n-alkanes, and until the second phase there were no data to test the mechanisms for the higher cycloalkanes. This project has been successful in providing the data needed to test the mechanisms for those compounds, allowing their atmospheric impacts to be predicted to a greater degree of reliability than was previously the case.

The alkane mechanisms derived using the estimation procedures and mechanism generation system associated with the SAPRC-99 mechanism (Carter, 2000) have been shown to give predictions that are consistent with the environmental chamber data obtained in both phases of this project. No adjustments had to be made to the estimated mechanisms to obtain the fits to attain successful model simulations of these data. The environmental chamber data represent a reasonable range of conditions in terms of relative NO_x levels, sensitivity of the mixture to radical levels, and the nature of the light source, which means that the testing of the mechanisms were reasonably comprehensive. Based on this, we conclude that the SAPRC-99 mechanism will probably give reasonably reliable predictions of the impacts of the C_{12} - C_{16} n-alkanes and of the C_{12} - C_{14} n-alkyl cyclohexanes on ozone formation and other measures of reactivity in the atmosphere, if the relevant scenario conditions are appropriately represented. Note that this mechanism has some substantial differences with the mechanisms used in our previous studies, and thus the alkane reactivity estimates in the Phase 1 report of Carter et al (1996) are superceded by this work.

It should be pointed out, however, that the available data do not definitively validate the mechanisms for all the higher alkane compounds. Because of experimental problems with handling low volatility compounds, data could not be obtained on normal alkanes heavier than n-hexadecane, even though such compounds still have sufficient volatility to react in the gas phase in the atmosphere, and contribute to ozone formation. However, based on the trends observed in this work and based on theoretical considerations, one would expect the $C_{>16}$ n-alkanes to be no more reactive than n-hexadecane, with the only uncertainty being how much less reactive they are. Thus if n-hexadecane is concluded to have “negligible” reactivity, it is probably reasonably safe to conclude that this is the case for the higher n-alkanes as well.

The situation is somewhat more uncertain in the case of the estimated reactivities of the branched and cyclic alkanes. The branched alkanes were not studied in this work, though data obtained under

separate funding indicated that the estimated mechanisms perform reasonably well in simulating results of experiments with several C_{10} branched alkanes (Carter et al, 2000b; Carter, 2000). A wide variety of branched and cyclic alkane isomers are possible for the higher carbon numbers, and it is only practical to study a small subset of the large number of possibilities. Although the data obtained in this project indicate that the mechanisms perform reasonably well for the n-alkyl cyclohexanes, data were not obtained to test the mechanisms derived for more branched cycloalkanes such as compounds with more than one substituent around the ring, or more than one ring. Therefore, reactivity estimates for unspeciated cyclic alkanes must necessarily be considered more uncertain. This would also be the case for the branched alkanes, though Carter et al (2000b) did obtain data on isomers with differing degrees of branching, though not with varying molecular weights.

Consistent with predictions using previous mechanisms (Carter, 1994a; Carter et al, 1996), the atmospheric ozone impacts for the higher alkanes were found to be highly dependent on conditions, both in an absolute sense and also relative to other VOCs such as ethane. Because of their strong radical inhibiting characteristics the $C_{\geq 12}$ alkanes were calculated to have relatively low ozone impacts, with ozone formation on a mass basis usually being less than 25% that of the mixture of compounds representing VOC emissions from all sources. However, the impacts relative to ethane, the compound that has been used as the standard defining "negligible" reactivity for VOC exemption purposes, are highly variable, depending not only on scenario conditions but also on how ozone impacts are quantified. In general, the relative ozone impacts of the higher alkanes are lower in scenarios with lower NO_x conditions (especially below EBIR levels) and the relative impacts on the maximum 8-hour average ozone tend to be lower (much lower some cases) than relative impacts on peak ozone yields. In general, the impacts of the $C_{\geq 12}$ alkanes on maximum 8-hour average ozone levels are less than those of ethane under most conditions, while their impacts on peak ozone yields tend to be greater than ethane, except for the lower NO_x base case scenarios. However, the results are highly variable and dependent on other scenario conditions besides NO_x.

Because of the relatively large dependence in calculated relative reactivities of the $C_{\geq 12}$ alkanes with scenario conditions, it is important that the set of scenarios used to assess their relative reactivities be reasonably representative of the distribution of conditions in the atmosphere. Although the EKMA scenarios used for the reactivity assessments in this work were designed to represent a range of conditions, they are obviously highly simplified representations of real urban areas. These simplifications are somewhat less of a concern when assessing ozone impacts of VOCs whose relative reactivities depend primarily on NO_x, since the use of the adjusted NO_x scenarios permit these NO_x effects to be systematically assessed. However, it is clear that other scenario conditions are affecting relative reactivities for the $C_{\geq 12}$ alkanes much greater than is the case for other VOCs, particularly at NO_x levels above EBIR, where VOC control is more effective than NO_x control for reducing ozone. Because of this, it may be appropriate to determine which scenario conditions are the most important in affecting predicted relative reactivities of these compounds, and to assure that the scenarios used to assess their reactivities represent these conditions appropriately.

REFERENCES

Arey, J., S. M. Aschmann, E. S. C. Kwok, and R. Atkinson (2000): Alkyl nitrate, hydroxyalkyl nitrate, and hydroxycarbonyl formation from the NO_x-air photooxidations of C_5-C_{10} n-alkanes. J. Phys. Chem. A, to be submitted for publication.

Atkinson, R. (1987): "A Structure-Activity Relationship for the Estimation of Rate Constants for the Gas-Phase Reactions of OH Radicals with Organic Compounds," Int. J. Chem. Kinet., 19, 799-828.

Atkinson, R. (1989): "Kinetics and Mechanisms of the Gas-Phase Reactions of the Hydroxyl Radical with Organic Compounds," J. Phys. Chem. Ref. Data, Monograph no 1.

Atkinson, R. (1997): "Gas Phase Tropospheric Chemistry of Volatile Organic Compounds: 1. Alkanes and Alkenes," J. Phys. Chem. Ref. Data, 26, 215-290.

Atkinson, R., S. M. Aschmann, W. P. L. Carter, A. M. Winer and J. N. Pitts, Jr. (1982): "Alkyl Nitrate Formation from the NO_x-Air Photooxidations of C_2-C_8 n-Alkanes," J. Phys. Chem. 86, 4562-4569.

Atkinson, R. and W. P. L. Carter (1984): "Kinetics and Mechanisms of the Gas-Phase Reactions of Ozone with Organic Compounds under Atmospheric Conditions," Chem. Rev. 84, 437-470.

Atkinson, R. et al. (2000) Manuscript on OH rate constants for branched alkanes. In preparation.

Baugues, K. (1990): "Preliminary Planning Information for Updating the Ozone Regulatory Impact Analysis Version of EKMA," Draft Document, Source Receptor Analysis Branch, Technical Support Division, U. S. Environmental Protection Agency, Research Triangle Park, NC, January.

Calvert, J. G., and J. N. Pitts, Jr. (1966): "Photochemistry," John Wiley and Sons, New York.

CARB (1999) California Air Resources Board, Proposed Regulation for Title 17, California Code of Regulations, Division 3, Chapter 1, Subchapter 8.5, Article 3.1, sections 94560- 94539.

Carter, W. P. L. (1990): "A Detailed Mechanism for the Gas-Phase Atmospheric Reactions of Organic Compounds," Atmos. Environ., 24A, 481-518.

Carter, W. P. L. (1994a): "Development of Ozone Reactivity Scales for Volatile Organic Compounds," J. Air & Waste Manage. Assoc., 44, 881-899.

Carter, W. P. L. (1994b): "Calculation of Reactivity Scales Using an Updated Carbon Bond IV Mechanism," Report Prepared for Systems Applications International Under Funding from the Auto/Oil Air Quality Improvement Research Program, April 12. Available at http://helium.ucr.edu/~carter/absts.htm#cb4rct.

Carter, W. P. L. (2000): "Documentation of the SAPRC-99 Chemical Mechanism for VOC Reactivity Assessment," Report to the California Air Resources Board, Contracts 92-329 and 95-308, May 8. Available at http://helium.ucr.edu/~carter/absts.htm#saprc99.

Carter, W. P. L., and R. Atkinson (1985): "Atmospheric Chemistry of Alkanes", J. Atmos. Chem., 3, 377-405, 1985.

Carter, W. P. L. and R. Atkinson (1987): "An Experimental Study of Incremental Hydrocarbon Reactivity," Environ. Sci. Technol., 21, 670-679

Carter, W. P. L. and R. Atkinson (1989a): "Alkyl Nitrate Formation from the Atmospheric Photooxidation of Alkanes; a Revised Estimation Method," J. Atm. Chem. 8, 165-173.

Carter, W. P. L. and R. Atkinson (1989b): "A Computer Modeling Study of Incremental Hydrocarbon Reactivity", Environ. Sci. Technol., 23, 864.

Carter, W. P. L., and F. W. Lurmann (1990): "Evaluation of the RADM Gas-Phase Chemical Mechanism," Final Report, EPA-600/3-90-001.

Carter, W. P. L. and F. W. Lurmann (1991): "Evaluation of a Detailed Gas-Phase Atmospheric Reaction Mechanism using Environmental Chamber Data," Atm. Environ. 25A, 2771-2806.

Carter, W. P. L., J. A. Pierce, I. L. Malkina, D. Luo and W. D. Long (1993): "Environmental Chamber Studies of Maximum Incremental Reactivities of Volatile Organic Compounds," Report to Coordinating Research Council, Project No. ME-9, California Air Resources Board Contract No. A032-0692; South Coast Air Quality Management District Contract No. C91323, United States Environmental Protection Agency Cooperative Agreement No. CR-814396-01-0, University Corporation for Atmospheric Research Contract No. 59166, and Dow Corning Corporation. April 1. Available at http://helium.ucr.edu/~carter/absts.htm#rct1rept.

Carter, W. P. L. and C. Venkataraman (1995): "Atmospheric Ozone Formation Potential of Common Aluminum Rolling Lubricant Constituents," Report to Alcoa Aluminum Co., April 9, 1995.

Carter, W. P. L., J. A. Pierce, D. Luo, and I. L. Malkina (1995a): "Environmental Chamber Studies of Maximum Incremental Reactivities of Volatile Organic Compounds," Atmos. Environ. 29, 2499-2511.

Carter, W. P. L., D. Luo, I. L. Malkina, and J. A. Pierce (1995b): "Environmental Chamber Studies of Atmospheric Reactivities of Volatile Organic Compounds. Effects of Varying ROG Surrogate and NO_x," Final report to Coordinating Research Council, Inc., Project ME-9, California Air Resources Board, Contract A032-0692, and South Coast Air Quality Management District, Contract C91323. March 24. Available at http://helium.ucr.edu/~carter/absts.htm#rct2rept.

Carter, W. P. L., D. Luo, I. L. Malkina, and D. Fitz (1995c): "The University of California, Riverside Environmental Chamber Data Base for Evaluating Oxidant Mechanism. Indoor Chamber Experiments through 1993," Report submitted to the U. S. Environmental Protection Agency, EPA/AREAL, Research Triangle Park, NC., March 20. Available at http://helium.ucr.edu/~carter/absts.htm#databas.

Carter, W. P. L., D. Luo, I. L. Malkina, and J. A. Pierce (1995d): "Environmental Chamber Studies of Atmospheric Reactivities of Volatile Organic Compounds. Effects of Varying Chamber and Light Source," Final report to National Renewable Energy Laboratory, Contract XZ-2-12075, Coordinating Research Council, Inc., Project M-9, California Air Resources Board, Contract A032-0692, and South Coast Air Quality Management District, Contract C91323, March 26. Available at http://helium.ucr.edu/~carter/absts.htm#explrept.

Carter, W. P. L., D. Luo, and I. L. Malkina (1996): "Investigation of Atmospheric Ozone Formation Potentials of C_{12} - C_{16} n-Alkanes," Report to the Aluminum Association, October 28. Available at http://cert.ucr.edu/~carter/absts.htm#alkrept.

Carter, W. P. L., D. Luo, and I. L. Malkina (1997a): "Environmental Chamber Studies for Development of an Updated Photochemical Mechanism for VOC Reactivity Assessment," Final report to the California Air Resources Board, the Coordinating Research Council, and the National Renewable Energy Laboratory, November 26. Available at http://helium.ucr.edu/~carter/absts.htm#rct3rept.

Carter, W. P. L., D. Luo, and I. L. Malkina (1997b): "Investigation of the Atmospheric Ozone Formation Potentials of Selected Mineral Spirits Mixtures," Report to Safety-Kleen Corporation, July 25. Available at http://cert.ucr.edu/~carter/absts.htm#msrept.

Carter. W. P. L., D. Luo and I. L. Malkina (2000a): "Investigation of Atmospheric Reactivities of Selected Consumer Product VOCs," Report to California Air Resources Board, May 30. Available at http://helium.ucr.edu/~carter/absts.htm#cpreport.

Carter, W. P. L., D. Luo, and I. L. Malkina (2000b): "Investigation of the Ozone Formation Potentials of Selected Branched Alkanes and Mineral Spirits Samples," Report to the Safety-Kleen Corporation, in preparation.

Chang, T. Y. and S. J. Rudy (1990): "Ozone-Forming Potential of Organic Emissions from Alternative-Fueled Vehicles," Atmos. Environ., 24A, 2421-2430.

Croes, B. E., Technical Support Division, California Air Resources Board, personal communication (1991).

Croes, B. E., et al. (1994): "Southern California Air Quality Study Data Archive," Research Division, California Air Resources Board.

Dasgupta, P. K, Dong, S. and Hwang, H. (1988): "Continuous Liquid Phase Fluorometry Coupled to a Diffusion Scrubber for the Determination of Atmospheric Formaldehyde, Hydrogen Peroxide, and Sulfur Dioxide," Atmos. Environ. 22, 949-963.

Dasgupta, P.K, Dong, S. and Hwang, H. (1990): Aerosol Science and Technology 12, 98-104

Dimitriades, B. (1999): "Scientific Basis of an Improved EPA Policy on Control of Organic Emissions for Ambient Ozone Reduction," J. Air & Waste Manage. Assoc. 49, 831-838

Dodge, M. C. (1984): "Combined effects of organic reactivity and NMHC/NOx ratio on photochemical oxidant formation -- a modeling study," Atmos. Environ., 18, 1657.

Eberhard, J., C. Muller, D. W. Stocker and J. A. Kerr (1995): "Isomerization of Alkoxy Radicals under Atmospheric Conditions," Environ. Sci. Technol. 29, 232.

EPA (1984): "Guideline for Using the Carbon Bond Mechanism in City-Specific EKMA," EPA-450/4-84-005, February.

Gery, M. W., R. D. Edmond and G. Z. Whitten (1987): "Tropospheric Ultraviolet Radiation. Assessment of Existing Data and Effects on Ozone Formation," Final Report, EPA-600/3-87-047, October.

Gipson, G. L., W. P. Freas, R. A. Kelly and E. L. Meyer (1981): "Guideline for Use of City-Specific EKMA in Preparing Ozone SIPs, EPA-450/4-80-027, March.

Gipson, G. L. and W. P. Freas (1983): "Use of City-Specific EKMA in the Ozone RIA," U. S. Environmental Protection Agency, July.

Johnson, G. M. (1983): "Factors Affecting Oxidant Formation in Sydney Air," in "The Urban Atmosphere -- Sydney, a Case Study." Eds. J. N. Carras and G. M. Johnson (CSIRO, Melbourne), pp. 393-408.

Jeffries, H. E. (1991): "UNC Solar Radiation Models," unpublished draft report for EPA Cooperative Agreements CR813107, CR813964 and CR815779".

Jeffries, H. E., K. G. Sexton, J. R. Arnold, and T. L. Kale (1989): "Validation Testing of New Mechanisms with Outdoor Chamber Data. Volume 2: Analysis of VOC Data for the CB4 and CAL Photochemical Mechanisms," Final Report, EPA-600/3-89-010b.

Jeffries, H. E. and R. Crouse (1991): "Scientific and Technical Issues Related to the Application of Incremental Reactivity. Part II: Explaining Mechanism Differences," Report prepared for Western States Petroleum Association, Glendale, CA, October.

Kwok, E. S. C., and R. Atkinson (1995): "Estimation of Hydroxyl Radical Reaction Rate Constants for Gas-Phase Organic Compounds Using a Structure-Reactivity Relationship: An Update," Atmos. Environ 29, 1685-1695.

Kwok, E. S. C., J. Arey and R. Atkinson (1996): "Alkoxy radical isomerization in the OH radical-initiated reactions of C4-C8 n-alkanes," J. Phys. Chem., 100, 214-219.

Lurmann, F. W. and H. H. Main (1992): "Analysis of the Ambient VOC Data Collected in the Southern California Air Quality Study," Final Report to California Air Resources Board Contract No. A832-130, February.

McBride, S., M. Oravetz, and A.G. Russell. 1997. "Cost-Benefit and Uncertainty Issues Using Organic Reactivity to Regulate Urban Ozone." Environ. Sci. Technol. 35, A238-44.

RRWG (1999): "VOC Reactivity Policy White Paper," Prepared by the Reactivity Research Work Group Policy Team, October 1. Available at http://www.cgenv.com/Narsto/reactinfo.html.

Zafonte, L., P. L. Rieger, and J. R. Holmes (1977): "Nitrogen Dioxide Photolysis in the Los Angeles Atmosphere," Environ. Sci. Technol. 11, 483-487.

APPENDIX A.
MECHANISM LISTING AND TABULATIONS

This Appendix gives a complete listing of the mechanisms used in the model simulations in this report. Table A-1 contains a list of all the model species used in the mechanism, and Table A-2 lists the reactions and rate parameters, and Table A-3 lists the absorption cross sections and quantum yields for the photolysis reactions. In addition, Finally, Table A-4 gives the chamber-dependent parameters used in the model simulations of the chamber experiments.

Table A-1. Listing of the model species in the mechanism used in the model simulations discussed in this report.

Type and Name	Description
	Species used in Base Mechanism
Constant Species.	
O2	Oxygen
M	Air
H2O	Water
H2	Hydrogen Molecules
HV	Light
Active Inorganic Species.	
O3	Ozone
NO	Nitric Oxide
NO2	Nitrogen Dioxide
NO3	Nitrate Radical
N2O5	Nitrogen Pentoxide
HONO	Nitrous Acid
HNO3	Nitric Acid
HNO4	Peroxynitric Acid
HO2H	Hydrogen Peroxide
CO	Carbon Monoxide
SO2	Sulfur Dioxide
Active Radical Species and Operators.	
HO.	Hydroxyl Radicals
HO2.	Hydroperoxide Radicals
C-O2.	Methyl Peroxy Radicals
RO2-R.	Peroxy Radical Operator representing NO to NO2 conversion with HO2 formation.
R2O2.	Peroxy Radical Operator representing NO to NO2 conversion without HO2 formation.
RO2-N.	Peroxy Radical Operator representing NO consumption with organic nitrate formation.
CCO-O2.	Acetyl Peroxy Radicals
RCO-O2.	Peroxy Propionyl and higher peroxy acyl Radicals

Table A-1 (continued)

Type and Name	Description
BZCO-O2.	Peroxyacyl radical formed from Aromatic Aldehydes
MA-RCO3.	Peroxyacyl radicals formed from methacrolein and other acroleins.
Steady State Radical Species	
O3P	Ground State Oxygen Atoms
O*1D2	Excited Oxygen Atoms
TBU-O.	t-Butoxy Radicals
BZ-O.	Phenoxy Radicals
BZ(NO2)-O.	Nitro-substituted Phenoxy Radical
HOCOO.	Radical formed when Formaldehyde reacts with HO2
PAN and PAN Analogues	
PAN	Peroxy Acetyl Nitrate
PAN2	PPN and other higher alkyl PAN analogues
PBZN	PAN analogues formed from Aromatic Aldehydes
MA-PAN	PAN analogue formed from Methacrolein
Explicit and Lumped Molecule Reactive Organic Product Species	
HCHO	Formaldehyde
CCHO	Acetaldehyde
RCHO	Lumped C3+ Aldehydes
ACET	Acetone
MEK	Ketones and other non-aldehyde oxygenated products that react with OH radicals slower than 5×10^{-12} cm^3 $molec^{-2}$ sec^{-1}.
MEOH	Methanol
COOH	Methyl Hydroperoxide
ROOH	Lumped higher organic hydroperoxides
GLY	Glyoxal
MGLY	Methyl Glyoxal
BACL	Biacetyl
PHEN	Phenol
CRES	Cresols
NPHE	Nitrophenols
BALD	Aromatic aldehydes (e.g., benzaldehyde)
METHACRO	Methacrolein
MVK	Methyl Vinyl Ketone
ISO-PROD	Lumped isoprene product species
Lumped Parameter Products	
PROD2	Ketones and other non-aldehyde oxygenated products that react with OH radicals faster than 5×10^{-12} cm^3 $molec^{-2}$ sec^{-1}.
RNO3	Lumped Organic Nitrates
Uncharacterized Reactive Aromatic Ring Fragmentation Products	
DCB1	Reactive Aromatic Fragmentation Products that do not undergo significant photodecomposition to radicals.
DCB2	Reactive Aromatic Fragmentation Products which photolyze with alpha-dicarbonyl-like action spectrum.
DCB3	Reactive Aromatic Fragmentation Products which photolyze with acrolein action spectrum.

Table A-1 (continued)

Type and Name	Description
Non-Reacting Species	
CO2	Carbon Dioxide
XC	Lost Carbon
XN	Lost Nitrogen
SULF	Sulfates (SO_3 or H_2SO_4)
Low Reactivity Compounds or Unknown Products Represented as Unreactive	
H2	Hydrogen
HCOOH	Formic Acid
CCO-OH	Acetic Acid
RCO-OH	Higher organic acids
CCO-OOH	Peroxy Acetic Acid
RCO-OOH	Higher organic peroxy acids
NROG	Unspecified Unreactive Carbon
	Base ROG VOC Species used in the Chamber Simulations
N-C4	n-Butane
N-C6	n-Hexane
N-C8	n-Octane
ETHENE	Ethene
PROPENE	Propene
T-2-BUTE	*Trans*-2-Butene
TOLUENE	Toluene
M-XYLENE	m-Xylene
	Test Compounds Studied for this Project
N-C12	n-Dodecane
N-C14	n-Tetradecane
N-C15	n-Pentadecane
N-C16	n-Hexadecane
C6-CYCC6	Hexyl Cyclohexane
C8-CYCC6	Octyl Cyclohexane
	Lumped Higher Ketone Products from the Alkane Test Compounds
PRD-NC12	Lumped higher ketones formed in the reaction of OH with n-dodecane. The compounds represented by this model species are listed in Table 3.
PRD-NC14	Lumped higher ketones formed in the reaction of OH with n-tetradecane. The compounds represented by this model species are analogous to those listed in Table 3 for n-dodecane.
PRD-NC15	Lumped higher ketones formed in the reaction of OH with n-pentadecane. The compounds represented by this model species are analogous to those listed in Table 3 for n-dodecane.
PRD-NC16	Lumped higher ketones formed in the reaction of OH with n-hexadecane. The compounds represented by this model species are analogous to those listed in Table 3 for n-dodecane.
PRD-CC12	Lumped higher ketones formed in the reaction of OH with hexyl cyclohexane. The compounds represented by this model species are listed in Table 3.

Table A-1 (continued)

Type and Name	Description
PRD-CC14	Lumped higher ketones formed in the reaction of OH with octyl cyclohexane. The compounds represented by this model species are analogous to those listed in Table 3 for hexyl cyclohexane.
	Explicit and Lumped VOC Species used in the Ambient Simulations
Primary Organics Represented explicitly	
CH4	Methane
ETHENE	Ethene
ISOPRENE	Isoprene
Example Test VOCs not in the Base Mechanism	
ETHANE	Ethane
Lumped Parameter Species	
ALK1	Alkanes and other non-aromatic compounds that react only with OH, and have kOH < 5 x 10^2 ppm-1 min-1. (Primarily ethane)
ALK2	Alkanes and other non-aromatic compounds that react only with OH, and have kOH between 5 x 10^2 and 2.5 x 10^3 ppm-1 min-1. (Primarily propane and acetylene)
ALK3	Alkanes and other non-aromatic compounds that react only with OH, and have kOH between 2.5 x 10^3 and 5 x 10^3 ppm-1 min-1.
ALK4	Alkanes and other non-aromatic compounds that react only with OH, and have kOH between 5 x 10^3 and 1 x 10^4 ppm-1 min-1.
ALK5	Alkanes and other non-aromatic compounds that react only with OH, and have kOH greater than 1 x 10^4 ppm-1 min-1.
ARO1	Aromatics with kOH < 2x10^4 ppm-1 min-1.
ARO2	Aromatics with kOH > 2x10^4 ppm-1 min-1.
OLE1	Alkenes (other than ethene) with kOH < 7x10^4 ppm-1 min-1.
OLE2	Alkenes with kOH > 7x10^4 ppm-1 min-1.
TERP	Terpenes

Table A-2. Listing of the reactions in the mechanism used in the model simulations discussed in this report. See Carter (2000) for documentation.

Label	Rate Parameters [a] k(298)	A	Ea	B	Reaction and Products [b]
Inorganic Reactions					
1		Phot Set= NO2			NO2 + HV = NO + O3P
2	5.79e-34	5.68e-34	0.00	-2.8	O3P + O2 + M = O3 + M
3	7.96e-15	8.00e-12	4.09		O3P + O3 = #2 O2
4	1.01e-31	1.00e-31	0.00	-1.6	O3P + NO + M = NO2 + M
5	9.72e-12	6.50e-12	-0.24		O3P + NO2 = NO + O2
6	1.82e-12	Falloff, F=0.80			O3P + NO2 = NO3 + M
	0:	9.00e-32	0.00	-2.0	
	inf:	2.20e-11	0.00	0.0	
8	1.81e-14	1.80e-12	2.72		O3 + NO = NO2 + O2
9	3.52e-17	1.40e-13	4.91		O3 + NO2 = O2 + NO3
10	2.60e-11	1.80e-11	-0.22		NO + NO3 = #2 NO2
11	1.95e-38	3.30e-39	-1.05		NO + NO + O2 = #2 NO2
12	1.54e-12	Falloff, F=0.45			NO2 + NO3 = N2O5
	0:	2.80e-30	0.00	-3.5	
	inf:	2.00e-12	0.00	0.2	
13	5.28e-2	Falloff, F=0.45			N2O5 = NO2 + NO3
	0:	1.00e-3	21.86	-3.5	
	inf:	9.70e+14	22.02	0.1	
14	2.60e-22	2.60e-22			N2O5 + H2O = #2 HNO3
15		(Slow)			N2O5 + HV = NO3 + NO + O3P
16		(Slow)			N2O5 + HV = NO3 + NO2
17	6.56e-16	4.50e-14	2.50		NO2 + NO3 = NO + NO2 + O2
18		Phot Set= NO3NO			NO3 + HV = NO + O2
19		Phot Set= NO3NO2			NO3 + HV = NO2 + O3P
20		Phot Set= O3O3P			O3 + HV = O3P + O2
21		Phot Set= O3O1D			O3 + HV = O*1D2 + O2
22	2.20e-10	2.20e-10			O*1D2 + H2O = #2 HO.
23	2.87e-11	2.09e-11	-0.19		O*1D2 + M = O3P + M
24	7.41e-12	Falloff, F=0.60			HO. + NO = HONO
	0:	7.00e-31	0.00	-2.6	
	inf:	3.60e-11	0.00	-0.1	
25		Phot Set= HONO-NO			HONO + HV = HO. + NO
26		Phot Set= HONO-NO2			HONO + HV = HO2. + NO2
27	6.46e-12	2.70e-12	-0.52		HO. + HONO = H2O + NO2
28	8.98e-12	Falloff, F=0.60			HO. + NO2 = HNO3
	0:	2.43e-30	0.00	-3.1	
	inf:	1.67e-11	0.00	-2.1	
29	2.00e-11	2.00e-11			HO. + NO3 = HO2. + NO2
30	1.47e-13	k = k0+k3M/(1+k3M/k2)			HO. + HNO3 = H2O + NO3
	k0:	7.20e-15	-1.56	0.0	
	k2:	4.10e-16	-2.86	0.0	
	k3:	1.90e-33	-1.44	0.0	
31		Phot Set= HNO3			HNO3 + HV = HO. + NO2
32	2.09e-13	k = k1 + k2 [M]			HO. + CO = HO2. + CO2
	k1:	1.30e-13	0.00	0.0	
	k2:	3.19e-33	0.00	0.0	

Table A-2 (continued)

Label	Rate Parameters [a] k(298)	A	Ea	B	Reaction and Products [b]
33	6.63e-14	1.90e-12	1.99		HO. + O3 = HO2. + O2
34	8.41e-12	3.40e-12	-0.54		HO2. + NO = HO. + NO2
35	1.38e-12	Falloff, F=0.60			HO2. + NO2 = HNO4
	0:	1.80e-31	0.00	-3.2	
	inf:	4.70e-12	0.00	0.0	
36	7.55e-2	Falloff, F=0.50			HNO4 = HO2. + NO2
	0:	4.10e-5	21.16	0.0	
	inf:	5.70e+15	22.20	0.0	
37	Phot Set= HO2NO2				HNO4 + HV = #.61 {HO2. + NO2} + #.39 {HO. + NO3}
38	5.02e-12	1.50e-12	-0.72		HNO4 + HO. = H2O + NO2 + O2
39	1.87e-15	1.40e-14	1.19		HO2. + O3 = HO. + #2 O2
40A	2.87e-12	k = k1 + k2 [M]			HO2. + HO2. = HO2H + O2
	k1:	2.20e-13	-1.19	0.0	
	k2:	1.85e-33	-1.95	0.0	
40B	6.46e-30	k = k1 + k2 [M]			HO2. + HO2. + H2O = HO2H + O2 + H2O
	k1:	3.08e-34	-5.56	0.0	
	k2:	2.59e-54	-6.32	0.0	
41	4.00e-12	4.00e-12			NO3 + HO2. = #.8 {HO. + NO2 + O2} + #.2 {HNO3 + O2}
42	2.28e-16	8.50e-13	4.87		NO3 + NO3 = #2 NO2 + O2
43	Phot Set= H2O2				HO2H + HV = #2 HO.
44	1.70e-12	2.90e-12	0.32		HO2H + HO. = HO2. + H2O
45	1.11e-10	4.80e-11	-0.50		HO. + HO2. = H2O + O2
S2OH	9.77e-13	Falloff, F=0.45			HO. + SO2 = HO2. + SULF
	0:	4.00e-31	0.00	-3.3	
	inf:	2.00e-12	0.00	0.0	
H2OH	6.70e-15	7.70e-12	4.17		HO. + H2 = HO2. + H2O
Methyl peroxy and methoxy reactions					
MER1	7.29e-12	2.80e-12	-0.57		C-O2. + NO = NO2 + HCHO + HO2.
MER4	5.21e-12	3.80e-13	-1.55		C-O2. + HO2. = COOH + O2
MEN3	1.30e-12	1.30e-12			C-O2. + NO3 = HCHO + HO2. + NO2
MER5	2.65e-13	2.45e-14	-1.41		C-O2. + C-O2. = MEOH + HCHO + O2
MER6	1.07e-13	5.90e-13	1.01		C-O2. + C-O2. = #2 {HCHO + HO2.}
Peroxy Racical Operators					
RRNO	9.04e-12	2.70e-12	-0.72		RO2-R. + NO = NO2 + HO2.
RRH2	1.49e-11	1.90e-13	-2.58		RO2-R. + HO2. = ROOH + O2 + #-3 XC
RRN3	2.30e-12	2.30e-12			RO2-R. + NO3 = NO2 + O2 + HO2.
RRME	2.00e-13	2.00e-13			RO2-R. + C-O2. = HO2. + #.75 HCHO + #.25 MEOH
RRR2	3.50e-14	3.50e-14			RO2-R. + RO2-R. = HO2.
R2NO	Same k as rxn RRNO				R2O2. + NO = NO2
R2H2	Same k as rxn RRH2				R2O2. + HO2. = HO2.
R2N3	Same k as rxn RRN3				R2O2. + NO3 = NO2
R2ME	Same k as rxn RRME				R2O2. + C-O2. = C-O2.
R2RR	Same k as rxn RRR2				R2O2. + RO2-R. = RO2-R.
R2R3	Same k as rxn RRR2				R2O2. + R2O2. =
RNNO	Same k as rxn RRNO				RO2-N. + NO = RNO3
RNH2	Same k as rxn RRH2				RO2-N. + HO2. = ROOH + #3 XC

Table A-2 (continued)

Label	Rate Parameters [a] k(298)	A	Ea	B	Reaction and Products [b]
RNME	Same k as rxn RRME				RO2-N. + C-O2. = HO2. + #.25 MEOH + #.5 {MEK + PROD2} + #.75 HCHO + XC
RNN3	Same k as rxn RRN3				RO2-N. + NO3 = NO2 + O2 + HO2. + MEK + #2 XC
RNRR	Same k as rxn RRR2				RO2-N. + RO2-R. = HO2. + #.5 {MEK + PROD2} + O2 + XC
RNR2	Same k as rxn RRR2				RO2-N. + R2O2. = RO2-N.
RNRN	Same k as rxn RRR2				RO2-N. + RO2-N. = MEK + HO2. + PROD2 + O2 + #2 XC
APN2	1.05e-11	Falloff, F=0.30			CCO-O2. + NO2 = PAN
	0:	2.70e-28	0.00	-7.1	
	inf:	1.20e-11	0.00	-0.9	
DPAN	5.21e-4	Falloff, F=0.30			PAN = CCO-O2. + NO2
	0:	4.90e-3	24.05	0.0	
	inf:	4.00e+16	27.03	0.0	
APNO	2.13e-11	7.80e-12	-0.60		CCO-O2. + NO = C-O2. + CO2 + NO2
APH2	1.41e-11	4.30e-13	-2.07		CCO-O2. + HO2. = #.75 {CCO-OOH +O2} + #.25 {CCO-OH + O3}
APN3	4.00e-12	4.00e-12			CCO-O2. + NO3 = C-O2. + CO2 + NO2 + O2
APME	9.64e-12	1.80e-12	-0.99		CCO-O2. + C-O2. = CCO-OH + HCHO + O2
APRR	7.50e-12	7.50e-12			CCO-O2. + RO2-R. = CCO-OH
APR2	Same k as rxn APRR				CCO-O2. + R2O2. = CCO-O2.
APRN	Same k as rxn APRR				CCO-O2. + RO2-N. = CCO-OH + PROD2
APAP	1.55e-11	2.90e-12	-0.99		CCO-O2. + CCO-O2. = #2 {C-O2. + CO2} + O2
PPN2	1.21e-11	1.20e-11	0.00	-0.9	RCO-O2. + NO2 = PAN2
PAN2	4.43e-4	2.00e+15	25.44		PAN2 = RCO-O2. + NO2
PPNO	2.80e-11	1.25e-11	-0.48		RCO-O2. + NO = NO2 + CCHO + RO2-R. + CO2
PPH2	Same k as rxn APH2				RCO-O2. + HO2. = #.75 {RCO-OOH + O2} + #.25 {RCO-OH + O3}
PPN3	Same k as rxn APN3				RCO-O2. + NO3 = NO2 + CCHO + RO2-R. + CO2 + O2
PPME	Same k as rxn APME				RCO-O2. + C-O2. = RCO-OH + HCHO + O2
PPRR	Same k as rxn APRR				RCO-O2. + RO2-R. = RCO-OH + O2
PPR2	Same k as rxn APRR				RCO-O2. + R2O2. = RCO-O2.
PPRN	Same k as rxn APRR				RCO-O2. + RO2-N. = RCO-OH + PROD2 + O2
PPAP	Same k as rxn APAP				RCO-O2. + CCO-O2. = #2 CO2 + C-O2. + CCHO + RO2-R. + O2
PPPP	Same k as rxn APAP				RCO-O2. + RCO-O2. = #2 {CCHO + RO2-R. + CO2}
BPN2	1.37e-11	1.37e-11			BZCO-O2. + NO2 = PBZN
BPAN	3.12e-4	7.90e+16	27.82		PBZN = BZCO-O2. + NO2
BPNO	Same k as rxn PPNO				BZCO-O2. + NO = NO2 + CO2 + BZ-O. + R2O2.
BPH2	Same k as rxn APH2				BZCO-O2. + HO2. = #.75 {RCO-OOH + O2} + #.25 {RCO-OH + O3} + #4 XC
BPN3	Same k as rxn APN3				BZCO-O2. + NO3 = NO2 + CO2 + BZ-O. + R2O2. + O2
BPME	Same k as rxn APME				BZCO-O2. + C-O2. = RCO-OH + HCHO + O2 + #4 XC
BPRR	Same k as rxn APRR				BZCO-O2. + RO2-R. = RCO-OH + O2 + #4 XC
BPR2	Same k as rxn APRR				BZCO-O2. + R2O2. = BZCO-O2.
BPRN	Same k as rxn APRR				BZCO-O2. + RO2-N. = RCO-OH + PROD2 + O2 + #4 XC
BPAP	Same k as rxn APAP				BZCO-O2. + CCO-O2. = #2 CO2 + C-O2. + BZ-O. + R2O2.
BPPP	Same k as rxn APAP				BZCO-O2. + RCO-O2. = #2 CO2 + CCHO + RO2-R. + BZ-O. + R2O2.
BPBP	Same k as rxn APAP				BZCO-O2. + BZCO-O2. = #2 {BZ-O. + R2O2. + CO2}

Table A-2 (continued)

Label	Rate Parameters [a] k(298)	A	Ea	B	Reaction and Products [b]
MPN2	Same k as rxn PPN2				MA-RCO3. + NO2 = MA-PAN
MPPN	3.55e-4	1.60e+16	26.80		MA-PAN = MA-RCO3. + NO2
MPNO	Same k as rxn PPNO				MA-RCO3. + NO = NO2 + CO2 + HCHO + CCO-O2.
MPH2	Same k as rxn APH2				MA-RCO3. + HO2. = #.75 {RCO-OOH + O2} + #.25 {RCO-OH + O3} + XC
MPN3	Same k as rxn APN3				MA-RCO3. + NO3 = NO2 + CO2 + HCHO + CCO-O2. + O2
MPME	Same k as rxn APME				MA-RCO3. + C-O2. = RCO-OH + HCHO + XC + O2
MPRR	Same k as rxn APRR				MA-RCO3. + RO2-R. = RCO-OH + XC
MPR2	Same k as rxn APRR				MA-RCO3. + R2O2. = MA-RCO3.
MPRN	Same k as rxn APRR				MA-RCO3. + RO2-N. = #2 RCO-OH + O2 + #4 XC
MPAP	Same k as rxn APAP				MA-RCO3. + CCO-O2. = #2 CO2 + C-O2. + HCHO + CCO-O2. + O2
MPPP	Same k as rxn APAP				MA-RCO3. + RCO-O2. = HCHO + CCO-O2. + CCHO + RO2-R. + #2 CO2
MPBP	Same k as rxn APAP				MA-RCO3. + BZCO-O2. = HCHO + CCO-O2. + BZ-O. + R2O2. + #2 CO2
MPMP	Same k as rxn APAP				MA-RCO3. + MA-RCO3. = #2 {HCHO + CCO-O2. + CO2}
Other Organic Radical Species					
TBON	2.40e-11	2.40e-11			TBU-O. + NO2 = RNO3 + #-2 XC
TBOD	9.87e+2	7.50e+14	16.20		TBU-O. = ACET + C-O2.
BRN2	3.80e-11	2.30e-11	-0.30		BZ-O. + NO2 = NPHE
BRH2	Same k as rxn RRH2				BZ-O. + HO2. = PHEN
BRXX	1.00e-3	1.00e-3			BZ-O. = PHEN
BNN2	Same k as rxn BRN2				BZ(NO2)-O. + NO2 = #2 XN + #6 XC
BNH2	Same k as rxn RRH2				BZ(NO2)-O. + HO2. = NPHE
BNXX	Same k as rxn BRXX				BZ(NO2)-O. = NPHE
Explicit and Lumped Molecule Organic Products					
FAHV	Phot Set= HCHO_R				HCHO + HV = #2 HO2. + CO
FAVS	Phot Set= HCHO_M				HCHO + HV = H2 + CO
FAOH	9.20e-12	8.60e-12	-0.04		HCHO + HO. = HO2. + CO + H2O
FAH2	7.90e-14	9.70e-15	-1.24		HCHO + HO2. = HOCOO.
FAHR	1.51e+2	2.40e+12	13.91		HOCOO. = HO2. + HCHO
FAHN	Same k as rxn MER1				HOCOO. + NO = HCOOH + NO2 + HO2.
FAN3	5.74e-16	2.00e-12	4.83		HCHO + NO3 = HNO3 + HO2. + CO
AAOH	1.58e-11	5.60e-12	-0.62		CCHO + HO. = CCO-O2. + H2O
AAHV	Phot Set= CCHO_R				CCHO + HV = CO + HO2. + C-O2.
AAN3	2.73e-15	1.40e-12	3.70		CCHO + NO3 = HNO3 + CCO-O2.
PAOH	2.00e-11	2.00e-11			RCHO + HO. = #.034 RO2-R. + #.001 RO2-N. + #.965 RCO-O2. + #.034 CO + #.034 CCHO + #-0.003 XC
PAHV	Phot Set= C2CHO				RCHO + HV = CCHO + RO2-R. + CO + HO2.
PAN3	3.67e-15	1.40e-12	3.52		RCHO + NO3 = HNO3 + RCO-O2.
K3OH	1.92e-13	1.10e-12	1.03		ACET + HO. = HCHO + CCO-O2. + R2O2.
K3HV	Phot Set= ACETONE				ACET + HV = CCO-O2. + C-O2.

Table A-2 (continued)

Label	Rate Parameters [a] k(298)	A	Ea	B	Reaction and Products [b]
K4OH	1.18e-12	1.30e-12	0.05	2.0	MEK + HO. = #.37 RO2-R. + #.042 RO2-N. + #.616 R2O2. + #.492 CCO-O2. + #.096 RCO-O2. + #.115 HCHO + #.482 CCHO + #.37 RCHO + #.287 XC
K4HV	Phot Set= KETONE, qy= 1.5e-1				MEK + HV = CCO-O2. + CCHO + RO2-R.
MeOH	9.14e-13	3.10e-12	0.72	2.0	MEOH + HO. = HCHO + HO2.
MER9	5.49e-12	2.90e-12	-0.38		COOH + HO. = H2O + #.35 {HCHO + HO.} + #.65 C-O2.
MERA	Phot Set= COOH				COOH + HV = HCHO + HO2. + HO.
LPR9	1.10e-11	1.10e-11			ROOH + HO. = H2O + RCHO + #.34 RO2-R. + #.66 HO.
LPRA	Phot Set= COOH				ROOH + HV = RCHO + HO2. + HO.
GLHV	Phot Set= GLY_R				GLY + HV = #2 {CO + HO2.}
GLVM	Phot Set= GLY_ABS, qy= 6.0e-3				GLY + HV = HCHO + CO
GLOH	1.10e-11	1.10e-11			GLY + HO. = #.63 HO2. + #1.26 CO + #.37 RCO-O2. + #-.37 XC
GLN3	9.63e-16	2.80e-12	4.72		GLY + NO3 = HNO3 + #.63 HO2. + #1.26 CO + #.37 RCO-O2. + #-.37 XC
MGHV	Phot Set= MGLY_ADJ				MGLY + HV = HO2. + CO + CCO-O2.
MGOH	1.50e-11	1.50e-11			MGLY + HO. = CO + CCO-O2.
MGN3	2.43e-15	1.40e-12	3.77		MGLY + NO3 = HNO3 + CO + CCO-O2.
BAHV	Phot Set= BACL_ADJ				BACL + HV = #2 CCO-O2.
PHOH	2.63e-11	2.63e-11			PHEN + HO. = #.24 BZ-O. + #.76 RO2-R. + #.23 GLY + #4.1 XC
PHN3	3.78e-12	3.78e-12			PHEN + NO3 = HNO3 + BZ-O.
CROH	4.20e-11	4.20e-11			CRES + HO. = #.24 BZ-O. + #.76 RO2-R. + #.23 MGLY + #4.87 XC
CRN3	1.37e-11	1.37e-11			CRES + NO3 = HNO3 + BZ-O. + XC
NPN3	Same k as rxn PHN3				NPHE + NO3 = HNO3 + BZ(NO2)-O.
BZOH	1.29e-11	1.29e-11			BALD + HO. = BZCO-O2.
BZHV	Phot Set= BZCHO, qy= 5.0e-2				BALD + HV = #7 XC
BZNT	2.62e-15	1.40e-12	3.72		BALD + NO3 = HNO3 + BZCO-O2.
MAOH	3.36e-11	1.86e-11	-0.35		METHACRO + HO. = #.5 RO2-R. + #.416 CO + #.084 HCHO + #.416 MEK + #.084 MGLY + #.5 MA-RCO3. + #-0.416 XC
MAO3	1.13e-18	1.36e-15	4.20		METHACRO + O3 = #.008 HO2. + #.1 RO2-R. + #.208 HO. + #.1 RCO-O2. + #.45 CO + #.117 CO2 + #.2 HCHO + #.9 MGLY + #.333 HCOOH + #-0.1 XC
MAN3	4.58e-15	1.50e-12	3.43		METHACRO + NO3 = #.5 {HNO3 + RO2-R. + CO +MA-RCO3.} + #1.5 XC + #.5 XN
MAOP	6.34e-12	6.34e-12			METHACRO + O3P = RCHO + XC
MAHV	Phot Set= ACROLEIN, qy= 4.1e-3				METHACRO + HV = #.34 HO2. + #.33 RO2-R. + #.33 HO. + #.67 CCO-O2. + #.67 CO + #.67 HCHO + #.33 MA-RCO3. + #-0 XC

Table A-2 (continued)

Label	Rate Parameters [a] k(298)	A	Ea	B	Reaction and Products [b]
MVOH	1.89e-11	4.14e-12	-0.90		MVK + HO. = #.3 RO2-R. + #.025 RO2-N. + #.675 R2O2. + #.675 CCO-O2. + #.3 HCHO + #.675 RCHO + #.3 MGLY + #-0.725 XC
MVO3	4.58e-18	7.51e-16	3.02		MVK + O3 = #.064 HO2. + #.05 RO2-R. + #.164 HO. + #.05 RCO-O2. + #.475 CO + #.124 CO2 + #.1 HCHO + #.95 MGLY + #.351 HCOOH + #-0.05 XC
MVN3		(Slow)			MVK + NO3 = #4 XC + XN
MVOP	4.32e-12	4.32e-12			MVK + O3P = #.45 RCHO + #.55 MEK + #.45 XC
MVHV	Phot Set= ACROLEIN, qy= 2.1e-3				MVK + HV = #.3 C-O2. + #.7 CO + #.7 PROD2 + #.3 MA-RCO3. + #-2.4 XC
IPOH	6.19e-11	6.19e-11			ISO-PROD + HO. = #.67 RO2-R. + #.041 RO2-N. + #.289 MA-RCO3. + #.336 CO + #.055 HCHO + #.129 CCHO + #.013 RCHO + #.15 MEK + #.332 PROD2 + #.15 GLY + #.174 MGLY + #-0.504 XC
IPO3	4.18e-18	4.18e-18			ISO-PROD + O3 = #.4 HO2. + #.048 RO2-R. + #.048 RCO-O2. + #.285 HO. + #.498 CO + #.14 CO2 + #.125 HCHO + #.047 CCHO + #.21 MEK + #.023 GLY + #.742 MGLY + #.1 HCOOH + #.372 RCO-OH + #-.33 XC
IPN3	1.00e-13	1.00e-13			ISO-PROD + NO3 = #.799 RO2-R. + #.051 RO2-N. + #.15 MA-RCO3. + #.572 CO + #.15 HNO3 + #.227 HCHO + #.218 RCHO + #.008 MGLY + #.572 RNO3 + #.28 XN + #-.815 XC
IPHV	Phot Set= ACROLEIN, qy= 4.1e-3				ISO-PROD + HV = #1.233 HO2. + #.467 CCO-O2. + #.3 RCO-O2. + #1.233 CO + #.3 HCHO + #.467 CCHO + #.233 MEK + #-.233 XC
Lumped Parameter Organic Products					
K6OH	1.50e-11	1.50e-11			PROD2 + HO. = #.379 HO2. + #.473 RO2-R. + #.07 RO2-N. + #.029 CCO-O2. + #.049 RCO-O2. + #.213 HCHO + #.084 CCHO + #.558 RCHO + #.115 MEK + #.329 PROD2 + #.886 XC
K6HV	Phot Set= KETONE, qy= 2.0e-2				PROD2 + HV = #.96 RO2-R. + #.04 RO2-N. + #.515 R2O2. + #.667 CCO-O2. + #.333 RCO-O2. + #.506 HCHO + #.246 CCHO + #.71 RCHO + #.299 XC
RNOH	7.80e-12	7.80e-12			RNO3 + HO. = #.338 NO2 + #.113 HO2. + #.376 RO2-R. + #.173 RO2-N. + #.596 R2O2. + #.01 HCHO + #.439 CCHO + #.213 RCHO + #.006 ACET + #.177 MEK + #.048 PROD2 + #.31 RNO3 + #.351 XN + #.56 XC
RNHV	Phot Set= IC3ONO2				RNO3 + HV = NO2 + #.341 HO2. + #.564 RO2-R. + #.095 RO2-N. + #.152 R2O2. + #.134 HCHO + #.431 CCHO + #.147 RCHO + #.02 ACET + #.243 MEK + #.435 PROD2 + #.35 XC
Uncharacterized Reactive Aromatic Ring Fragmentation Products					
D1OH	5.00e-11	5.00e-11			DCB1 + HO. = RCHO + RO2-R. + CO
D1HV		(Slow)			DCB1 + HV = HO2. + #2 CO + RO2-R. + GLY + R2O2.
D1O3	2.00e-18	2.00e-18			DCB1 + O3 = #1.5 HO2. + #.5 HO. + #1.5 CO + #.5 CO2 + GLY
D2OH	5.00e-11	5.00e-11			DCB2 + HO. = R2O2. + RCHO + CCO-O2.
D2HV	Phot Set= MGLY_ABS, qy= 3.7e-1				DCB2 + HV = RO2-R. + #.5 {CCO-O2. + HO2.} + CO + R2O2. + #.5 {GLY + MGLY + XC}

Table A-2 (continued)

Label	Rate Parameters [a] k(298)	A	Ea	B	Reaction and Products [b]
D3OH	5.00e-11	5.00e-11			DCB3 + HO. = R2O2. + RCHO + CCO-O2.
D3HV	Phot Set= ACROLEIN, qy= 7.3e+0				DCB3 + HV = RO2-R. + #.5 {CCO-O2. + HO2.} + CO + R2O2. + #.5 {GLY + MGLY + XC}
Base ROG VOCs Used in the Chamber Simulations and Explicit VOCs in the Ambient Simulations					
c1OH	6.37e-15	2.15e-12	3.45		CH4 + HO. = H2O + C-O2.
c2OH	2.54e-13	1.37e-12	0.99	2.0	ETHANE + HO. = RO2-R. + CCHO
c4OH	2.44e-12	1.52e-12	-0.29	2.0	N-C4 + HO. = #.921 RO2-R. + #.079 RO2-N. + #.413 R2O2. + #.632 CCHO + #.12 RCHO + #.485 MEK + #-0.038 XC
c6OH	5.47e-12	1.38e-12	-0.82	2.0	N-C6 + HO. = #.775 RO2-R. + #.225 RO2-N. + #.787 R2O2. + #.011 CCHO + #.113 RCHO + #.688 PROD2 + #.162 XC
c8OH	8.70e-12	2.48e-12	-0.75	2.0	N-C8 + HO. = #.646 RO2-R. + #.354 RO2-N. + #.786 R2O2. + #.024 RCHO + #.622 PROD2 + #2.073 XC
etOH	8.52e-12	1.96e-12	-0.87		ETHENE + HO. = RO2-R. + #1.61 HCHO + #.195 CCHO
etO3	1.59e-18	9.14e-15	5.13		ETHENE + O3 = #.12 HO. + #.12 HO2. + #.5 CO + #.13 CO2 + HCHO + #.37 HCOOH
etN3	2.05e-16	4.39e-13	4.53	2.0	ETHENE + NO3 = RO2-R. + RCHO + #-1 XC + XN
etOA	7.29e-13	1.04e-11	1.57		ETHENE + O3P = #.5 HO2. + #.2 RO2-R. + #.3 C-O2. + #.491 CO + #.191 HCHO + #.25 CCHO + #.009 GLY + #.5 XC
prOH	2.63e-11	4.85e-12	-1.00		PROPENE + HO. = #.984 RO2-R. + #.016 RO2-N. + #.984 HCHO + #.984 CCHO + #-0.048 XC
prO3	1.01e-17	5.51e-15	3.73		PROPENE + O3 = #.32 HO. + #.06 HO2. + #.26 C-O2. + #.51 CO + #.135 CO2 + #.5 HCHO + #.5 CCHO + #.185 HCOOH + #.17 CCO-OH + #.07 INERT + #.07 XC
prN3	9.49e-15	4.59e-13	2.30		PROPENE + NO3 = #.949 RO2-R. + #.051 RO2-N. + #2.693 XC + XN
prOP	3.98e-12	1.18e-11	0.64		PROPENE + O3P = #.45 RCHO + #.55 MEK + #-0.55 XC
t2OH	6.40e-11	1.01e-11	-1.09		T-2-BUTE + HO. = #.965 RO2-R. + #.035 RO2-N. + #1.93 CCHO + #-0.07 XC
t2O3	1.90e-16	6.64e-15	2.10		T-2-BUTE + O3 = #.52 HO. + #.52 C-O2. + #.52 CO + #.14 CO2 + CCHO + #.34 CCO-OH + #.14 INERT + #.14 XC
t2N3	3.91e-13	1.10e-13	-0.76	2.0	T-2-BUTE + NO3 = #.705 NO2 + #.215 RO2-R. + #.08 RO2-N. + #.705 R2O2. + #1.41 CCHO + #.215 RNO3 + #-0.59 XC + #.08 XN
t2OP	2.18e-11	2.18e-11			T-2-BUTE + O3P = MEK
isOH	9.82e-11	2.50e-11	-0.81		ISOPRENE + HO. = #.907 RO2-R. + #.093 RO2-N. + #.079 R2O2. + #.624 HCHO + #.23 METHACRO + #.32 MVK + #.357 ISO-PROD + #-0.167 XC
isO3	1.28e-17	7.86e-15	3.80		ISOPRENE + O3 = #.266 HO. + #.066 RO2-R. + #.008 RO2-N. + #.126 R2O2. + #.192 MA-RCO3. + #.275 CO + #.122 CO2 + #.592 HCHO + #.1 PROD2 + #.39 METHACRO + #.16 MVK + #.204 HCOOH + #.15 RCO-OH + #-0.259 XC
isN3	6.74e-13	3.03e-12	0.89		ISOPRENE + NO3 = #.187 NO2 + #.749 RO2-R. + #.064 RO2-N. + #.187 R2O2. + #.936 ISO-PROD + #-0.064 XC + #.813 XN
isOP	3.60e-11	3.60e-11			ISOPRENE + O3P = #.01 RO2-N. + #.24 R2O2. + #.25 C-O2. + #.24 MA-RCO3. + #.24 HCHO + #.75 PROD2 + #-1.01 XC
tlOH	5.95e-12	1.81e-12	-0.71	0.0	TOLUENE + HO. = #.234 HO2. + #.758 RO2-R. + #.008 RO2-N. + #.116 GLY + #.135 MGLY + #.234 CRES + #.085 BALD + #.46 DCB1 + #.156 DCB2 + #.057 DCB3 + #1.178 XC

Table A-2 (continued)

Label	Rate Parameters [a] k(298)	A	Ea	B	Reaction and Products [b]
mxOH	2.36e-11	2.36e-11	0.00	0.0	M-XYLENE + HO. = #.21 HO2. + #.782 RO2-R. + #.008 RO2-N. + #.107 GLY + #.335 MGLY + #.21 CRES + #.037 BALD + #.347 DCB1 + #.29 DCB2 + #.108 DCB3 + #1.628 XC
Lumped Organic Species used in the Ambient Reactivity Simulations					
t1OH	8.27e-11	1.83e-11	-0.89		TERP + HO. = #.75 RO2-R. + #.25 RO2-N. + #.5 R2O2. + #.276 HCHO + #.474 RCHO + #.276 PROD2 + #5.146 XC
t1O3	6.88e-17	1.08e-15	1.63		TERP + O3 = #.567 HO. + #.033 HO2. + #.031 RO2-R. + #.18 RO2-N. + #.729 R2O2. + #.123 CCO-O2. + #.201 RCO-O2. + #.157 CO + #.037 CO2 + #.235 HCHO + #.205 RCHO + #.13 ACET + #.276 PROD2 + #.001 GLY + #.031 BACL + #.103 HCOOH + #.189 RCO-OH + #4.183 XC
t1N3	6.57e-12	3.66e-12	-0.35		TERP + NO3 = #.474 NO2 + #.276 RO2-R. + #.25 RO2-N. + #.75 R2O2. + #.474 RCHO + #.276 RNO3 + #5.421 XC + #.25 XN
t1OP	3.27e-11	3.27e-11			TERP + O3P = #.147 RCHO + #.853 PROD2 + #4.441 XC
a1OH	2.54e-13	1.37e-12	0.99	2.0	ALK1 + HO. = RO2-R. + CCHO
a2OH	1.04e-12	9.87e-12	1.33		ALK2 + HO. = #.246 HO. + #.121 HO2. + #.612 RO2-R. + #.021 RO2-N. + #.16 CO + #.039 HCHO + #.155 RCHO + #.417 ACET + #.248 GLY + #.121 HCOOH + #0.338 XC
a3OH	2.38e-12	1.02e-11	0.86		ALK3 + HO. = #.695 RO2-R. + #.07 RO2-N. + #.559 R2O2. + #.236 TBU-O. + #.026 HCHO + #.445 CCHO + #.122 RCHO + #.024 ACET + #.332 MEK + #-0.05 XC
a4OH	4.39e-12	5.95e-12	0.18		ALK4 + HO. = #.835 RO2-R. + #.143 RO2-N. + #.936 R2O2. + #.011 C-O2. + #.011 CCO-O2. + #.002 CO + #.024 HCHO + #.455 CCHO + #.244 RCHO + #.452 ACET + #.11 MEK + #.125 PROD2 + #-0.105 XC
a5OH	9.34e-12	1.11e-11	0.10		ALK5 + HO. = #.653 RO2-R. + #.347 RO2-N. + #.948 R2O2. + #.026 HCHO + #.099 CCHO + #.204 RCHO + #.072 ACET + #.089 MEK + #.417 PROD2 + #2.008 XC
b1OH	5.95e-12	1.81e-12	-0.71		ARO1 + HO. = #.224 HO2. + #.765 RO2-R. + #.011 RO2-N. + #.055 PROD2 + #.118 GLY + #.119 MGLY + #.017 PHEN + #.207 CRES + #.059 BALD + #.491 DCB1 + #.108 DCB2 + #.051 DCB3 + #1.288 XC
b2OH	2.64e-11	2.64e-11	0.00		ARO2 + HO. = #.187 HO2. + #.804 RO2-R. + #.009 RO2-N. + #.097 GLY + #.287 MGLY + #.087 BACL + #.187 CRES + #.05 BALD + #.561 DCB1 + #.099 DCB2 + #.093 DCB3 + #1.68 XC
o1OH	3.23e-11	7.10e-12	-0.90		OLE1 + HO. = #.91 RO2-R. + #.09 RO2-N. + #.205 R2O2. + #.732 HCHO + #.294 CCHO + #.497 RCHO + #.005 ACET + #.119 PROD2 + #.92 XC
o1O3	1.06e-17	2.62e-15	3.26		OLE1 + O3 = #.155 HO. + #.056 HO2. + #.022 RO2-R. + #.001 RO2-N. + #.076 C-O2. + #.345 CO + #.086 CO2 + #.5 HCHO + #.154 CCHO + #.363 RCHO + #.001 ACET + #.215 PROD2 + #.185 HCOOH + #.05 CCO-OH + #.119 RCO-OH + #.654 XC
o1N3	1.26e-14	4.45e-14	0.75		OLE1 + NO3 = #.824 RO2-R. + #.176 RO2-N. + #.488 R2O2. + #.009 CCHO + #.037 RCHO + #.024 ACET + #.511 RNO3 + #.677 XC + #.489 XN

Table A-2 (continued)

Label	Rate Parameters [a] k(298)	A	Ea	B	Reaction and Products [b]
o1OP	4.90e-12	1.07e-11	0.47		OLE1 + O3P = #.45 RCHO + #.437 MEK + #.113 PROD2 + #1.224 XC
o2OH	6.33e-11	1.74e-11	-0.76		OLE2 + HO. = #.918 RO2-R. + #.082 RO2-N. + #.001 R2O2. + #.244 HCHO + #.732 CCHO + #.511 RCHO + #.127 ACET + #.072 MEK + #.061 BALD + #.025 METHACRO + #.025 ISO-PROD + #-.054 XC
o2O3	1.07e-16	5.02e-16	0.92		OLE2 + O3 = #.378 HO. + #.003 HO2. + #.033 RO2-R. + #.002 RO2-N. + #.137 R2O2. + #.197 C-O2. + #.137 CCO-O2. + #.006 RCO-O2. + #.265 CO + #.07 CO2 + #.269 HCHO + #.456 CCHO + #.305 RCHO + #.045 ACET + #.026 MEK + #.006 PROD2 + #.042 BALD + #.026 METHACRO + #.073 HCOOH + #.129 CCO-OH + #.303 RCO-OH + #.155 XC
o2N3	7.27e-13	7.27e-13	0.00		OLE2 + NO3 = #.391 NO2 + #.442 RO2-R. + #.136 RO2-N. + #.711 R2O2. + #.03 C-O2. + #.079 HCHO + #.507 CCHO + #.151 RCHO + #.102 ACET + #.001 MEK + #.015 BALD + #.048 MVK + #.321 RNO3 + #.075 XC + #.288 XN
o2OP	2.09e-11	2.09e-11			OLE2 + O3P = #.013 HO2. + #.012 RO2-R. + #.001 RO2-N. + #.012 CO + #.069 RCHO + #.659 MEK + #.259 PROD2 + #.012 METHACRO + #.537 XC
Test Compounds Studied for This Project [c]					
	1.39e-11	1.39e-11			N-C12 + HO. = #.542 RO2-R. + #.458 RO2-N. + #.768 R2O2. + #.011 RCHO + #6.034 XC + #.53 PRD-NC12
	2.53e-11	2.53e-11			PRD-NC12 + HO. = #.141 HO2. + #.588 RO2-R. + #.199 RO2-N. + #.004 R2O2. + #.006 CCO-O2. + #.066 RCO-O2. + #.007 HCHO + #.034 CCHO + #.425 RCHO + #.536 PROD2 + #.032 XC
	1.80e-11	1.80e-11			N-C14 + HO. = #.53 RO2-R. + #.47 RO2-N. + #.765 R2O2. + #.009 RCHO + #8.027 XC + #.521 PRD-NC14
	2.84e-11	2.84e-11			PRD-NC14 + HO. = #.051 HO2. + #.652 RO2-R. + #.235 RO2-N. + #.008 R2O2. + #.004 CCO-O2. + #.058 RCO-O2. + #.005 HCHO + #.025 CCHO + #.375 RCHO + #.534 PROD2 + #.023 XC
	2.10e-11	2.10e-11			N-C15 + HO. = #.527 RO2-R. + #.473 RO2-N. + #.764 R2O2. + #.008 RCHO + #9.025 XC + #.519 PRD-NC15
	2.99e-11	2.99e-11			PRD-NC15 + HO. = #.019 HO2. + #.674 RO2-R. + #.249 RO2-N. + #.015 R2O2. + #.004 CCO-O2. + #.055 RCO-O2. + #.004 HCHO + #.022 CCHO + #.357 RCHO + #.533 PROD2 + #.02 XC
	2.30e-11	2.30e-11			N-C16 + HO. = #.525 RO2-R. + #.475 RO2-N. + #.763 R2O2. + #.008 RCHO + #10.023 XC + #.517 PRD-NC16
	3.14e-11	3.14e-11			PRD-NC16 + HO. = #.002 HO2. + #.681 RO2-R. + #.261 RO2-N. + #.035 R2O2. + #.003 CCO-O2. + #.052 RCO-O2. + #.004 HCHO + #.019 CCHO + #.338 RCHO + #.533 PROD2 + #.018 XC
	1.78e-11	1.78e-11			C6-CYCC6 + HO. = #.527 RO2-R. + #.473 RO2-N. + #.849 R2O2. + #.093 RCHO + #6.118 XC + #.461 PRD-CC12

Table A-2 (continued)

Label	Rate Parameters [a] k(298)	A	Ea	B	Reaction and Products [b]
	2.61e-11	2.61e-11			PRD-CC12 + HO. = #.036 HO2. + #.574 RO2-R. + #.298 RO2-N. + #.313 R2O2. + #.003 CCO-O2. + #.089 RCO-O2. + #.042 HCHO + #.013 CCHO + #.407 RCHO + #.396 PROD2 + #.271 XC
	2.05e-11	2.05e-11			C8-CYCC6 + HO. = #.511 RO2-R. + #.489 RO2-N. + #.847 R2O2. + #.063 RCHO + #8.099 XC + #.463 PRD-CC14
	2.99e-11	2.99e-11			PRD-CC14 + HO. = #.058 HO2. + #.554 RO2-R. + #.311 RO2-N. + #.32 R2O2. + #.004 CCO-O2. + #.074 RCO-O2. + #.012 HCHO + #.01 CCHO + #.347 RCHO + #.454 PROD2 + #.112 XC

[a] Except as indicated, the rate constants are given by $k(T) = A \cdot (T/300)^B \cdot e^{-Ea/RT}$, where the units of k and A are cm^3 $molec^{-1}$ s^{-1}, Ea are kcal mol^{-1}, T is ^oK, and R=0.0019872 kcal mol^{-1} deg^{-1}. The following special rate constant expressions are used: Phot Set = *name*: The absorption cross sections and quantum yields for the photolysis reaction are given in Table A-3, where "*name*" indicates the photolysis set used. If a "qy=*number*" notation is given, the number given is the overall quantum yield, which is assumed to be wavelength independent. Falloff: The rate constant as a function of temperature and pressure is calculated using $k(T,M) = \{k0(T)\cdot[M]/[1 + k0(T)\cdot[M]/kinf(T)]\}\cdot F^Z$, where $Z = \{1 + [\log_{10}\{k0(T)\cdot[M])/kinf(T)\}]^2\}^{-1}$, [M] is the total pressure in molecules cm^{-3}, F is as indicated on the table, and the temperature dependences of k0 and kinf are as indicated on the table. (Slow): The reaction is assumed to be negligible and is not included in the mechanism. It is shown on the listing for documentation purposes only. k = k0+k3M(1+k3M/k2): The rate constant as a function of temperature and pressure is calculated using $k(T,M) = k0(T) + k3(T)\cdot[M] \cdot(1 + k3(T)\cdot[M]/k2(T))$, where [M] is the total bath gas (air) concentration in molecules cm^{-3}, and the temperature dependences for k0, k2 and k3 are as indicated on the table. k = k1 + k2 [M]: The rate constant as a function of temperature and pressure is calculated using $k(T,M) = k1(T) + k2(T)\cdot[M]$, where [M] is the total bath gas (air) concentration in molecules cm^{-3}, and the temperature dependences for k1, and k2 are as indicated on the table. Same k as Rxn *label*: The rate constant is the same as the reaction with the indicated label.

[b] Format of reaction listing: "=" separates reactants from products; "*#number*" indicates stoichiometric coefficient, "*#coefficient { product list }*" means that the stoichiometric coefficient is applied to all the products listed. See Table A-1 for a listing of the model species used.

[c] Mechanisms for the alkanes derived using the SAPRC-99 mechanism generation system, with measured rate constant. Mechanisms for the lumped higher ketone product model species were derived by weighted averages of the estimated mechanisms derived for the individual product compounds See Carter (2000) for a discussion of adjusted product mechanisms.

Table A-3. Listing of the absorption cross-sections and quantum yields for the photolysis reactions.

WL (nm)	Abs (cm^2)	QY	WL (nm)	Abs (cm^2)	QY	WL (nm)	Abs (cm^2)	QY	WL (nm)	Abs (cm^2)	QY	WL (nm)	Abs (cm^2)	QY
							NO2							
205.0	4.31e-19	1.000	210.0	4.72e-19	1.000	215.0	4.95e-19	1.000	220.0	4.56e-19	1.000	225.0	3.79e-19	1.000
230.0	2.74e-19	1.000	235.0	1.67e-19	1.000	240.0	9.31e-20	1.000	245.0	4.74e-20	1.000	250.0	2.48e-20	1.000
255.0	1.95e-20	1.000	260.0	2.24e-20	1.000	265.0	2.73e-20	1.000	270.0	4.11e-20	1.000	275.0	4.90e-20	1.000
280.0	5.92e-20	1.000	285.0	7.39e-20	1.000	290.0	9.00e-20	1.000	295.0	1.09e-19	1.000	300.0	1.31e-19	1.000
305.0	1.57e-19	1.000	310.0	1.86e-19	1.000	315.0	2.15e-19	0.990	320.0	2.48e-19	0.990	325.0	2.81e-19	0.990
330.0	3.13e-19	0.990	335.0	3.43e-19	0.990	340.0	3.80e-19	0.990	345.0	4.07e-19	0.990	350.0	4.31e-19	0.990
355.0	4.72e-19	0.990	360.0	4.83e-19	0.980	365.0	5.17e-19	0.980	370.0	5.32e-19	0.980	375.0	5.51e-19	0.980
380.0	5.64e-19	0.970	385.0	5.76e-19	0.970	390.0	5.93e-19	0.960	395.0	5.85e-19	0.935	400.0	6.02e-19	0.820
405.0	5.78e-19	0.355	410.0	6.00e-19	0.130	411.0	5.93e-19	0.110	412.0	5.86e-19	0.094	413.0	5.79e-19	0.083
414.0	5.72e-19	0.070	415.0	5.65e-19	0.059	416.0	5.68e-19	0.048	417.0	5.71e-19	0.039	418.0	5.75e-19	0.030
419.0	5.78e-19	0.023	420.0	5.81e-19	0.018	421.0	5.72e-19	0.012	422.0	5.64e-19	0.008	423.0	5.55e-19	0.004
424.0	5.47e-19	0.000												
							NO3NO							
585.0	2.89e-18	0.000	586.0	3.32e-18	0.050	587.0	4.16e-18	0.100	588.0	5.04e-18	0.150	589.0	6.13e-18	0.200
590.0	5.96e-18	0.250	591.0	5.44e-18	0.280	592.0	5.11e-18	0.310	593.0	4.58e-18	0.340	594.0	4.19e-18	0.370
595.0	4.29e-18	0.400	596.0	4.62e-18	0.370	597.0	4.36e-18	0.340	598.0	3.67e-18	0.310	599.0	3.10e-18	0.280
600.0	2.76e-18	0.250	601.0	2.86e-18	0.240	602.0	3.32e-18	0.230	603.0	3.80e-18	0.220	604.0	4.37e-18	0.210
605.0	4.36e-18	0.200	606.0	3.32e-18	0.200	607.0	2.40e-18	0.200	608.0	1.85e-18	0.200	609.0	1.71e-18	0.200
610.0	1.77e-18	0.200	611.0	1.91e-18	0.180	612.0	2.23e-18	0.160	613.0	2.63e-18	0.140	614.0	2.55e-18	0.120
615.0	2.26e-18	0.100	616.0	2.09e-18	0.100	617.0	2.11e-18	0.100	618.0	2.39e-18	0.100	619.0	2.56e-18	0.100
620.0	3.27e-18	0.100	621.0	5.24e-18	0.090	622.0	1.02e-17	0.080	623.0	1.47e-17	0.070	624.0	1.21e-17	0.060
625.0	8.38e-18	0.050	626.0	7.30e-18	0.050	627.0	7.53e-18	0.050	628.0	7.37e-18	0.050	629.0	6.98e-18	0.050
630.0	6.76e-18	0.050	631.0	4.84e-18	0.046	632.0	3.27e-18	0.042	633.0	2.17e-18	0.038	634.0	1.64e-18	0.034
635.0	1.44e-18	0.030	636.0	1.69e-18	0.024	637.0	2.07e-18	0.018	638.0	2.03e-18	0.012	639.0	1.58e-18	0.006
640.0	1.23e-18	0.000												
							NO3NO2							
400.0	0.00e+00	1.000	401.0	0.00e+00	1.000	402.0	0.00e+00	1.000	403.0	2.00e-20	1.000	404.0	0.00e+00	1.000
405.0	3.00e-20	1.000	406.0	2.00e-20	1.000	407.0	1.00e-20	1.000	408.0	3.00e-20	1.000	409.0	0.00e+00	1.000
410.0	1.00e-20	1.000	411.0	2.00e-20	1.000	412.0	5.00e-20	1.000	413.0	5.00e-20	1.000	414.0	2.00e-20	1.000
415.0	6.00e-20	1.000	416.0	6.00e-20	1.000	417.0	7.00e-20	1.000	418.0	5.00e-20	1.000	419.0	8.00e-20	1.000
420.0	8.00e-20	1.000	421.0	8.00e-20	1.000	422.0	9.00e-20	1.000	423.0	1.10e-19	1.000	424.0	9.00e-20	1.000
425.0	7.00e-20	1.000	426.0	1.40e-19	1.000	427.0	1.40e-19	1.000	428.0	1.20e-19	1.000	429.0	1.10e-19	1.000
430.0	1.70e-19	1.000	431.0	1.30e-19	1.000	432.0	1.50e-19	1.000	433.0	1.80e-19	1.000	434.0	1.80e-19	1.000
435.0	1.60e-19	1.000	436.0	1.50e-19	1.000	437.0	1.80e-19	1.000	438.0	2.10e-19	1.000	439.0	2.00e-19	1.000
440.0	1.90e-19	1.000	441.0	1.80e-19	1.000	442.0	2.10e-19	1.000	443.0	1.80e-19	1.000	444.0	1.90e-19	1.000
445.0	2.00e-19	1.000	446.0	2.40e-19	1.000	447.0	2.90e-19	1.000	448.0	2.40e-19	1.000	449.0	2.80e-19	1.000
450.0	2.90e-19	1.000	451.0	3.00e-19	1.000	452.0	3.30e-19	1.000	453.0	3.10e-19	1.000	454.0	3.60e-19	1.000
455.0	3.60e-19	1.000	456.0	3.60e-19	1.000	457.0	4.00e-19	1.000	458.0	3.70e-19	1.000	459.0	4.20e-19	1.000
460.0	4.00e-19	1.000	461.0	3.90e-19	1.000	462.0	4.00e-19	1.000	463.0	4.10e-19	1.000	464.0	4.80e-19	1.000
465.0	5.10e-19	1.000	466.0	5.40e-19	1.000	467.0	5.70e-19	1.000	468.0	5.60e-19	1.000	469.0	5.80e-19	1.000
470.0	5.90e-19	1.000	471.0	6.20e-19	1.000	472.0	6.40e-19	1.000	473.0	6.20e-19	1.000	474.0	6.20e-19	1.000
475.0	6.80e-19	1.000	476.0	7.80e-19	1.000	477.0	7.70e-19	1.000	478.0	7.30e-19	1.000	479.0	7.30e-19	1.000
480.0	7.00e-19	1.000	481.0	7.10e-19	1.000	482.0	7.10e-19	1.000	483.0	7.20e-19	1.000	484.0	7.70e-19	1.000
485.0	8.20e-19	1.000	486.0	9.10e-19	1.000	487.0	9.20e-19	1.000	488.0	9.50e-19	1.000	489.0	9.60e-19	1.000
490.0	1.03e-18	1.000	491.0	9.90e-19	1.000	492.0	9.90e-19	1.000	493.0	1.01e-18	1.000	494.0	1.01e-18	1.000
495.0	1.06e-18	1.000	496.0	1.21e-18	1.000	497.0	1.22e-18	1.000	498.0	1.20e-18	1.000	499.0	1.17e-18	1.000
500.0	1.13e-18	1.000	501.0	1.11e-18	1.000	502.0	1.11e-18	1.000	503.0	1.11e-18	1.000	504.0	1.26e-18	1.000
505.0	1.28e-18	1.000	506.0	1.34e-18	1.000	507.0	1.28e-18	1.000	508.0	1.27e-18	1.000	509.0	1.35e-18	1.000
510.0	1.51e-18	1.000	511.0	1.73e-18	1.000	512.0	1.77e-18	1.000	513.0	1.60e-18	1.000	514.0	1.58e-18	1.000
515.0	1.58e-18	1.000	516.0	1.56e-18	1.000	517.0	1.49e-18	1.000	518.0	1.44e-18	1.000	519.0	1.54e-18	1.000
520.0	1.68e-18	1.000	521.0	1.83e-18	1.000	522.0	1.93e-18	1.000	523.0	1.77e-18	1.000	524.0	1.64e-18	1.000
525.0	1.58e-18	1.000	526.0	1.63e-18	1.000	527.0	1.81e-18	1.000	528.0	2.10e-18	1.000	529.0	2.39e-18	1.000
530.0	2.23e-18	1.000	531.0	2.09e-18	1.000	532.0	2.02e-18	1.000	533.0	1.95e-18	1.000	534.0	2.04e-18	1.000
535.0	2.30e-18	1.000	536.0	2.57e-18	1.000	537.0	2.58e-18	1.000	538.0	2.34e-18	1.000	539.0	2.04e-18	1.000
540.0	2.10e-18	1.000	541.0	2.04e-18	1.000	542.0	1.88e-18	1.000	543.0	1.68e-18	1.000	544.0	1.70e-18	1.000
545.0	1.96e-18	1.000	546.0	2.42e-18	1.000	547.0	2.91e-18	1.000	548.0	2.98e-18	1.000	549.0	2.71e-18	1.000
550.0	2.48e-18	1.000	551.0	2.43e-18	1.000	552.0	2.47e-18	1.000	553.0	2.53e-18	1.000	554.0	2.78e-18	1.000
555.0	3.11e-18	1.000	556.0	3.26e-18	1.000	557.0	3.29e-18	1.000	558.0	3.51e-18	1.000	559.0	3.72e-18	1.000
560.0	3.32e-18	1.000	561.0	2.98e-18	1.000	562.0	2.90e-18	1.000	563.0	2.80e-18	1.000	564.0	2.72e-18	1.000
565.0	2.73e-18	1.000	566.0	2.85e-18	1.000	567.0	2.81e-18	1.000	568.0	2.85e-18	1.000	569.0	2.89e-18	1.000
570.0	2.79e-18	1.000	571.0	2.76e-18	1.000	572.0	2.74e-18	1.000	573.0	2.78e-18	1.000	574.0	2.86e-18	1.000
575.0	3.08e-18	1.000	576.0	3.27e-18	1.000	577.0	3.38e-18	1.000	578.0	3.31e-18	1.000	579.0	3.24e-18	1.000
580.0	3.34e-18	1.000	581.0	3.55e-18	1.000	582.0	3.28e-18	1.000	583.0	2.93e-18	1.000	584.0	2.82e-18	1.000
585.0	2.89e-18	1.000	586.0	3.32e-18	0.950	587.0	4.16e-18	0.900	588.0	5.04e-18	0.850	589.0	6.13e-18	0.800
590.0	5.96e-18	0.750	591.0	5.44e-18	0.720	592.0	5.11e-18	0.690	593.0	4.58e-18	0.660	594.0	4.19e-18	0.630
595.0	4.29e-18	0.600	596.0	4.62e-18	0.590	597.0	4.36e-18	0.580	598.0	3.67e-18	0.570	599.0	3.10e-18	0.560
600.0	2.76e-18	0.550	601.0	2.86e-18	0.540	602.0	3.32e-18	0.530	603.0	3.80e-18	0.520	604.0	4.37e-18	0.510
605.0	4.36e-18	0.400	606.0	3.32e-18	0.380	607.0	2.40e-18	0.360	608.0	1.85e-18	0.340	609.0	1.71e-18	0.320

Table A-3 (continued)

WL (nm)	Abs (cm^2)	QY	WL (nm)	Abs (cm^2)	QY	WL (nm)	Abs (cm^2)	QY	WL (nm)	Abs (cm^2)	QY	WL (nm)	Abs (cm^2)	QY
610.0	1.77e-18	0.300	611.0	1.91e-18	0.290	612.0	2.23e-18	0.280	613.0	2.63e-18	0.270	614.0	2.55e-18	0.260
615.0	2.26e-18	0.250	616.0	2.09e-18	0.240	617.0	2.11e-18	0.230	618.0	2.39e-18	0.220	619.0	2.56e-18	0.210
620.0	3.27e-18	0.200	621.0	5.24e-18	0.190	622.0	1.02e-17	0.180	623.0	1.47e-17	0.170	624.0	1.21e-17	0.160
625.0	8.38e-18	0.150	626.0	7.30e-18	0.130	627.0	7.53e-18	0.110	628.0	7.37e-18	0.090	629.0	6.98e-18	0.070
630.0	6.76e-18	0.050	631.0	4.84e-18	0.040	632.0	3.27e-18	0.030	633.0	2.17e-18	0.020	634.0	1.64e-18	0.010
635.0	1.44e-18	0.000												
							O3O3P							
280.0	3.94e-18	0.095	281.0	3.62e-18	0.093	282.0	3.31e-18	0.090	283.0	2.99e-18	0.088	284.0	2.70e-18	0.086
285.0	2.46e-18	0.084	286.0	2.22e-18	0.082	287.0	1.98e-18	0.079	288.0	1.75e-18	0.077	289.0	1.59e-18	0.075
290.0	1.42e-18	0.073	291.0	1.25e-18	0.070	292.0	1.09e-18	0.068	293.0	9.81e-19	0.066	294.0	8.73e-19	0.064
295.0	7.65e-19	0.061	296.0	6.58e-19	0.059	297.0	5.81e-19	0.057	298.0	5.18e-19	0.055	299.0	4.55e-19	0.052
300.0	3.92e-19	0.050	301.0	3.35e-19	0.035	302.0	3.01e-19	0.025	303.0	2.66e-19	0.015	304.0	2.32e-19	0.010
305.0	1.97e-19	0.020	306.0	1.73e-19	0.050	307.0	1.55e-19	0.123	308.0	1.37e-19	0.227	309.0	1.18e-19	0.333
310.0	9.98e-20	0.400	311.0	8.92e-20	0.612	312.0	7.94e-20	0.697	313.0	6.96e-20	0.738	314.0	5.99e-20	0.762
315.0	5.01e-20	0.765	316.0	4.51e-20	0.779	317.0	4.00e-20	0.791	318.0	3.50e-20	0.806	319.0	2.99e-20	0.822
320.0	2.49e-20	0.852	321.0	2.23e-20	0.879	322.0	1.97e-20	0.903	323.0	1.72e-20	0.908	324.0	1.46e-20	0.920
325.0	1.20e-20	0.930	326.0	1.08e-20	0.934	327.0	9.67e-21	0.938	328.0	8.50e-21	0.942	329.0	7.34e-21	0.946
330.0	6.17e-21	0.950	331.0	5.48e-21	0.950	332.0	4.80e-21	0.950	333.0	4.11e-21	0.950	334.0	3.43e-21	0.950
335.0	2.74e-21	0.950	336.0	2.43e-21	0.960	337.0	2.11e-21	0.970	338.0	1.80e-21	0.980	339.0	1.48e-21	0.990
340.0	1.17e-21	1.000	350.0	0.00e+00	1.000	400.0	0.00e+00	1.000	410.0	1.20e-23	1.000	420.0	2.20e-23	1.000
440.0	1.12e-22	1.000	460.0	3.28e-22	1.000	480.0	6.84e-22	1.000	500.0	1.22e-21	1.000	520.0	1.82e-21	1.000
540.0	2.91e-21	1.000	560.0	3.94e-21	1.000	580.0	4.59e-21	1.000	600.0	5.11e-21	1.000	620.0	4.00e-21	1.000
640.0	2.96e-21	1.000	660.0	2.09e-21	1.000	680.0	1.36e-21	1.000	700.0	9.10e-22	1.000	750.0	3.20e-22	1.000
800.0	1.60e-22	1.000	900.0	0.00e+00	1.000									
							O3O1D							
280.0	3.94e-18	0.905	281.0	3.62e-18	0.907	282.0	3.31e-18	0.910	283.0	2.99e-18	0.912	284.0	2.70e-18	0.914
285.0	2.46e-18	0.916	286.0	2.22e-18	0.918	287.0	1.98e-18	0.921	288.0	1.75e-18	0.923	289.0	1.59e-18	0.925
290.0	1.42e-18	0.927	291.0	1.25e-18	0.930	292.0	1.09e-18	0.932	293.0	9.81e-19	0.934	294.0	8.73e-19	0.936
295.0	7.65e-19	0.939	296.0	6.58e-19	0.941	297.0	5.81e-19	0.943	298.0	5.18e-19	0.945	299.0	4.55e-19	0.948
300.0	3.92e-19	0.950	301.0	3.35e-19	0.965	302.0	3.01e-19	0.975	303.0	2.66e-19	0.985	304.0	2.32e-19	0.990
305.0	1.97e-19	0.980	306.0	1.73e-19	0.950	307.0	1.55e-19	0.877	308.0	1.37e-19	0.773	309.0	1.18e-19	0.667
310.0	9.98e-20	0.600	311.0	8.92e-20	0.388	312.0	7.94e-20	0.303	313.0	6.96e-20	0.262	314.0	5.99e-20	0.238
315.0	5.01e-20	0.235	316.0	4.51e-20	0.221	317.0	4.00e-20	0.209	318.0	3.50e-20	0.194	319.0	2.99e-20	0.178
320.0	2.49e-20	0.148	321.0	2.23e-20	0.121	322.0	1.97e-20	0.097	323.0	1.72e-20	0.092	324.0	1.46e-20	0.080
325.0	1.20e-20	0.070	326.0	1.08e-20	0.066	327.0	9.67e-21	0.062	328.0	8.50e-21	0.058	329.0	7.34e-21	0.054
330.0	6.17e-21	0.050	331.0	5.48e-21	0.050	332.0	4.80e-21	0.050	333.0	4.11e-21	0.050	334.0	3.43e-21	0.050
335.0	2.74e-21	0.050	336.0	2.43e-21	0.040	337.0	2.11e-21	0.030	338.0	1.80e-21	0.020	339.0	1.48e-21	0.010
340.0	1.17e-21	0.000												
							HONO-NO							
309.0	0.00e+00	0.410	310.0	1.30e-20	0.410	311.0	1.90e-20	0.411	312.0	2.80e-20	0.421	313.0	2.20e-20	0.432
314.0	3.60e-20	0.443	315.0	3.00e-20	0.454	316.0	1.40e-20	0.464	317.0	3.10e-20	0.475	318.0	5.60e-20	0.486
319.0	3.60e-20	0.496	320.0	4.90e-20	0.507	321.0	7.80e-20	0.518	322.0	4.90e-20	0.529	323.0	5.10e-20	0.539
324.0	7.10e-20	0.550	325.0	5.00e-20	0.561	326.0	2.90e-20	0.571	327.0	6.60e-20	0.582	328.0	1.17e-19	0.593
329.0	6.10e-20	0.604	330.0	1.11e-19	0.614	331.0	1.79e-19	0.625	332.0	8.70e-20	0.636	333.0	7.60e-20	0.646
334.0	9.60e-20	0.657	335.0	9.60e-20	0.668	336.0	7.20e-20	0.679	337.0	5.30e-20	0.689	338.0	1.00e-19	0.700
339.0	1.88e-19	0.711	340.0	1.00e-19	0.721	341.0	1.70e-19	0.732	342.0	3.86e-19	0.743	343.0	1.49e-19	0.754
344.0	9.70e-20	0.764	345.0	1.09e-19	0.775	346.0	1.23e-19	0.786	347.0	1.04e-19	0.796	348.0	9.10e-20	0.807
349.0	7.90e-20	0.818	350.0	1.12e-19	0.829	351.0	2.12e-19	0.839	352.0	1.55e-19	0.850	353.0	1.91e-19	0.861
354.0	5.81e-19	0.871	355.0	3.64e-19	0.882	356.0	1.41e-19	0.893	357.0	1.17e-19	0.904	358.0	1.20e-19	0.914
359.0	1.04e-19	0.925	360.0	9.00e-20	0.936	361.0	8.30e-20	0.946	362.0	8.00e-20	0.957	363.0	9.60e-20	0.968
364.0	1.46e-19	0.979	365.0	1.68e-19	0.989	366.0	1.83e-19	1.000	367.0	3.02e-19	1.000	368.0	5.20e-19	1.000
369.0	3.88e-19	1.000	370.0	1.78e-19	1.000	371.0	1.13e-19	1.000	372.0	1.00e-19	1.000	373.0	7.70e-20	1.000
374.0	6.20e-20	1.000	375.0	5.30e-20	1.000	376.0	5.30e-20	1.000	377.0	5.00e-20	1.000	378.0	5.80e-20	1.000
379.0	8.00e-20	1.000	380.0	9.60e-20	1.000	381.0	1.13e-19	1.000	382.0	1.59e-19	1.000	383.0	2.10e-19	1.000
384.0	2.41e-19	1.000	385.0	2.03e-19	1.000	386.0	1.34e-19	1.000	387.0	9.00e-20	1.000	388.0	5.60e-20	1.000
389.0	3.40e-20	1.000	390.0	2.70e-20	1.000	391.0	2.00e-20	1.000	392.0	1.50e-20	1.000	393.0	1.10e-20	1.000
394.0	6.00e-21	1.000	395.0	1.00e-20	1.000	396.0	4.00e-21	1.000	400.0	0.00e+00	1.000			
							HONO-NO2							
309.0	0.00e+00	0.590	310.0	1.30e-20	0.590	311.0	1.90e-20	0.589	312.0	2.80e-20	0.579	313.0	2.20e-20	0.568
314.0	3.60e-20	0.557	315.0	3.00e-20	0.546	316.0	1.40e-20	0.536	317.0	3.10e-20	0.525	318.0	5.60e-20	0.514
319.0	3.60e-20	0.504	320.0	4.90e-20	0.493	321.0	7.80e-20	0.482	322.0	4.90e-20	0.471	323.0	5.10e-20	0.461
324.0	7.10e-20	0.450	325.0	5.00e-20	0.439	326.0	2.90e-20	0.429	327.0	6.60e-20	0.418	328.0	1.17e-19	0.407
329.0	6.10e-20	0.396	330.0	1.11e-19	0.386	331.0	1.79e-19	0.375	332.0	8.70e-20	0.364	333.0	7.60e-20	0.354
334.0	9.60e-20	0.343	335.0	9.60e-20	0.332	336.0	7.20e-20	0.321	337.0	5.30e-20	0.311	338.0	1.00e-19	0.300
339.0	1.88e-19	0.289	340.0	1.00e-19	0.279	341.0	1.70e-19	0.268	342.0	3.86e-19	0.257	343.0	1.49e-19	0.246
344.0	9.70e-20	0.236	345.0	1.09e-19	0.225	346.0	1.23e-19	0.214	347.0	1.04e-19	0.204	348.0	9.10e-20	0.193
349.0	7.90e-20	0.182	350.0	1.12e-19	0.171	351.0	2.12e-19	0.161	352.0	1.55e-19	0.150	353.0	1.91e-19	0.139
354.0	5.81e-19	0.129	355.0	3.64e-19	0.118	356.0	1.41e-19	0.107	357.0	1.17e-19	0.096	358.0	1.20e-19	0.086
359.0	1.04e-19	0.075	360.0	9.00e-20	0.064	361.0	8.30e-20	0.054	362.0	8.00e-20	0.043	363.0	9.60e-20	0.032

Table A-3 (continued)

WL (nm)	Abs (cm^2)	QY	WL (nm)	Abs (cm^2)	QY	WL (nm)	Abs (cm^2)	QY	WL (nm)	Abs (cm^2)	QY	WL (nm)	Abs (cm^2)	QY
364.0	1.46e-19	0.021	365.0	1.68e-19	0.011	366.0	1.83e-19	0.000						
							HNO3							
190.0	1.36e-17	1.000	195.0	1.02e-17	1.000	200.0	5.88e-18	1.000	205.0	2.80e-18	1.000	210.0	1.04e-18	1.000
215.0	3.65e-19	1.000	220.0	1.49e-19	1.000	225.0	8.81e-20	1.000	230.0	5.75e-20	1.000	235.0	3.75e-20	1.000
240.0	2.58e-20	1.000	245.0	2.11e-20	1.000	250.0	1.97e-20	1.000	255.0	1.95e-20	1.000	260.0	1.91e-20	1.000
265.0	1.80e-20	1.000	270.0	1.62e-20	1.000	275.0	1.38e-20	1.000	280.0	1.12e-20	1.000	285.0	8.58e-21	1.000
290.0	6.15e-21	1.000	295.0	4.12e-21	1.000	300.0	2.63e-21	1.000	305.0	1.50e-21	1.000	310.0	8.10e-22	1.000
315.0	4.10e-22	1.000	320.0	2.00e-22	1.000	325.0	9.50e-23	1.000	330.0	4.30e-23	1.000	335.0	2.20e-23	1.000
340.0	1.00e-23	1.000	345.0	6.00e-24	1.000	350.0	4.00e-24	1.000	355.0	0.00e+00	1.000			
							HO2NO2							
190.0	1.01e-17	1.000	195.0	8.16e-18	1.000	200.0	5.63e-18	1.000	205.0	3.67e-18	1.000	210.0	2.39e-18	1.000
215.0	1.61e-18	1.000	220.0	1.18e-18	1.000	225.0	9.32e-19	1.000	230.0	7.88e-19	1.000	235.0	6.80e-19	1.000
240.0	5.79e-19	1.000	245.0	4.97e-19	1.000	250.0	4.11e-19	1.000	255.0	3.49e-19	1.000	260.0	2.84e-19	1.000
265.0	2.29e-19	1.000	270.0	1.80e-19	1.000	275.0	1.33e-19	1.000	280.0	9.30e-20	1.000	285.0	6.20e-20	1.000
290.0	3.90e-20	1.000	295.0	2.40e-20	1.000	300.0	1.40e-20	1.000	305.0	8.50e-21	1.000	310.0	5.30e-21	1.000
315.0	3.90e-21	1.000	320.0	2.40e-21	1.000	325.0	1.50e-21	1.000	330.0	9.00e-22	1.000	335.0	0.00e+00	1.000
							H2O2							
190.0	6.72e-19	1.000	195.0	5.63e-19	1.000	200.0	4.75e-19	1.000	205.0	4.08e-19	1.000	210.0	3.57e-19	1.000
215.0	3.07e-19	1.000	220.0	2.58e-19	1.000	225.0	2.17e-19	1.000	230.0	1.82e-19	1.000	235.0	1.50e-19	1.000
240.0	1.24e-19	1.000	245.0	1.02e-19	1.000	250.0	8.30e-20	1.000	255.0	6.70e-20	1.000	260.0	5.30e-20	1.000
265.0	4.20e-20	1.000	270.0	3.30e-20	1.000	275.0	2.60e-20	1.000	280.0	2.00e-20	1.000	285.0	1.50e-20	1.000
290.0	1.20e-20	1.000	295.0	9.00e-21	1.000	300.0	6.80e-21	1.000	305.0	5.10e-21	1.000	310.0	3.90e-21	1.000
315.0	2.90e-21	1.000	320.0	2.20e-21	1.000	325.0	1.60e-21	1.000	330.0	1.30e-21	1.000	335.0	1.00e-21	1.000
340.0	7.00e-22	1.000	345.0	5.00e-22	1.000	350.0	4.00e-22	1.000	355.0	0.00e+00	1.000			
							HCHO_R							
240.0	6.40e-22	0.270	241.0	5.60e-22	0.272	242.0	1.05e-21	0.274	243.0	1.15e-21	0.276	244.0	8.20e-22	0.278
245.0	1.03e-21	0.280	246.0	9.80e-22	0.282	247.0	1.35e-21	0.284	248.0	1.91e-21	0.286	249.0	2.82e-21	0.288
250.0	2.05e-21	0.290	251.0	1.70e-21	0.291	252.0	2.88e-21	0.292	253.0	2.55e-21	0.293	254.0	2.55e-21	0.294
255.0	3.60e-21	0.295	256.0	5.09e-21	0.296	257.0	3.39e-21	0.297	258.0	2.26e-21	0.298	259.0	5.04e-21	0.299
260.0	5.05e-21	0.300	261.0	5.49e-21	0.308	262.0	5.20e-21	0.316	263.0	9.33e-21	0.324	264.0	8.23e-21	0.332
265.0	4.30e-21	0.340	266.0	4.95e-21	0.348	267.0	1.24e-20	0.356	268.0	1.11e-20	0.364	269.0	8.78e-21	0.372
270.0	9.36e-21	0.380	271.0	1.79e-20	0.399	272.0	1.23e-20	0.418	273.0	6.45e-21	0.437	274.0	6.56e-21	0.456
275.0	2.23e-20	0.475	276.0	2.42e-20	0.494	277.0	1.40e-20	0.513	278.0	1.05e-20	0.532	279.0	2.55e-20	0.551
280.0	2.08e-20	0.570	281.0	1.48e-20	0.586	282.0	8.81e-21	0.602	283.0	1.07e-20	0.618	284.0	4.49e-20	0.634
285.0	3.59e-20	0.650	286.0	1.96e-20	0.666	287.0	1.30e-20	0.682	288.0	3.36e-20	0.698	289.0	2.84e-20	0.714
290.0	1.30e-20	0.730	291.0	1.75e-20	0.735	292.0	8.32e-21	0.740	293.0	3.73e-20	0.745	294.0	6.54e-20	0.750
295.0	3.95e-20	0.755	296.0	2.33e-20	0.760	297.0	1.51e-20	0.765	298.0	4.04e-20	0.770	299.0	2.87e-20	0.775
300.0	8.71e-21	0.780	301.0	1.72e-20	0.780	302.0	1.06e-20	0.780	303.0	3.20e-20	0.780	304.0	6.90e-20	0.780
305.0	4.91e-20	0.780	306.0	4.63e-20	0.780	307.0	2.10e-20	0.780	308.0	1.49e-20	0.780	309.0	3.41e-20	0.780
310.0	1.95e-20	0.780	311.0	5.21e-21	0.764	312.0	1.12e-20	0.748	313.0	1.12e-20	0.732	314.0	4.75e-20	0.716
315.0	5.25e-20	0.700	316.0	2.90e-20	0.684	317.0	5.37e-20	0.668	318.0	2.98e-20	0.652	319.0	9.18e-21	0.636
320.0	1.26e-20	0.620	321.0	1.53e-20	0.585	322.0	6.69e-21	0.550	323.0	3.45e-21	0.515	324.0	8.16e-21	0.480
325.0	1.85e-20	0.445	326.0	5.95e-20	0.410	327.0	3.49e-20	0.375	328.0	1.09e-20	0.340	329.0	3.35e-20	0.305
330.0	3.32e-20	0.270	331.0	1.07e-20	0.243	332.0	2.89e-21	0.216	333.0	2.15e-21	0.189	334.0	1.71e-21	0.162
335.0	1.43e-21	0.135	336.0	1.94e-21	0.108	337.0	4.17e-21	0.081	338.0	2.36e-20	0.054	339.0	4.71e-20	0.027
340.0	2.48e-20	0.000												
							HCHO_M							
240.0	6.40e-22	0.490	241.0	5.60e-22	0.490	242.0	1.05e-21	0.490	243.0	1.15e-21	0.490	244.0	8.20e-22	0.490
245.0	1.03e-21	0.490	246.0	9.80e-22	0.490	247.0	1.35e-21	0.490	248.0	1.91e-21	0.490	249.0	2.82e-21	0.490
250.0	2.05e-21	0.490	251.0	1.70e-21	0.490	252.0	2.88e-21	0.490	253.0	2.55e-21	0.490	254.0	2.55e-21	0.490
255.0	3.60e-21	0.490	256.0	5.09e-21	0.490	257.0	3.39e-21	0.490	258.0	2.26e-21	0.490	259.0	5.04e-21	0.490
260.0	5.05e-21	0.490	261.0	5.49e-21	0.484	262.0	5.20e-21	0.478	263.0	9.33e-21	0.472	264.0	8.23e-21	0.466
265.0	4.30e-21	0.460	266.0	4.95e-21	0.454	267.0	1.24e-20	0.448	268.0	1.11e-20	0.442	269.0	8.78e-21	0.436
270.0	9.36e-21	0.430	271.0	1.79e-20	0.419	272.0	1.23e-20	0.408	273.0	6.45e-21	0.397	274.0	6.56e-21	0.386
275.0	2.23e-20	0.375	276.0	2.42e-20	0.364	277.0	1.40e-20	0.353	278.0	1.05e-20	0.342	279.0	2.55e-20	0.331
280.0	2.08e-20	0.320	281.0	1.48e-20	0.312	282.0	8.81e-21	0.304	283.0	1.07e-20	0.296	284.0	4.49e-20	0.288
285.0	3.59e-20	0.280	286.0	1.96e-20	0.272	287.0	1.30e-20	0.264	288.0	3.36e-20	0.256	289.0	2.84e-20	0.248
290.0	1.30e-20	0.240	291.0	1.75e-20	0.237	292.0	8.32e-21	0.234	293.0	3.73e-20	0.231	294.0	6.54e-20	0.228
295.0	3.95e-20	0.225	296.0	2.33e-20	0.222	297.0	1.51e-20	0.219	298.0	4.04e-20	0.216	299.0	2.87e-20	0.213
300.0	8.71e-21	0.210	301.0	1.72e-20	0.211	302.0	1.06e-20	0.212	303.0	3.20e-20	0.213	304.0	6.90e-20	0.214
305.0	4.91e-20	0.215	306.0	4.63e-20	0.216	307.0	2.10e-20	0.217	308.0	1.49e-20	0.218	309.0	3.41e-20	0.219
310.0	1.95e-20	0.220	311.0	5.21e-21	0.236	312.0	1.12e-20	0.252	313.0	1.12e-20	0.268	314.0	4.75e-20	0.284
315.0	5.25e-20	0.300	316.0	2.90e-20	0.316	317.0	5.37e-20	0.332	318.0	2.98e-20	0.348	319.0	9.18e-21	0.364
320.0	1.26e-20	0.380	321.0	1.53e-20	0.408	322.0	6.69e-21	0.436	323.0	3.45e-21	0.464	324.0	8.16e-21	0.492
325.0	1.85e-20	0.520	326.0	5.95e-20	0.548	327.0	3.49e-20	0.576	328.0	1.09e-20	0.604	329.0	3.35e-20	0.632
330.0	3.32e-20	0.660	331.0	1.07e-20	0.650	332.0	2.89e-21	0.640	333.0	2.15e-21	0.630	334.0	1.71e-21	0.620
335.0	1.43e-21	0.610	336.0	1.94e-21	0.600	337.0	4.17e-21	0.590	338.0	2.36e-20	0.580	339.0	4.71e-20	0.570
340.0	2.48e-20	0.560	341.0	7.59e-21	0.525	342.0	6.81e-21	0.490	343.0	1.95e-20	0.455	344.0	1.14e-20	0.420
345.0	3.23e-21	0.385	346.0	1.13e-21	0.350	347.0	6.60e-22	0.315	348.0	1.22e-21	0.280	349.0	3.20e-22	0.245

Table A-3 (continued)

WL (nm)	Abs (cm^2)	QY	WL (nm)	Abs (cm^2)	QY	WL (nm)	Abs (cm^2)	QY	WL (nm)	Abs (cm^2)	QY	WL (nm)	Abs (cm^2)	QY
350.0	3.80e-22	0.210	351.0	1.04e-21	0.192	352.0	7.13e-21	0.174	353.0	2.21e-20	0.156	354.0	1.54e-20	0.138
355.0	6.76e-21	0.120	356.0	1.35e-21	0.102	357.0	3.60e-22	0.084	358.0	5.70e-23	0.066	359.0	5.80e-22	0.048
360.0	8.20e-22	0.000												
							CCHO_R							
262.0	2.44e-20	0.326	266.0	3.05e-20	0.358	270.0	3.42e-20	0.390	274.0	4.03e-20	0.466	278.0	4.19e-20	0.542
280.0	4.50e-20	0.580	281.0	4.69e-20	0.575	282.0	4.72e-20	0.570	283.0	4.75e-20	0.565	284.0	4.61e-20	0.560
285.0	4.49e-20	0.555	286.0	4.44e-20	0.550	287.0	4.59e-20	0.545	288.0	4.72e-20	0.540	289.0	4.77e-20	0.535
290.0	4.89e-20	0.530	291.0	4.78e-20	0.520	292.0	4.68e-20	0.510	293.0	4.53e-20	0.500	294.0	4.33e-20	0.490
295.0	4.27e-20	0.480	296.0	4.24e-20	0.470	297.0	4.38e-20	0.460	298.0	4.41e-20	0.450	299.0	4.26e-20	0.440
300.0	4.16e-20	0.430	301.0	3.99e-20	0.418	302.0	3.86e-20	0.406	303.0	3.72e-20	0.394	304.0	3.48e-20	0.382
305.0	3.42e-20	0.370	306.0	3.42e-20	0.354	307.0	3.36e-20	0.338	308.0	3.33e-20	0.322	309.0	3.14e-20	0.306
310.0	2.93e-20	0.290	311.0	2.76e-20	0.266	312.0	2.53e-20	0.242	313.0	2.47e-20	0.218	314.0	2.44e-20	0.194
315.0	2.20e-20	0.170	316.0	2.04e-20	0.156	317.0	2.07e-20	0.142	318.0	1.98e-20	0.128	319.0	1.87e-20	0.114
320.0	1.72e-20	0.100	321.0	1.48e-20	0.088	322.0	1.40e-20	0.076	323.0	1.24e-20	0.064	324.0	1.09e-20	0.052
325.0	1.14e-20	0.040	326.0	1.07e-20	0.032	327.0	8.58e-21	0.024	328.0	7.47e-21	0.016	329.0	7.07e-21	0.008
							C2CHO							
294.0	5.80e-20	0.890	295.0	5.57e-20	0.885	296.0	5.37e-20	0.880	297.0	5.16e-20	0.875	298.0	5.02e-20	0.870
299.0	5.02e-20	0.865	300.0	5.04e-20	0.860	301.0	5.09e-20	0.855	302.0	5.07e-20	0.850	303.0	4.94e-20	0.818
304.0	4.69e-20	0.786	305.0	4.32e-20	0.755	306.0	4.04e-20	0.723	307.0	3.81e-20	0.691	308.0	3.65e-20	0.659
309.0	3.62e-20	0.627	310.0	3.60e-20	0.596	311.0	3.53e-20	0.564	312.0	3.50e-20	0.532	313.0	3.32e-20	0.500
314.0	3.06e-20	0.480	315.0	2.77e-20	0.460	316.0	2.43e-20	0.440	317.0	2.18e-20	0.420	318.0	2.00e-20	0.400
319.0	1.86e-20	0.380	320.0	1.83e-20	0.360	321.0	1.78e-20	0.340	322.0	1.66e-20	0.320	323.0	1.58e-20	0.300
324.0	1.49e-20	0.280	325.0	1.30e-20	0.260	326.0	1.13e-20	0.248	327.0	9.96e-21	0.236	328.0	8.28e-21	0.223
329.0	6.85e-21	0.211	330.0	5.75e-21	0.199	331.0	4.94e-21	0.187	332.0	4.66e-21	0.174	333.0	4.30e-21	0.162
334.0	3.73e-21	0.150	335.0	3.25e-21	0.133	336.0	2.80e-21	0.117	337.0	2.30e-21	0.100	338.0	1.85e-21	0.083
339.0	1.66e-21	0.067	340.0	1.55e-21	0.050	341.0	1.19e-21	0.033	342.0	7.60e-22	0.017	343.0	4.50e-22	0.000
							ACETONE							
250.0	2.47e-20	0.760	254.0	3.04e-20	0.776	258.0	3.61e-20	0.792	262.0	4.15e-20	0.768	266.0	4.58e-20	0.704
270.0	4.91e-20	0.640	274.0	5.06e-20	0.604	278.0	5.07e-20	0.568	280.0	5.05e-20	0.550	281.0	5.01e-20	0.525
282.0	4.94e-20	0.500	283.0	4.86e-20	0.475	284.0	4.76e-20	0.450	285.0	4.68e-20	0.425	286.0	4.58e-20	0.400
287.0	4.50e-20	0.375	288.0	4.41e-20	0.350	289.0	4.29e-20	0.325	290.0	4.19e-20	0.302	291.0	4.08e-20	0.284
292.0	3.94e-20	0.266	293.0	3.81e-20	0.249	294.0	3.67e-20	0.232	295.0	3.52e-20	0.217	296.0	3.35e-20	0.201
297.0	3.20e-20	0.187	298.0	3.07e-20	0.173	299.0	2.91e-20	0.160	300.0	2.77e-20	0.147	301.0	2.66e-20	0.135
302.0	2.53e-20	0.124	303.0	2.37e-20	0.114	304.0	2.24e-20	0.104	305.0	2.11e-20	0.095	306.0	1.95e-20	0.086
307.0	1.80e-20	0.078	308.0	1.66e-20	0.071	309.0	1.54e-20	0.064	310.0	1.41e-20	0.057	311.0	1.28e-20	0.052
312.0	1.17e-20	0.046	313.0	1.08e-20	0.042	314.0	9.67e-21	0.037	315.0	8.58e-21	0.033	316.0	7.77e-21	0.029
317.0	6.99e-21	0.026	318.0	6.08e-21	0.023	319.0	5.30e-21	0.020	320.0	4.67e-21	0.018	321.0	4.07e-21	0.016
322.0	3.44e-21	0.014	323.0	2.87e-21	0.012	324.0	2.43e-21	0.011	325.0	2.05e-21	0.009	326.0	1.68e-21	0.008
327.0	1.35e-21	0.007	328.0	1.08e-21	0.006	329.0	8.60e-22	0.005	330.0	6.70e-22	0.005	331.0	5.10e-22	0.004
332.0	4.00e-22	0.003	333.0	3.10e-22	0.003	334.0	2.60e-22	0.002	335.0	1.70e-22	0.002	336.0	1.40e-22	0.002
337.0	1.10e-22	0.002	338.0	9.00e-23	0.001	339.0	6.00e-23	0.001	340.0	5.00e-23	0.001	341.0	5.00e-23	0.001
342.0	3.00e-23	0.001	343.0	4.00e-23	0.001	344.0	2.00e-23	0.000						
							KETONE							
198.5	3.95e-19	1.000	199.0	1.61e-19	1.000	199.5	7.75e-20	1.000	200.0	3.76e-20	1.000	200.5	2.51e-20	1.000
201.0	1.83e-20	1.000	201.5	1.36e-20	1.000	202.0	1.16e-20	1.000	202.5	8.97e-21	1.000	203.0	4.62e-21	1.000
203.5	3.18e-21	1.000	204.0	2.42e-21	1.000	204.5	2.01e-21	1.000	205.0	1.77e-21	1.000	205.5	1.64e-21	1.000
206.0	1.54e-21	1.000	206.5	1.52e-21	1.000	207.0	1.54e-21	1.000	207.5	1.62e-21	1.000	208.0	1.64e-21	1.000
208.5	1.60e-21	1.000	209.0	1.57e-21	1.000	209.5	1.49e-21	1.000	210.0	1.47e-21	1.000	210.5	1.52e-21	1.000
211.0	1.50e-21	1.000	211.5	1.62e-21	1.000	212.0	1.81e-21	1.000	212.5	2.10e-21	1.000	213.0	2.23e-21	1.000
213.5	2.06e-21	1.000	214.0	1.69e-21	1.000	214.5	1.49e-21	1.000	215.0	1.42e-21	1.000	215.5	1.42e-21	1.000
216.0	1.42e-21	1.000	216.5	1.48e-21	1.000	217.0	1.48e-21	1.000	217.5	1.53e-21	1.000	218.0	1.56e-21	1.000
218.5	1.67e-21	1.000	219.0	1.68e-21	1.000	219.5	1.78e-21	1.000	220.0	1.85e-21	1.000	220.5	1.92e-21	1.000
221.0	2.01e-21	1.000	221.5	2.11e-21	1.000	222.0	2.23e-21	1.000	222.5	2.33e-21	1.000	223.0	2.48e-21	1.000
223.5	2.60e-21	1.000	224.0	2.74e-21	1.000	224.5	2.85e-21	1.000	225.0	3.04e-21	1.000	225.5	3.15e-21	1.000
226.0	3.33e-21	1.000	226.5	3.55e-21	1.000	227.0	3.73e-21	1.000	227.5	3.93e-21	1.000	228.0	4.11e-21	1.000
228.5	4.34e-21	1.000	229.0	4.56e-21	1.000	229.5	4.75e-21	1.000	230.0	5.01e-21	1.000	230.5	5.27e-21	1.000
231.0	5.53e-21	1.000	231.5	5.83e-21	1.000	232.0	6.15e-21	1.000	232.5	6.45e-21	1.000	233.0	6.73e-21	1.000
233.5	7.02e-21	1.000	234.0	7.42e-21	1.000	234.5	7.83e-21	1.000	235.0	8.11e-21	1.000	235.5	8.45e-21	1.000
236.0	8.82e-21	1.000	236.5	9.21e-21	1.000	237.0	9.65e-21	1.000	237.5	1.00e-20	1.000	238.0	1.05e-20	1.000
238.5	1.10e-20	1.000	239.0	1.15e-20	1.000	239.5	1.20e-20	1.000	240.0	1.23e-20	1.000	240.5	1.28e-20	1.000
241.0	1.32e-20	1.000	241.5	1.38e-20	1.000	242.0	1.44e-20	1.000	242.5	1.50e-20	1.000	243.0	1.57e-20	1.000
243.5	1.63e-20	1.000	244.0	1.68e-20	1.000	244.5	1.75e-20	1.000	245.0	1.81e-20	1.000	245.5	1.88e-20	1.000
246.0	1.96e-20	1.000	246.5	2.03e-20	1.000	247.0	2.11e-20	1.000	247.5	2.19e-20	1.000	248.0	2.25e-20	1.000
248.5	2.33e-20	1.000	249.0	2.40e-20	1.000	249.5	2.48e-20	1.000	250.0	2.56e-20	1.000	250.5	2.64e-20	1.000
251.0	2.73e-20	1.000	251.5	2.81e-20	1.000	252.0	2.88e-20	1.000	252.5	2.98e-20	1.000	253.0	3.07e-20	1.000
253.5	3.16e-20	1.000	254.0	3.25e-20	1.000	254.5	3.34e-20	1.000	255.0	3.43e-20	1.000	255.5	3.51e-20	1.000
256.0	3.59e-20	1.000	256.5	3.67e-20	1.000	257.0	3.75e-20	1.000	257.5	3.84e-20	1.000	258.0	3.94e-20	1.000
258.5	4.03e-20	1.000	259.0	4.13e-20	1.000	259.5	4.22e-20	1.000	260.0	4.28e-20	1.000	260.5	4.33e-20	1.000
261.0	4.41e-20	1.000	261.5	4.49e-20	1.000	262.0	4.57e-20	1.000	262.5	4.65e-20	1.000	263.0	4.72e-20	1.000
263.5	4.78e-20	1.000	264.0	4.85e-20	1.000	264.5	4.92e-20	1.000	265.0	4.99e-20	1.000	265.5	5.04e-20	1.000
266.0	5.12e-20	1.000	266.5	5.22e-20	1.000	267.0	5.28e-20	1.000	267.5	5.34e-20	1.000	268.0	5.41e-20	1.000

Table A-3 (continued)

WL (nm)	Abs (cm^2)	QY	WL (nm)	Abs (cm^2)	QY	WL (nm)	Abs (cm^2)	QY	WL (nm)	Abs (cm^2)	QY	WL (nm)	Abs (cm^2)	QY
268.5	5.46e-20	1.000	269.0	5.51e-20	1.000	269.5	5.55e-20	1.000	270.0	5.59e-20	1.000	270.5	5.63e-20	1.000
271.0	5.66e-20	1.000	271.5	5.70e-20	1.000	272.0	5.74e-20	1.000	272.5	5.78e-20	1.000	273.0	5.81e-20	1.000
273.5	5.86e-20	1.000	274.0	5.90e-20	1.000	274.5	5.93e-20	1.000	275.0	5.96e-20	1.000	275.5	5.97e-20	1.000
276.0	5.98e-20	1.000	276.5	5.98e-20	1.000	277.0	5.99e-20	1.000	277.5	5.99e-20	1.000	278.0	5.98e-20	1.000
278.5	5.96e-20	1.000	279.0	5.96e-20	1.000	279.5	5.95e-20	1.000	280.0	5.94e-20	1.000	280.5	5.92e-20	1.000
281.0	5.90e-20	1.000	281.5	5.88e-20	1.000	282.0	5.86e-20	1.000	282.5	5.83e-20	1.000	283.0	5.79e-20	1.000
283.5	5.75e-20	1.000	284.0	5.71e-20	1.000	284.5	5.67e-20	1.000	285.0	5.61e-20	1.000	285.5	5.56e-20	1.000
286.0	5.51e-20	1.000	286.5	5.45e-20	1.000	287.0	5.41e-20	1.000	287.5	5.37e-20	1.000	288.0	5.33e-20	1.000
288.5	5.27e-20	1.000	289.0	5.21e-20	1.000	289.5	5.15e-20	1.000	290.0	5.08e-20	1.000	290.5	4.99e-20	1.000
291.0	4.89e-20	1.000	291.5	4.82e-20	1.000	292.0	4.73e-20	1.000	292.5	4.62e-20	1.000	293.0	4.53e-20	1.000
293.5	4.41e-20	1.000	294.0	4.32e-20	1.000	294.5	4.23e-20	1.000	295.0	4.15e-20	1.000	295.5	4.11e-20	1.000
296.0	4.01e-20	1.000	296.5	3.94e-20	1.000	297.0	3.88e-20	1.000	297.5	3.77e-20	1.000	298.0	3.69e-20	1.000
298.5	3.63e-20	1.000	299.0	3.54e-20	1.000	299.5	3.46e-20	1.000	300.0	3.36e-20	1.000	300.5	3.24e-20	1.000
301.0	3.16e-20	1.000	301.5	3.06e-20	1.000	302.0	2.95e-20	1.000	302.5	2.82e-20	1.000	303.0	2.70e-20	1.000
303.5	2.59e-20	1.000	304.0	2.49e-20	1.000	304.5	2.42e-20	1.000	305.0	2.34e-20	1.000	305.5	2.28e-20	1.000
306.0	2.19e-20	1.000	306.5	2.11e-20	1.000	307.0	2.04e-20	1.000	307.5	1.93e-20	1.000	308.0	1.88e-20	1.000
308.5	1.80e-20	1.000	309.0	1.73e-20	1.000	309.5	1.66e-20	1.000	310.0	1.58e-20	1.000	310.5	1.48e-20	1.000
311.0	1.42e-20	1.000	311.5	1.34e-20	1.000	312.0	1.26e-20	1.000	312.5	1.17e-20	1.000	313.0	1.13e-20	1.000
313.5	1.08e-20	1.000	314.0	1.04e-20	1.000	314.5	9.69e-21	1.000	315.0	8.91e-21	1.000	315.5	8.61e-21	1.000
316.0	7.88e-21	1.000	316.5	7.25e-21	1.000	317.0	6.92e-21	1.000	317.5	6.43e-21	1.000	318.0	6.07e-21	1.000
318.5	5.64e-21	1.000	319.0	5.19e-21	1.000	319.5	4.66e-21	1.000	320.0	4.36e-21	1.000	320.5	3.95e-21	1.000
321.0	3.64e-21	1.000	321.5	3.38e-21	1.000	322.0	3.17e-21	1.000	322.5	2.80e-21	1.000	323.0	2.62e-21	1.000
323.5	2.29e-21	1.000	324.0	2.13e-21	1.000	324.5	1.93e-21	1.000	325.0	1.70e-21	1.000	325.5	1.58e-21	1.000
326.0	1.48e-21	1.000	326.5	1.24e-21	1.000	327.0	1.20e-21	1.000	327.5	1.04e-21	1.000	328.0	9.51e-22	1.000
328.5	8.44e-22	1.000	329.0	7.26e-22	1.000	329.5	6.70e-22	1.000	330.0	6.08e-22	1.000	330.5	5.15e-22	1.000
331.0	4.56e-22	1.000	331.5	4.13e-22	1.000	332.0	3.56e-22	1.000	332.5	3.30e-22	1.000	333.0	2.97e-22	1.000
333.5	2.67e-22	1.000	334.0	2.46e-22	1.000	334.5	2.21e-22	1.000	335.0	1.93e-22	1.000	335.5	1.56e-22	1.000
336.0	1.47e-22	1.000	336.5	1.37e-22	1.000	337.0	1.27e-22	1.000	337.5	1.19e-22	1.000	338.0	1.09e-22	1.000
338.5	1.01e-22	1.000	339.0	9.09e-23	1.000	339.5	8.22e-23	1.000	340.0	7.66e-23	1.000	340.5	7.43e-23	1.000
341.0	6.83e-23	1.000	341.5	6.72e-23	1.000	342.0	6.04e-23	1.000	342.5	4.78e-23	1.000	343.0	0.00e+00	1.000
							COOH							
210.0	3.12e-19	1.000	215.0	2.09e-19	1.000	220.0	1.54e-19	1.000	225.0	1.22e-19	1.000	230.0	9.62e-20	1.000
235.0	7.61e-20	1.000	240.0	6.05e-20	1.000	245.0	4.88e-20	1.000	250.0	3.98e-20	1.000	255.0	3.23e-20	1.000
260.0	2.56e-20	1.000	265.0	2.11e-20	1.000	270.0	1.70e-20	1.000	275.0	1.39e-20	1.000	280.0	1.09e-20	1.000
285.0	8.63e-21	1.000	290.0	6.91e-21	1.000	295.0	5.51e-21	1.000	300.0	4.13e-21	1.000	305.0	3.13e-21	1.000
310.0	2.39e-21	1.000	315.0	1.82e-21	1.000	320.0	1.37e-21	1.000	325.0	1.05e-21	1.000	330.0	7.90e-22	1.000
335.0	6.10e-22	1.000	340.0	4.70e-22	1.000	345.0	3.50e-22	1.000	350.0	2.70e-22	1.000	355.0	2.10e-22	1.000
360.0	1.60e-22	1.000	365.0	1.20e-22	1.000	370.0	0.00e+00	1.000						
							GLY_R							
230.0	2.87e-21	1.000	235.0	2.87e-21	1.000	240.0	4.30e-21	1.000	245.0	5.73e-21	1.000	250.0	8.60e-21	1.000
255.0	1.15e-20	1.000	260.0	1.43e-20	1.000	265.0	1.86e-20	1.000	270.0	2.29e-20	1.000	275.0	2.58e-20	1.000
280.0	2.87e-20	1.000	285.0	3.30e-20	1.000	290.0	3.15e-20	1.000	295.0	3.30e-20	1.000	300.0	3.58e-20	1.000
305.0	2.72e-20	1.000	310.0	2.72e-20	1.000	312.5	2.87e-20	1.000	315.0	2.29e-20	1.000	320.0	1.43e-20	1.000
325.0	1.15e-20	1.000	327.5	1.43e-20	1.000	330.0	1.15e-20	1.000	335.0	2.87e-21	1.000	340.0	0.00e+00	1.000
345.0	0.00e+00	1.000	350.0	0.00e+00	1.000	355.0	0.00e+00	1.000	360.0	2.29e-21	1.000	365.0	2.87e-21	1.000
370.0	8.03e-21	1.000	375.0	1.00e-20	1.000	380.0	1.72e-20	0.972	382.0	1.58e-20	0.855	384.0	1.49e-20	0.737
386.0	1.49e-20	0.619	388.0	2.87e-20	0.502	390.0	3.15e-20	0.384	391.0	3.24e-20	0.326	392.0	3.04e-20	0.267
393.0	2.23e-20	0.208	394.0	2.63e-20	0.149	395.0	3.04e-20	0.090	396.0	2.63e-20	0.032	397.0	2.43e-20	0.000
398.0	3.24e-20	0.000	399.0	3.04e-20	0.000	400.0	2.84e-20	0.000	401.0	3.24e-20	0.000	402.0	4.46e-20	0.000
403.0	5.27e-20	0.000	404.0	4.26e-20	0.000	405.0	3.04e-20	0.000	406.0	3.04e-20	0.000	407.0	2.84e-20	0.000
408.0	2.43e-20	0.000	409.0	2.84e-20	0.000	410.0	6.08e-20	0.000	411.0	5.07e-20	0.000	411.5	6.08e-20	0.000
412.0	4.86e-20	0.000	413.0	8.31e-20	0.000	413.5	6.48e-20	0.000	414.0	7.50e-20	0.000	414.5	8.11e-20	0.000
415.0	8.11e-20	0.000	415.5	6.89e-20	0.000	416.0	4.26e-20	0.000	417.0	4.86e-20	0.000	418.0	5.88e-20	0.000
							GLY_ABS							
230.0	2.87e-21	1.000	235.0	2.87e-21	1.000	240.0	4.30e-21	1.000	245.0	5.73e-21	1.000	250.0	8.60e-21	1.000
255.0	1.15e-20	1.000	260.0	1.43e-20	1.000	265.0	1.86e-20	1.000	270.0	2.29e-20	1.000	275.0	2.58e-20	1.000
280.0	2.87e-20	1.000	285.0	3.30e-20	1.000	290.0	3.15e-20	1.000	295.0	3.30e-20	1.000	300.0	3.58e-20	1.000
305.0	2.72e-20	1.000	310.0	2.72e-20	1.000	312.5	2.87e-20	1.000	315.0	2.29e-20	1.000	320.0	1.43e-20	1.000
325.0	1.15e-20	1.000	327.5	1.43e-20	1.000	330.0	1.15e-20	1.000	335.0	2.87e-21	1.000	340.0	0.00e+00	1.000
355.0	0.00e+00	1.000	360.0	2.29e-21	1.000	365.0	2.87e-21	1.000	370.0	8.03e-21	1.000	375.0	1.00e-20	1.000
380.0	1.72e-20	1.000	382.0	1.58e-20	1.000	384.0	1.49e-20	1.000	386.0	1.49e-20	1.000	388.0	2.87e-20	1.000
390.0	3.15e-20	1.000	391.0	3.24e-20	1.000	392.0	3.04e-20	1.000	393.0	2.23e-20	1.000	394.0	2.63e-20	1.000
395.0	3.04e-20	1.000	396.0	2.63e-20	1.000	397.0	2.43e-20	1.000	398.0	3.24e-20	1.000	399.0	3.04e-20	1.000
400.0	2.84e-20	1.000	401.0	3.24e-20	1.000	402.0	4.46e-20	1.000	403.0	5.27e-20	1.000	404.0	4.26e-20	1.000
405.0	3.04e-20	1.000	406.0	3.04e-20	1.000	407.0	2.84e-20	1.000	408.0	2.43e-20	1.000	409.0	2.84e-20	1.000
410.0	6.08e-20	1.000	411.0	5.07e-20	1.000	411.5	6.08e-20	1.000	412.0	4.86e-20	1.000	413.0	8.31e-20	1.000
413.5	6.48e-20	1.000	414.0	7.50e-20	1.000	414.5	8.11e-20	1.000	415.0	8.11e-20	1.000	415.5	6.89e-20	1.000
416.0	4.26e-20	1.000	417.0	4.86e-20	1.000	418.0	5.88e-20	1.000	419.0	6.69e-20	1.000	420.0	3.85e-20	1.000
421.0	5.67e-20	1.000	421.5	4.46e-20	1.000	422.0	5.27e-20	1.000	422.5	1.05e-19	1.000	423.0	8.51e-20	1.000
424.0	6.08e-20	1.000	425.0	7.29e-20	1.000	426.0	1.18e-19	1.000	426.5	1.30e-19	1.000	427.0	1.07e-19	1.000
428.0	1.66e-19	1.000	429.0	4.05e-20	1.000	430.0	5.07e-20	1.000	431.0	4.86e-20	1.000	432.0	4.05e-20	1.000

Table A-3 (continued)

WL (nm)	Abs (cm^2)	QY	WL (nm)	Abs (cm^2)	QY	WL (nm)	Abs (cm^2)	QY	WL (nm)	Abs (cm^2)	QY	WL (nm)	Abs (cm^2)	QY
433.0	3.65e-20	1.000	434.0	4.05e-20	1.000	434.5	6.08e-20	1.000	435.0	5.07e-20	1.000	436.0	8.11e-20	1.000
436.5	1.13e-19	1.000	437.0	5.27e-20	1.000	438.0	1.01e-19	1.000	438.5	1.38e-19	1.000	439.0	7.70e-20	1.000
440.0	2.47e-19	1.000	441.0	8.11e-20	1.000	442.0	6.08e-20	1.000	443.0	7.50e-20	1.000	444.0	9.32e-20	1.000
445.0	1.13e-19	1.000	446.0	5.27e-20	1.000	447.0	2.43e-20	1.000	448.0	2.84e-20	1.000	449.0	3.85e-20	1.000
450.0	6.08e-20	1.000	451.0	1.09e-19	1.000	451.5	9.32e-20	1.000	452.0	1.22e-19	1.000	453.0	2.39e-19	1.000
454.0	1.70e-19	1.000	455.0	3.40e-19	1.000	455.5	4.05e-19	1.000	456.0	1.01e-19	1.000	457.0	1.62e-20	1.000
458.0	1.22e-20	1.000	458.5	1.42e-20	1.000	459.0	4.05e-21	1.000	460.0	4.05e-21	1.000	460.5	6.08e-21	1.000
461.0	2.03e-21	1.000	462.0	0.00e+00	1.000									
						MGLY_ADJ								
219.0	9.84e-21	1.000	219.5	1.04e-20	1.000	220.0	1.06e-20	1.000	220.5	1.11e-20	1.000	221.0	1.15e-20	1.000
221.5	1.18e-20	1.000	222.0	1.22e-20	1.000	222.5	1.24e-20	1.000	223.0	1.26e-20	1.000	223.5	1.26e-20	1.000
224.0	1.25e-20	1.000	224.5	1.24e-20	1.000	225.0	1.25e-20	1.000	225.5	1.27e-20	1.000	226.0	1.27e-20	1.000
226.5	1.29e-20	1.000	227.0	1.31e-20	1.000	227.5	1.32e-20	1.000	228.0	1.35e-20	1.000	228.5	1.37e-20	1.000
229.0	1.40e-20	1.000	229.5	1.42e-20	1.000	230.0	1.48e-20	1.000	230.5	1.53e-20	1.000	231.0	1.57e-20	1.000
231.5	1.59e-20	1.000	232.0	1.61e-20	1.000	232.5	1.62e-20	1.000	233.0	1.61e-20	1.000	233.5	1.68e-20	1.000
234.0	1.74e-20	1.000	234.5	1.80e-20	1.000	235.0	1.84e-20	1.000	235.5	1.87e-20	1.000	236.0	1.89e-20	1.000
236.5	1.91e-20	1.000	237.0	1.93e-20	1.000	237.5	1.94e-20	1.000	238.0	1.96e-20	1.000	238.5	1.96e-20	1.000
239.0	2.01e-20	1.000	239.5	2.04e-20	1.000	240.0	2.08e-20	1.000	240.5	2.10e-20	1.000	241.0	2.14e-20	1.000
241.5	2.16e-20	1.000	242.0	2.19e-20	1.000	242.5	2.20e-20	1.000	243.0	2.23e-20	1.000	243.5	2.26e-20	1.000
244.0	2.28e-20	1.000	244.5	2.29e-20	1.000	245.0	2.30e-20	1.000	245.5	2.32e-20	1.000	246.0	2.33e-20	1.000
246.5	2.35e-20	1.000	247.0	2.38e-20	1.000	247.5	2.41e-20	1.000	248.0	2.46e-20	1.000	248.5	2.51e-20	1.000
249.0	2.57e-20	1.000	249.5	2.61e-20	1.000	250.0	2.65e-20	1.000	250.5	2.67e-20	1.000	251.0	2.69e-20	1.000
251.5	2.69e-20	1.000	252.0	2.71e-20	1.000	252.5	2.72e-20	1.000	253.0	2.73e-20	1.000	253.5	2.74e-20	1.000
254.0	2.76e-20	1.000	254.5	2.78e-20	1.000	255.0	2.82e-20	1.000	255.5	2.87e-20	1.000	256.0	2.93e-20	1.000
256.5	2.98e-20	1.000	257.0	3.07e-20	1.000	257.5	3.12e-20	1.000	258.0	3.17e-20	1.000	258.5	3.21e-20	1.000
259.0	3.26e-20	1.000	259.5	3.28e-20	1.000	260.0	3.29e-20	1.000	260.5	3.31e-20	1.000	261.0	3.33e-20	1.000
261.5	3.34e-20	1.000	262.0	3.36e-20	1.000	262.5	3.38e-20	1.000	263.0	3.42e-20	1.000	263.5	3.44e-20	1.000
264.0	3.48e-20	1.000	264.5	3.54e-20	1.000	265.0	3.59e-20	1.000	265.5	3.65e-20	1.000	266.0	3.73e-20	1.000
266.5	3.80e-20	1.000	267.0	3.87e-20	1.000	267.5	3.95e-20	1.000	268.0	4.02e-20	1.000	268.5	4.08e-20	1.000
269.0	4.13e-20	1.000	269.5	4.17e-20	1.000	270.0	4.20e-20	1.000	270.5	4.22e-20	1.000	271.0	4.22e-20	1.000
271.5	4.22e-20	1.000	272.0	4.23e-20	1.000	272.5	4.24e-20	1.000	273.0	4.27e-20	1.000	273.5	4.29e-20	1.000
274.0	4.31e-20	1.000	274.5	4.33e-20	1.000	275.0	4.37e-20	1.000	275.5	4.42e-20	1.000	276.0	4.48e-20	1.000
276.5	4.56e-20	1.000	277.0	4.64e-20	1.000	277.5	4.71e-20	1.000	278.0	4.78e-20	1.000	278.5	4.83e-20	1.000
279.0	4.87e-20	1.000	279.5	4.90e-20	1.000	280.0	4.92e-20	1.000	280.5	4.93e-20	1.000	281.0	4.94e-20	1.000
281.5	4.92e-20	1.000	282.0	4.90e-20	1.000	282.5	4.86e-20	1.000	283.0	4.83e-20	1.000	283.5	4.79e-20	1.000
284.0	4.76e-20	1.000	284.5	4.72e-20	1.000	285.0	4.70e-20	1.000	285.5	4.68e-20	1.000	286.0	4.66e-20	1.000
286.5	4.65e-20	1.000	287.0	4.65e-20	1.000	287.5	4.68e-20	1.000	288.0	4.73e-20	1.000	288.5	4.78e-20	1.000
289.0	4.84e-20	1.000	289.5	4.89e-20	1.000	290.0	4.92e-20	1.000	290.5	4.92e-20	1.000	291.0	4.90e-20	1.000
291.5	4.86e-20	1.000	292.0	4.81e-20	1.000	292.5	4.75e-20	1.000	293.0	4.70e-20	1.000	293.5	4.65e-20	1.000
294.0	4.58e-20	1.000	294.5	4.48e-20	1.000	295.0	4.38e-20	1.000	295.5	4.27e-20	1.000	296.0	4.17e-20	1.000
296.5	4.07e-20	1.000	297.0	3.99e-20	1.000	297.5	3.94e-20	1.000	298.0	3.88e-20	1.000	298.5	3.82e-20	1.000
299.0	3.76e-20	1.000	299.5	3.72e-20	1.000	300.0	3.69e-20	1.000	300.5	3.68e-20	1.000	301.0	3.70e-20	1.000
301.5	3.72e-20	1.000	302.0	3.74e-20	1.000	302.5	3.74e-20	1.000	303.0	3.75e-20	1.000	303.5	3.71e-20	1.000
304.0	3.62e-20	1.000	304.5	3.51e-20	1.000	305.0	3.38e-20	1.000	305.5	3.25e-20	1.000	306.0	3.15e-20	1.000
306.5	3.04e-20	1.000	307.0	2.92e-20	1.000	307.5	2.80e-20	1.000	308.0	2.71e-20	1.000	308.5	2.63e-20	1.000
309.0	2.52e-20	1.000	309.5	2.43e-20	1.000	310.0	2.34e-20	1.000	310.5	2.25e-20	1.000	311.0	2.19e-20	1.000
311.5	2.12e-20	1.000	312.0	2.06e-20	1.000	312.5	2.02e-20	1.000	313.0	1.96e-20	1.000	313.5	1.92e-20	1.000
314.0	1.91e-20	1.000	314.5	1.88e-20	1.000	315.0	1.86e-20	1.000	315.5	1.85e-20	1.000	316.0	1.86e-20	1.000
316.5	1.87e-20	1.000	317.0	1.87e-20	1.000	317.5	1.87e-20	1.000	318.0	1.83e-20	1.000	318.5	1.75e-20	1.000
319.0	1.69e-20	1.000	319.5	1.60e-20	1.000	320.0	1.50e-20	1.000	320.5	1.41e-20	1.000	321.0	1.34e-20	1.000
321.5	1.27e-20	1.000	322.0	1.21e-20	1.000	322.5	1.18e-20	1.000	323.0	1.14e-20	1.000	323.5	1.08e-20	1.000
324.0	1.01e-20	1.000	324.5	9.62e-21	1.000	325.0	9.28e-21	1.000	325.5	8.75e-21	1.000	326.0	8.49e-21	1.000
326.5	8.21e-21	1.000	327.0	7.71e-21	1.000	327.5	7.38e-21	1.000	328.0	7.18e-21	1.000	328.5	6.86e-21	1.000
329.0	6.71e-21	1.000	329.5	6.63e-21	1.000	330.0	6.46e-21	1.000	330.5	6.29e-21	1.000	331.0	6.21e-21	1.000
331.5	6.18e-21	1.000	332.0	6.20e-21	1.000	332.5	5.49e-21	1.000	333.0	5.21e-21	1.000	333.5	5.38e-21	1.000
334.0	5.35e-21	1.000	334.5	5.04e-21	1.000	335.0	4.94e-21	1.000	335.5	4.90e-21	1.000	336.0	4.52e-21	1.000
336.5	4.26e-21	1.000	337.0	4.11e-21	1.000	337.5	3.76e-21	1.000	338.0	3.61e-21	1.000	338.5	3.58e-21	1.000
339.0	3.47e-21	1.000	339.5	3.32e-21	1.000	340.0	3.22e-21	1.000	340.5	3.10e-21	1.000	341.0	3.00e-21	1.000
341.5	2.94e-21	1.000	342.0	2.89e-21	1.000	342.5	2.86e-21	1.000	343.0	2.88e-21	1.000	343.5	2.88e-21	1.000
344.0	2.89e-21	0.992	344.5	2.91e-21	0.984	345.0	2.95e-21	0.976	345.5	3.00e-21	0.968	346.0	3.08e-21	0.960
346.5	3.18e-21	0.953	347.0	3.25e-21	0.945	347.5	3.30e-21	0.937	348.0	3.39e-21	0.929	348.5	3.51e-21	0.921
349.0	3.63e-21	0.913	349.5	3.73e-21	0.905	350.0	3.85e-21	0.897	350.5	3.99e-21	0.889	351.0	4.27e-21	0.881
351.5	4.47e-21	0.873	352.0	4.63e-21	0.865	352.5	4.78e-21	0.858	353.0	4.92e-21	0.850	353.5	5.07e-21	0.842
354.0	5.23e-21	0.834	354.5	5.39e-21	0.826	355.0	5.56e-21	0.818	355.5	5.77e-21	0.810	356.0	5.97e-21	0.802
356.5	6.15e-21	0.794	357.0	6.35e-21	0.786	357.5	6.56e-21	0.778	358.0	6.76e-21	0.770	358.5	6.95e-21	0.763
359.0	7.20e-21	0.755	359.5	7.44e-21	0.747	360.0	7.64e-21	0.739	360.5	7.89e-21	0.731	361.0	8.15e-21	0.723
361.5	8.43e-21	0.715	362.0	8.71e-21	0.707	362.5	9.02e-21	0.699	363.0	9.33e-21	0.691	363.5	9.65e-21	0.683
364.0	1.00e-20	0.675	364.5	1.04e-20	0.668	365.0	1.08e-20	0.660	365.5	1.11e-20	0.652	366.0	1.15e-20	0.644
366.5	1.19e-20	0.636	367.0	1.23e-20	0.628	367.5	1.27e-20	0.620	368.0	1.31e-20	0.612	368.5	1.35e-20	0.604
369.0	1.40e-20	0.596	369.5	1.44e-20	0.588	370.0	1.47e-20	0.580	370.5	1.51e-20	0.573	371.0	1.55e-20	0.565
371.5	1.59e-20	0.557	372.0	1.64e-20	0.549	372.5	1.70e-20	0.541	373.0	1.73e-20	0.533	373.5	1.77e-20	0.525
374.0	1.81e-20	0.517	374.5	1.86e-20	0.509	375.0	1.90e-20	0.501	375.5	1.96e-20	0.493	376.0	2.02e-20	0.486

Table A-3 (continued)

WL (nm)	Abs (cm^2)	QY	WL (nm)	Abs (cm^2)	QY	WL (nm)	Abs (cm^2)	QY	WL (nm)	Abs (cm^2)	QY	WL (nm)	Abs (cm^2)	QY
376.5	2.06e-20	0.478	377.0	2.10e-20	0.470	377.5	2.14e-20	0.462	378.0	2.18e-20	0.454	378.5	2.24e-20	0.446
379.0	2.30e-20	0.438	379.5	2.37e-20	0.430	380.0	2.42e-20	0.422	380.5	2.47e-20	0.414	381.0	2.54e-20	0.406
381.5	2.62e-20	0.398	382.0	2.69e-20	0.391	382.5	2.79e-20	0.383	383.0	2.88e-20	0.375	383.5	2.96e-20	0.367
384.0	3.02e-20	0.359	384.5	3.10e-20	0.351	385.0	3.20e-20	0.343	385.5	3.29e-20	0.335	386.0	3.39e-20	0.327
386.5	3.51e-20	0.319	387.0	3.62e-20	0.311	387.5	3.69e-20	0.303	388.0	3.70e-20	0.296	388.5	3.77e-20	0.288
389.0	3.88e-20	0.280	389.5	3.97e-20	0.272	390.0	4.03e-20	0.264	390.5	4.12e-20	0.256	391.0	4.22e-20	0.248
391.5	4.29e-20	0.240	392.0	4.30e-20	0.232	392.5	4.38e-20	0.224	393.0	4.47e-20	0.216	393.5	4.55e-20	0.208
394.0	4.56e-20	0.201	394.5	4.59e-20	0.193	395.0	4.67e-20	0.185	395.5	4.80e-20	0.177	396.0	4.87e-20	0.169
396.5	4.96e-20	0.161	397.0	5.08e-20	0.153	397.5	5.19e-20	0.145	398.0	5.23e-20	0.137	398.5	5.39e-20	0.129
399.0	5.46e-20	0.121	399.5	5.54e-20	0.113	400.0	5.59e-20	0.106	400.5	5.77e-20	0.098	401.0	5.91e-20	0.090
401.5	5.99e-20	0.082	402.0	6.06e-20	0.074	402.5	6.20e-20	0.066	403.0	6.35e-20	0.058	403.5	6.52e-20	0.050
404.0	6.54e-20	0.042	404.5	6.64e-20	0.034	405.0	6.93e-20	0.026	405.5	7.15e-20	0.018	406.0	7.19e-20	0.011
406.5	7.32e-20	0.003	407.0	7.58e-20	0.000	407.5	7.88e-20	0.000	408.0	7.97e-20	0.000	408.5	7.91e-20	0.000
409.0	8.11e-20	0.000	409.5	8.41e-20	0.000	410.0	8.53e-20	0.000	410.5	8.59e-20	0.000	411.0	8.60e-20	0.000
411.5	8.80e-20	0.000	412.0	9.04e-20	0.000	412.5	9.45e-20	0.000	413.0	9.34e-20	0.000	413.5	9.37e-20	0.000
414.0	9.63e-20	0.000	414.5	9.71e-20	0.000	415.0	9.70e-20	0.000	415.5	9.65e-20	0.000	416.0	9.69e-20	0.000
416.5	9.89e-20	0.000	417.0	1.00e-19	0.000	417.5	1.02e-19	0.000	418.0	1.00e-19	0.000	418.5	1.02e-19	0.000
419.0	1.01e-19	0.000	419.5	1.01e-19	0.000	420.0	1.03e-19	0.000	420.5	1.01e-19	0.000	421.0	1.04e-19	0.000
							BACL_ADJ							
230.0	1.30e-20	1.000	232.5	1.46e-20	1.000	235.0	1.68e-20	1.000	237.5	1.84e-20	1.000	240.0	2.16e-20	1.000
242.5	2.49e-20	1.000	245.0	2.65e-20	1.000	247.5	2.71e-20	1.000	250.0	3.03e-20	1.000	252.5	3.46e-20	1.000
255.0	3.46e-20	1.000	257.5	3.57e-20	1.000	260.0	3.95e-20	1.000	262.5	4.17e-20	1.000	265.0	4.17e-20	1.000
267.5	4.22e-20	1.000	270.0	4.60e-20	1.000	272.5	4.54e-20	1.000	275.0	4.33e-20	1.000	277.5	4.22e-20	1.000
280.0	4.44e-20	1.000	282.5	4.33e-20	1.000	285.0	3.90e-20	1.000	287.5	3.57e-20	1.000	290.0	3.25e-20	1.000
292.5	2.92e-20	1.000	295.0	2.60e-20	1.000	297.5	2.16e-20	1.000	300.0	1.79e-20	1.000	302.5	1.73e-20	1.000
305.0	1.46e-20	1.000	307.5	1.08e-20	1.000	310.0	9.20e-21	1.000	312.5	7.03e-21	1.000	315.0	6.49e-21	1.000
317.5	5.41e-21	1.000	320.0	5.41e-21	1.000	322.5	5.41e-21	1.000	325.0	4.33e-21	1.000	327.5	3.25e-21	1.000
330.0	3.79e-21	1.000	332.5	3.79e-21	1.000	335.0	4.33e-21	1.000	337.5	4.87e-21	1.000	340.0	5.41e-21	1.000
342.5	5.95e-21	1.000	345.0	6.49e-21	1.000	347.5	7.03e-21	1.000	350.0	8.12e-21	0.995	352.5	7.57e-21	0.960
355.0	9.20e-21	0.925	357.5	9.74e-21	0.890	360.0	1.08e-20	0.855	362.5	1.19e-20	0.820	365.0	1.41e-20	0.785
367.5	1.51e-20	0.750	370.0	1.79e-20	0.715	372.5	2.00e-20	0.680	375.0	2.11e-20	0.645	377.5	2.33e-20	0.610
380.0	2.60e-20	0.575	382.5	2.81e-20	0.540	385.0	3.14e-20	0.505	387.5	3.46e-20	0.470	390.0	3.90e-20	0.435
392.5	4.11e-20	0.399	395.0	4.33e-20	0.364	397.5	4.38e-20	0.329	400.0	4.65e-20	0.294	402.5	4.81e-20	0.259
405.0	5.19e-20	0.224	407.5	5.84e-20	0.189	410.0	6.06e-20	0.154	412.5	6.49e-20	0.119	415.0	6.92e-20	0.084
417.5	6.87e-20	0.049	420.0	6.82e-20	0.014	422.5	6.71e-20	0.000	425.0	6.49e-20	0.000	427.5	5.95e-20	0.000
430.0	5.73e-20	0.000	432.5	6.28e-20	0.000	435.0	6.01e-20	0.000	437.5	5.84e-20	0.000	440.0	5.95e-20	0.000
442.5	6.49e-20	0.000	445.0	5.95e-20	0.000	447.5	4.98e-20	0.000	450.0	3.79e-20	0.000	452.5	2.81e-20	0.000
455.0	1.73e-20	0.000	457.5	1.08e-20	0.000	460.0	5.41e-21	0.000	462.5	3.79e-21	0.000	465.0	2.16e-21	0.000
467.5	1.08e-21	0.000	470.0	1.08e-21	0.000	472.5	0.00e+00	0.000						
							BZCHO							
299.0	1.78e-19	1.000	304.0	7.40e-20	1.000	306.0	6.91e-20	1.000	309.0	6.41e-20	1.000	313.0	6.91e-20	1.000
314.0	6.91e-20	1.000	318.0	6.41e-20	1.000	325.0	8.39e-20	1.000	332.0	7.65e-20	1.000	338.0	8.88e-20	1.000
342.0	8.88e-20	1.000	346.0	7.89e-20	1.000	349.0	7.89e-20	1.000	354.0	9.13e-20	1.000	355.0	8.14e-20	1.000
364.0	5.67e-20	1.000	368.0	6.66e-20	1.000	369.0	8.39e-20	1.000	370.0	8.39e-20	1.000	372.0	3.45e-20	1.000
374.0	3.21e-20	1.000	376.0	2.47e-20	1.000	377.0	2.47e-20	1.000	380.0	3.58e-20	1.000	382.0	9.90e-21	1.000
386.0	0.00e+00	1.000												
							ACROLEIN							
250.0	1.80e-21	1.000	252.0	2.05e-21	1.000	253.0	2.20e-21	1.000	254.0	2.32e-21	1.000	255.0	2.45e-21	1.000
256.0	2.56e-21	1.000	257.0	2.65e-21	1.000	258.0	2.74e-21	1.000	259.0	2.83e-21	1.000	260.0	2.98e-21	1.000
261.0	3.24e-21	1.000	262.0	3.47e-21	1.000	263.0	3.58e-21	1.000	264.0	3.93e-21	1.000	265.0	4.67e-21	1.000
266.0	5.10e-21	1.000	267.0	5.38e-21	1.000	268.0	5.73e-21	1.000	269.0	6.13e-21	1.000	270.0	6.64e-21	1.000
271.0	7.20e-21	1.000	272.0	7.77e-21	1.000	273.0	8.37e-21	1.000	274.0	8.94e-21	1.000	275.0	9.55e-21	1.000
276.0	1.04e-20	1.000	277.0	1.12e-20	1.000	278.0	1.19e-20	1.000	279.0	1.27e-20	1.000	280.0	1.27e-20	1.000
281.0	1.26e-20	1.000	282.0	1.26e-20	1.000	283.0	1.28e-20	1.000	284.0	1.33e-20	1.000	285.0	1.38e-20	1.000
286.0	1.44e-20	1.000	287.0	1.50e-20	1.000	288.0	1.57e-20	1.000	289.0	1.63e-20	1.000	290.0	1.71e-20	1.000
291.0	1.78e-20	1.000	292.0	1.86e-20	1.000	293.0	1.95e-20	1.000	294.0	2.05e-20	1.000	295.0	2.15e-20	1.000
296.0	2.26e-20	1.000	297.0	2.37e-20	1.000	298.0	2.48e-20	1.000	299.0	2.60e-20	1.000	300.0	2.73e-20	1.000
301.0	2.85e-20	1.000	302.0	2.99e-20	1.000	303.0	3.13e-20	1.000	304.0	3.27e-20	1.000	305.0	3.39e-20	1.000
306.0	3.51e-20	1.000	307.0	3.63e-20	1.000	308.0	3.77e-20	1.000	309.0	3.91e-20	1.000	310.0	4.07e-20	1.000
311.0	4.25e-20	1.000	312.0	4.39e-20	1.000	313.0	4.44e-20	1.000	314.0	4.50e-20	1.000	315.0	4.59e-20	1.000
316.0	4.75e-20	1.000	317.0	4.90e-20	1.000	318.0	5.05e-20	1.000	319.0	5.19e-20	1.000	320.0	5.31e-20	1.000
321.0	5.43e-20	1.000	322.0	5.52e-20	1.000	323.0	5.60e-20	1.000	324.0	5.67e-20	1.000	325.0	5.67e-20	1.000
326.0	5.62e-20	1.000	327.0	5.63e-20	1.000	328.0	5.71e-20	1.000	329.0	5.76e-20	1.000	330.0	5.80e-20	1.000
331.0	5.95e-20	1.000	332.0	6.23e-20	1.000	333.0	6.39e-20	1.000	334.0	6.38e-20	1.000	335.0	6.24e-20	1.000
336.0	6.01e-20	1.000	337.0	5.79e-20	1.000	338.0	5.63e-20	1.000	339.0	5.56e-20	1.000	340.0	5.52e-20	1.000
341.0	5.54e-20	1.000	342.0	5.53e-20	1.000	343.0	5.47e-20	1.000	344.0	5.41e-20	1.000	345.0	5.40e-20	1.000
346.0	5.48e-20	1.000	347.0	5.90e-20	1.000	348.0	6.08e-20	1.000	349.0	6.00e-20	1.000	350.0	5.53e-20	1.000
351.0	5.03e-20	1.000	352.0	4.50e-20	1.000	353.0	4.03e-20	1.000	354.0	3.75e-20	1.000	355.0	3.55e-20	1.000
356.0	3.45e-20	1.000	357.0	3.46e-20	1.000	358.0	3.49e-20	1.000	359.0	3.41e-20	1.000	360.0	3.23e-20	1.000
361.0	2.95e-20	1.000	362.0	2.81e-20	1.000	363.0	2.91e-20	1.000	364.0	3.25e-20	1.000	365.0	3.54e-20	1.000
366.0	3.30e-20	1.000	367.0	2.78e-20	1.000	368.0	2.15e-20	1.000	369.0	1.59e-20	1.000	370.0	1.19e-20	1.000

Table A-3 (continued)

WL (nm)	Abs (cm^2)	QY	WL (nm)	Abs (cm^2)	QY	WL (nm)	Abs (cm^2)	QY	WL (nm)	Abs (cm^2)	QY	WL (nm)	Abs (cm^2)	QY
371.0	8.99e-21	1.000	372.0	7.22e-21	1.000	373.0	5.86e-21	1.000	374.0	4.69e-21	1.000	375.0	3.72e-21	1.000
376.0	3.57e-21	1.000	377.0	3.55e-21	1.000	378.0	2.83e-21	1.000	379.0	1.69e-21	1.000	380.0	8.29e-24	1.000
381.0	0.00e+00	1.000												
							IC3ONO2							
185.0	1.79e-17	1.000	188.0	1.81e-17	1.000	190.0	1.79e-17	1.000	195.0	1.61e-17	1.000	200.0	1.26e-17	1.000
205.0	8.67e-18	1.000	210.0	4.98e-18	1.000	215.0	2.47e-18	1.000	220.0	1.17e-18	1.000	225.0	5.80e-19	1.000
230.0	3.10e-19	1.000	235.0	1.80e-19	1.000	240.0	1.10e-19	1.000	245.0	7.00e-20	1.000	250.0	5.70e-20	1.000
255.0	5.20e-20	1.000	260.0	4.90e-20	1.000	265.0	4.60e-20	1.000	270.0	4.10e-20	1.000	275.0	3.60e-20	1.000
280.0	2.90e-20	1.000	285.0	2.30e-20	1.000	290.0	1.70e-20	1.000	295.0	1.20e-20	1.000	300.0	8.10e-21	1.000
305.0	5.20e-21	1.000	310.0	3.20e-21	1.000	315.0	1.90e-21	1.000	320.0	1.10e-21	1.000	325.0	6.10e-22	1.000
330.0	3.70e-22	1.000	335.0	0.00e+00	1.000									
							MGLY_ABS							
219.0	9.84e-21	1.000	219.5	1.04e-20	1.000	220.0	1.06e-20	1.000	220.5	1.11e-20	1.000	221.0	1.15e-20	1.000
221.5	1.18e-20	1.000	222.0	1.22e-20	1.000	222.5	1.24e-20	1.000	223.0	1.26e-20	1.000	223.5	1.26e-20	1.000
224.0	1.25e-20	1.000	224.5	1.24e-20	1.000	225.0	1.25e-20	1.000	225.5	1.27e-20	1.000	226.0	1.27e-20	1.000
226.5	1.29e-20	1.000	227.0	1.31e-20	1.000	227.5	1.32e-20	1.000	228.0	1.35e-20	1.000	228.5	1.37e-20	1.000
229.0	1.40e-20	1.000	229.5	1.42e-20	1.000	230.0	1.48e-20	1.000	230.5	1.53e-20	1.000	231.0	1.57e-20	1.000
231.5	1.59e-20	1.000	232.0	1.61e-20	1.000	232.5	1.62e-20	1.000	233.0	1.61e-20	1.000	233.5	1.68e-20	1.000
234.0	1.74e-20	1.000	234.5	1.80e-20	1.000	235.0	1.84e-20	1.000	235.5	1.87e-20	1.000	236.0	1.89e-20	1.000
236.5	1.91e-20	1.000	237.0	1.93e-20	1.000	237.5	1.94e-20	1.000	238.0	1.96e-20	1.000	238.5	1.96e-20	1.000
239.0	2.01e-20	1.000	239.5	2.04e-20	1.000	240.0	2.08e-20	1.000	240.5	2.10e-20	1.000	241.0	2.14e-20	1.000
241.5	2.16e-20	1.000	242.0	2.19e-20	1.000	242.5	2.20e-20	1.000	243.0	2.23e-20	1.000	243.5	2.26e-20	1.000
244.0	2.28e-20	1.000	244.5	2.29e-20	1.000	245.0	2.30e-20	1.000	245.5	2.32e-20	1.000	246.0	2.33e-20	1.000
246.5	2.35e-20	1.000	247.0	2.38e-20	1.000	247.5	2.41e-20	1.000	248.0	2.46e-20	1.000	248.5	2.51e-20	1.000
249.0	2.57e-20	1.000	249.5	2.61e-20	1.000	250.0	2.65e-20	1.000	250.5	2.67e-20	1.000	251.0	2.69e-20	1.000
251.5	2.69e-20	1.000	252.0	2.71e-20	1.000	252.5	2.72e-20	1.000	253.0	2.73e-20	1.000	253.5	2.74e-20	1.000
254.0	2.76e-20	1.000	254.5	2.78e-20	1.000	255.0	2.82e-20	1.000	255.5	2.87e-20	1.000	256.0	2.93e-20	1.000
256.5	2.98e-20	1.000	257.0	3.07e-20	1.000	257.5	3.12e-20	1.000	258.0	3.17e-20	1.000	258.5	3.21e-20	1.000
259.0	3.26e-20	1.000	259.5	3.28e-20	1.000	260.0	3.29e-20	1.000	260.5	3.31e-20	1.000	261.0	3.33e-20	1.000
261.5	3.34e-20	1.000	262.0	3.36e-20	1.000	262.5	3.38e-20	1.000	263.0	3.42e-20	1.000	263.5	3.44e-20	1.000
264.0	3.48e-20	1.000	264.5	3.54e-20	1.000	265.0	3.59e-20	1.000	265.5	3.65e-20	1.000	266.0	3.73e-20	1.000
266.5	3.80e-20	1.000	267.0	3.87e-20	1.000	267.5	3.95e-20	1.000	268.0	4.02e-20	1.000	268.5	4.08e-20	1.000
269.0	4.13e-20	1.000	269.5	4.17e-20	1.000	270.0	4.20e-20	1.000	270.5	4.22e-20	1.000	271.0	4.22e-20	1.000
271.5	4.22e-20	1.000	272.0	4.23e-20	1.000	272.5	4.24e-20	1.000	273.0	4.27e-20	1.000	273.5	4.29e-20	1.000
274.0	4.31e-20	1.000	274.5	4.33e-20	1.000	275.0	4.37e-20	1.000	275.5	4.42e-20	1.000	276.0	4.48e-20	1.000
276.5	4.56e-20	1.000	277.0	4.64e-20	1.000	277.5	4.71e-20	1.000	278.0	4.78e-20	1.000	278.5	4.83e-20	1.000
279.0	4.87e-20	1.000	279.5	4.90e-20	1.000	280.0	4.92e-20	1.000	280.5	4.93e-20	1.000	281.0	4.94e-20	1.000
281.5	4.92e-20	1.000	282.0	4.90e-20	1.000	282.5	4.86e-20	1.000	283.0	4.83e-20	1.000	283.5	4.79e-20	1.000
284.0	4.76e-20	1.000	284.5	4.72e-20	1.000	285.0	4.70e-20	1.000	285.5	4.68e-20	1.000	286.0	4.66e-20	1.000
286.5	4.65e-20	1.000	287.0	4.65e-20	1.000	287.5	4.68e-20	1.000	288.0	4.73e-20	1.000	288.5	4.78e-20	1.000
289.0	4.84e-20	1.000	289.5	4.89e-20	1.000	290.0	4.92e-20	1.000	290.5	4.92e-20	1.000	291.0	4.90e-20	1.000
291.5	4.86e-20	1.000	292.0	4.81e-20	1.000	292.5	4.75e-20	1.000	293.0	4.70e-20	1.000	293.5	4.65e-20	1.000
294.0	4.58e-20	1.000	294.5	4.48e-20	1.000	295.0	4.38e-20	1.000	295.5	4.27e-20	1.000	296.0	4.17e-20	1.000
296.5	4.07e-20	1.000	297.0	3.99e-20	1.000	297.5	3.94e-20	1.000	298.0	3.88e-20	1.000	298.5	3.82e-20	1.000
299.0	3.76e-20	1.000	299.5	3.72e-20	1.000	300.0	3.69e-20	1.000	300.5	3.68e-20	1.000	301.0	3.70e-20	1.000
301.5	3.72e-20	1.000	302.0	3.74e-20	1.000	302.5	3.74e-20	1.000	303.0	3.75e-20	1.000	303.5	3.71e-20	1.000
304.0	3.62e-20	1.000	304.5	3.51e-20	1.000	305.0	3.38e-20	1.000	305.5	3.25e-20	1.000	306.0	3.15e-20	1.000
306.5	3.04e-20	1.000	307.0	2.92e-20	1.000	307.5	2.80e-20	1.000	308.0	2.71e-20	1.000	308.5	2.63e-20	1.000
309.0	2.52e-20	1.000	309.5	2.43e-20	1.000	310.0	2.34e-20	1.000	310.5	2.25e-20	1.000	311.0	2.19e-20	1.000
311.5	2.12e-20	1.000	312.0	2.06e-20	1.000	312.5	2.02e-20	1.000	313.0	1.96e-20	1.000	313.5	1.92e-20	1.000
314.0	1.91e-20	1.000	314.5	1.88e-20	1.000	315.0	1.86e-20	1.000	315.5	1.85e-20	1.000	316.0	1.86e-20	1.000
316.5	1.87e-20	1.000	317.0	1.87e-20	1.000	317.5	1.87e-20	1.000	318.0	1.83e-20	1.000	318.5	1.75e-20	1.000
319.0	1.69e-20	1.000	319.5	1.60e-20	1.000	320.0	1.50e-20	1.000	320.5	1.41e-20	1.000	321.0	1.34e-20	1.000
321.5	1.27e-20	1.000	322.0	1.21e-20	1.000	322.5	1.18e-20	1.000	323.0	1.14e-20	1.000	323.5	1.08e-20	1.000
324.0	1.01e-20	1.000	324.5	9.62e-21	1.000	325.0	9.28e-21	1.000	325.5	8.75e-21	1.000	326.0	8.49e-21	1.000
326.5	8.21e-21	1.000	327.0	7.71e-21	1.000	327.5	7.38e-21	1.000	328.0	7.18e-21	1.000	328.5	6.86e-21	1.000
329.0	6.71e-21	1.000	329.5	6.63e-21	1.000	330.0	6.46e-21	1.000	330.5	6.29e-21	1.000	331.0	6.21e-21	1.000
331.5	6.18e-21	1.000	332.0	6.20e-21	1.000	332.5	5.49e-21	1.000	333.0	5.21e-21	1.000	333.5	5.38e-21	1.000
334.0	5.35e-21	1.000	334.5	5.04e-21	1.000	335.0	4.94e-21	1.000	335.5	4.90e-21	1.000	336.0	4.52e-21	1.000
336.5	4.26e-21	1.000	337.0	4.11e-21	1.000	337.5	3.76e-21	1.000	338.0	3.61e-21	1.000	338.5	3.58e-21	1.000
339.0	3.47e-21	1.000	339.5	3.32e-21	1.000	340.0	3.22e-21	1.000	340.5	3.10e-21	1.000	341.0	3.00e-21	1.000
341.5	2.94e-21	1.000	342.0	2.89e-21	1.000	342.5	2.86e-21	1.000	343.0	2.88e-21	1.000	343.5	2.88e-21	1.000
344.0	2.89e-21	1.000	344.5	2.91e-21	1.000	345.0	2.95e-21	1.000	345.5	3.00e-21	1.000	346.0	3.08e-21	1.000
346.5	3.18e-21	1.000	347.0	3.25e-21	1.000	347.5	3.30e-21	1.000	348.0	3.39e-21	1.000	348.5	3.51e-21	1.000
349.0	3.63e-21	1.000	349.5	3.73e-21	1.000	350.0	3.85e-21	1.000	350.5	3.99e-21	1.000	351.0	4.27e-21	1.000
351.5	4.47e-21	1.000	352.0	4.63e-21	1.000	352.5	4.78e-21	1.000	353.0	4.92e-21	1.000	353.5	5.07e-21	1.000
354.0	5.23e-21	1.000	354.5	5.39e-21	1.000	355.0	5.56e-21	1.000	355.5	5.77e-21	1.000	356.0	5.97e-21	1.000
356.5	6.15e-21	1.000	357.0	6.35e-21	1.000	357.5	6.56e-21	1.000	358.0	6.76e-21	1.000	358.5	6.95e-21	1.000
359.0	7.20e-21	1.000	359.5	7.44e-21	1.000	360.0	7.64e-21	1.000	360.5	7.89e-21	1.000	361.0	8.15e-21	1.000
361.5	8.43e-21	1.000	362.0	8.71e-21	1.000	362.5	9.02e-21	1.000	363.0	9.33e-21	1.000	363.5	9.65e-21	1.000
364.0	1.00e-20	1.000	364.5	1.04e-20	1.000	365.0	1.08e-20	1.000	365.5	1.11e-20	1.000	366.0	1.15e-20	1.000

Table A-3 (continued)

WL (nm)	Abs (cm^2)	QY	WL (nm)	Abs (cm^2)	QY	WL (nm)	Abs (cm^2)	QY	WL (nm)	Abs (cm^2)	QY	WL (nm)	Abs (cm^2)	QY
366.5	1.19e-20	1.000	367.0	1.23e-20	1.000	367.5	1.27e-20	1.000	368.0	1.31e-20	1.000	368.5	1.35e-20	1.000
369.0	1.40e-20	1.000	369.5	1.44e-20	1.000	370.0	1.47e-20	1.000	370.5	1.51e-20	1.000	371.0	1.55e-20	1.000
371.5	1.59e-20	1.000	372.0	1.64e-20	1.000	372.5	1.70e-20	1.000	373.0	1.73e-20	1.000	373.5	1.77e-20	1.000
374.0	1.81e-20	1.000	374.5	1.86e-20	1.000	375.0	1.90e-20	1.000	375.5	1.96e-20	1.000	376.0	2.02e-20	1.000
376.5	2.06e-20	1.000	377.0	2.10e-20	1.000	377.5	2.14e-20	1.000	378.0	2.18e-20	1.000	378.5	2.24e-20	1.000
379.0	2.30e-20	1.000	379.5	2.37e-20	1.000	380.0	2.42e-20	1.000	380.5	2.47e-20	1.000	381.0	2.54e-20	1.000
381.5	2.62e-20	1.000	382.0	2.69e-20	1.000	382.5	2.79e-20	1.000	383.0	2.88e-20	1.000	383.5	2.96e-20	1.000
384.0	3.02e-20	1.000	384.5	3.10e-20	1.000	385.0	3.20e-20	1.000	385.5	3.29e-20	1.000	386.0	3.39e-20	1.000
386.5	3.51e-20	1.000	387.0	3.62e-20	1.000	387.5	3.69e-20	1.000	388.0	3.70e-20	1.000	388.5	3.77e-20	1.000
389.0	3.88e-20	1.000	389.5	3.97e-20	1.000	390.0	4.03e-20	1.000	390.5	4.12e-20	1.000	391.0	4.22e-20	1.000
391.5	4.29e-20	1.000	392.0	4.30e-20	1.000	392.5	4.38e-20	1.000	393.0	4.47e-20	1.000	393.5	4.55e-20	1.000
394.0	4.56e-20	1.000	394.5	4.59e-20	1.000	395.0	4.67e-20	1.000	395.5	4.80e-20	1.000	396.0	4.87e-20	1.000
396.5	4.96e-20	1.000	397.0	5.08e-20	1.000	397.5	5.19e-20	1.000	398.0	5.23e-20	1.000	398.5	5.39e-20	1.000
399.0	5.46e-20	1.000	399.5	5.54e-20	1.000	400.0	5.59e-20	1.000	400.5	5.77e-20	1.000	401.0	5.91e-20	1.000
401.5	5.99e-20	1.000	402.0	6.06e-20	1.000	402.5	6.20e-20	1.000	403.0	6.35e-20	1.000	403.5	6.52e-20	1.000
404.0	6.54e-20	1.000	404.5	6.64e-20	1.000	405.0	6.93e-20	1.000	405.5	7.15e-20	1.000	406.0	7.19e-20	1.000
406.5	7.32e-20	1.000	407.0	7.58e-20	1.000	407.5	7.88e-20	1.000	408.0	7.97e-20	1.000	408.5	7.91e-20	1.000
409.0	8.11e-20	1.000	409.5	8.41e-20	1.000	410.0	8.53e-20	1.000	410.5	8.59e-20	1.000	411.0	8.60e-20	1.000
411.5	8.80e-20	1.000	412.0	9.04e-20	1.000	412.5	9.45e-20	1.000	413.0	9.34e-20	1.000	413.5	9.37e-20	1.000
414.0	9.63e-20	1.000	414.5	9.71e-20	1.000	415.0	9.70e-20	1.000	415.5	9.65e-20	1.000	416.0	9.69e-20	1.000
416.5	9.89e-20	1.000	417.0	1.00e-19	1.000	417.5	1.02e-19	1.000	418.0	1.00e-19	1.000	418.5	1.02e-19	1.000
419.0	1.01e-19	1.000	419.5	1.01e-19	1.000	420.0	1.03e-19	1.000	420.5	1.01e-19	1.000	421.0	1.04e-19	1.000
421.5	1.05e-19	1.000	422.0	1.06e-19	1.000	422.5	1.04e-19	1.000	423.0	1.05e-19	1.000	423.5	1.05e-19	1.000
424.0	1.01e-19	1.000	424.5	1.01e-19	1.000	425.0	1.05e-19	1.000	425.5	1.03e-19	1.000	426.0	1.02e-19	1.000
426.5	1.01e-19	1.000	427.0	9.77e-20	1.000	427.5	9.81e-20	1.000	428.0	1.00e-19	1.000	428.5	1.02e-19	1.000
429.0	9.89e-20	1.000	429.5	9.85e-20	1.000	430.0	1.04e-19	1.000	430.5	1.08e-19	1.000	431.0	1.05e-19	1.000
431.5	1.02e-19	1.000	432.0	9.64e-20	1.000	432.5	1.01e-19	1.000	433.0	1.06e-19	1.000	433.5	1.09e-19	1.000
434.0	1.04e-19	1.000	434.5	1.03e-19	1.000	435.0	1.07e-19	1.000	435.5	1.16e-19	1.000	436.0	1.09e-19	1.000
436.5	1.11e-19	1.000	437.0	9.81e-20	1.000	437.5	9.71e-20	1.000	438.0	1.06e-19	1.000	438.5	1.16e-19	1.000
439.0	1.08e-19	1.000	439.5	1.05e-19	1.000	440.0	9.70e-20	1.000	440.5	1.01e-19	1.000	441.0	1.04e-19	1.000
441.5	1.07e-19	1.000	442.0	1.02e-19	1.000	442.5	9.68e-20	1.000	443.0	1.00e-19	1.000	443.5	1.14e-19	1.000
444.0	1.13e-19	1.000	444.5	1.03e-19	1.000	445.0	9.74e-20	1.000	445.5	8.46e-20	1.000	446.0	8.70e-20	1.000
446.5	9.97e-20	1.000	447.0	1.01e-19	1.000	447.5	9.15e-20	1.000	448.0	9.41e-20	1.000	448.5	8.99e-20	1.000
449.0	1.10e-19	1.000	449.5	9.12e-20	1.000	450.0	8.56e-20	1.000	450.5	8.28e-20	1.000	451.0	6.15e-20	1.000
451.5	5.56e-20	1.000	452.0	6.47e-20	1.000	452.5	7.27e-20	1.000	453.0	5.75e-20	1.000	453.5	5.08e-20	1.000
454.0	4.38e-20	1.000	454.5	3.81e-20	1.000	455.0	3.61e-20	1.000	455.5	3.61e-20	1.000	456.0	3.13e-20	1.000
456.5	2.72e-20	1.000	457.0	2.44e-20	1.000	457.5	2.22e-20	1.000	458.0	1.82e-20	1.000	458.5	1.43e-20	1.000
459.0	1.32e-20	1.000	459.5	1.05e-20	1.000	460.0	8.95e-21	1.000	460.5	8.90e-21	1.000	461.0	7.94e-21	1.000
461.5	7.04e-21	1.000	462.0	6.46e-21	1.000	462.5	5.63e-21	1.000	463.0	4.78e-21	1.000	463.5	3.94e-21	1.000
464.0	3.26e-21	1.000	464.5	2.97e-21	1.000	465.0	2.65e-21	1.000	465.5	2.46e-21	1.000	466.0	2.27e-21	1.000
466.5	2.08e-21	1.000	467.0	1.86e-21	1.000	467.5	1.76e-21	1.000	468.0	1.60e-21	1.000	468.5	1.44e-21	1.000
469.0	1.34e-21	1.000	469.5	1.20e-21	1.000	470.0	1.07e-21	1.000	470.5	1.02e-21	1.000	471.0	9.92e-22	1.000
471.5	9.97e-22	1.000	472.0	8.87e-22	1.000	472.5	8.27e-22	1.000	473.0	7.76e-22	1.000	473.5	7.15e-22	1.000
474.0	6.71e-22	1.000	474.5	6.67e-22	1.000	475.0	6.10e-22	1.000	475.5	6.17e-22	1.000	476.0	5.54e-22	1.000
476.5	5.22e-22	1.000	477.0	5.10e-22	1.000	477.5	5.17e-22	1.000	478.0	4.80e-22	1.000	478.5	4.71e-22	1.000
479.0	4.60e-22	1.000	479.5	4.35e-22	1.000	480.0	3.90e-22	1.000	480.5	3.71e-22	1.000	481.0	3.62e-22	1.000
481.5	3.52e-22	1.000	482.0	3.05e-22	1.000	482.5	3.05e-22	1.000	483.0	2.86e-22	1.000	483.5	2.53e-22	1.000
484.0	2.75e-22	1.000	484.5	2.59e-22	1.000	485.0	2.47e-22	1.000	485.5	2.36e-22	1.000	486.0	2.12e-22	1.000
486.5	1.89e-22	1.000	487.0	1.93e-22	1.000	487.5	1.86e-22	1.000	488.0	1.82e-22	1.000	488.5	1.75e-22	1.000
489.0	1.74e-22	1.000	489.5	1.72e-22	1.000	490.0	1.66e-22	1.000	490.5	1.75e-22	1.000	491.0	1.54e-22	1.000
491.5	1.74e-22	1.000	492.0	1.63e-22	1.000	492.5	1.53e-22	1.000	493.0	1.52e-22	1.000	493.5	5.85e-23	1.000
494.0	0.00e+00	1.000												

Table A-4. Chamber wall effect and background characterization parameters used in the environmental chamber model simulations for mechanism evaluation.

Cham.	Set [a]	Value	Discussion
RN-I (ppb)			Ratio of the rate of **wall + hν -> HONO** to the NO_2 photolysis rate.
DTC	10	8.14e+9 exp(-9712/T)	Average of value of RS-I that gave best fits to n-butane - NOx chamber experiments carried out in this chamber. The initial HONO was optimized at the same time. If a temperature dependence is shown, it was derived from the temperature dependence of the RN-I values that best fit characterization data in outdoor chamber experiments, with the same activation energy used in all cases. If a temperature dependence is not shown, then the temperature variation for experiments in this set is small compared to the run-to-run variability in the best fit RN-I values. Note that the radical source in Sets 3, 12, 13, and 16 runs was anomalously high. Any dependence of apparent radical source on initial NOx levels in Teflon bag chambers was found to be much less than the run-to-run variability.
	11	0.080	
CTC	≤7	0.064	Same procedure as for the DTC. The runs in Set 9 had slightly higher radical source than most other CTC experiments, so a slightly higher radical source parameter is used for those runs.
	9	0.097	
HONO-F (unitless)			Ratio of the initial HONO concentration to the measured initial NO2. [The initial NO2 in the experiment is reduced by a factor of 1 - (HONO-F)]. Unless the characterization data indicate otherwise, it is assumed that the initial HONO is introduced with the NO2 injection, so is it is assumed to be proportional to the initial NO2 concentration.
DTC	10	0.8%	Average of value of initial HONO to initial NO2 that gave best fits to n-butane - NOx chamber experiments carried out in this chamber. The RN-I parameter was optimized at the same time.
	11	0.6%	
CTC	All	0.08	Same procedure as for CTC
E-NO2/K1 (ppb)			Ratio of rate of NO2 offgasing from the walls to the NO2 photolysis rate.
All Teflon Bag Chambers		0	The NOx offgasing caused by representing the radical source by HONO offgasing appears to be sufficient for accounting for NOx offgasing effects in most cases. RN-I parameters adjusted to fit experiments sensitive to the radical source are consistent with NOx offgasing rates adjusted to fit pure air or aldehyde - air runs, to within the uncertainty and variability.
K(NO2W) (min^{-1})			Rate of unimolecular loss (or hydrolysis) of NO2 to the walls.
All Teflon Bag Chambers		1.6e-4	Based on dark NO2 decay and HONO formation measured in the ETC by Pitts et al. (1984). Assumed to be the same in all Teflon bag chambers, regardless of volume.
YHONO			Yield of HONO in the unimolecular reaction (hydrolysis) of NO2 on the walls.
All Teflon Bag Chambers		0.2	Based on dark NO2 decay and HONO formation measured in the ETC by Pitts et al. (1984). Assumed to be the same in all Teflon bag chambers, regardless of volume.
K(O3W) (min^{-1})			Unimolecular loss rate of O3 to the walls.
DTC	All	1.5e-4	Based on results of O_3 decay in Teflon bag chambers experiments as discussed by Carter et al (1995c).
CTC	All	8.5e-5	Based on results of O_3 decay experiments in this chamber

Table A-4 (continued)

Cham. Set [a]	Value	Discussion
k(N26I) (min^{-1})		Rate constant for **N2O5 -> 2 Wall-NOx**. This represents the humidity-independent portion of the wall loss of N_2O_5, or the intercept of plots of rates of N_2O_5 loss against humidity.
All Teflon Bag Chambers	2.8e-3	Based on N_2O_5 decay rate measurements made by Tuazon et al (1983) for the ETC. Assumed to be independent of chamber size (Carter et al, 1995c).
k(N26S) (ppm^{-1} min^{-1})		Rate constant for **N2O5 + H2O -> 2 Wall-NOx.** This represents the humidity dependent portion of the wall loss of N_2O_5, or the slope of plots of rates of N_2O_5 loss against humidity.
All Teflon Bag Chambers	1.1e-6	Based on N_2O_5 decay rate measurements made by Tuazon et al (1983) for the ETC. Assumed to be independent of chamber size (Carter et al, 1995c).
k(XSHC) (min^{-1})		Rate constant for **OH -> HO2**. This represents the effects of reaction of OH with reactive VOCs in the background air or offgased from the chamber walls. This parameter does not significantly affect model simulations of experiments other than pure air runs.
All Teflon Bag Chambers	250	Estimated from modeling several pure air in the ITC (Carter et al, 1996d), and also consistent with simulations of pure air runs in the ETC (Carter et al, 1997a).
H2O (ppm)		Default water vapor concentration for runs where no humidity data are available.
DTC all CTC	1.0e+3	Experiments in this chamber were carried out using dried purified air. The limited humidity data for such runs indicate that the humidity was less than 5%, probably no more than ~2.5%, and possibly much less than that. The default value corresponds to ~2.5 - 3% RH for the conditions of most experiments.

[a] Set refers to the characterization set, which refers to the group of experiments assumed to have the same run conditions and represented using the same chamber-dependent parameters. See Carter et al (1995) for more discussion. All DTC experiments for the first phase of this program (DTC271-293) are in DTC characterization set 10 and those for the second phase (DTC299 and later) are in characterization set 11. All CTC experiments for the first phase of the program are in CTC characterization set 6. For the CTC runs in the second phase, runs CTC155 through CTC168 are in set 7, and runs CTC230 to CTC247 were in set 9.